Dissertation

Development of radiolabeled probes for the prediction of therapeutic effects of EGFR-tyrosine kinase inhibitors

Muammar Fawwaz

February 2021

Dissertation

Development of radiolabeled probes for the prediction of therapeutic effects of EGFR-tyrosine kinase inhibitors

Graduate School of Medical Sciences
Kanazawa University

Division: Pharmaceutical Sciences
Laboratory: Clinical and Analytical Sciences

School registration no. : 1729012007
Name : Muammar Fawwaz
Primary supervisor name : Kazuma Ogawa

Index

List of Schemes

List of Tables

List of Figures

List of Abbreviations

ANOVA	Analysis of variance
ATP	Adenosine triphosphate
BCA	Bicinchoninic acid
Boc_2O	di-*tert*-Butyl dicarbonate
BrCO1686	*N*-(3-((2-((4-(4-acetylpiperazin-1-yl)-2-methoxyphenyl)amino)-5-(trifluoromethyl)pyrimidin-4-yl)amino)-5-(bromophenyl)acrylamide
CCK	Protein assay kit and cell counting kit
CH_3I	Iodomethane
$CDCl_3$	Chloroform-d
CPM	Count per minute
^{13}C-NMR	Carbon nuclear magnetic resonance
DMSO	Dimethyl sulfoxide
DMSO-*d*6	Dimethyl sulfoxide-d6
DIPEA	*N, N*-diisopropylethylamine
DART-MS	Direct analysis in real time mass spectra
DIPEA	*N*, *N*-diisopropylethylamine
DMA	Dimethylacetamide
EGFR	Epidermal growth factor receptor
EDTA	Ethylene diamine tetra acetate
FAB-MS	Fast atom bombardment mass spectra
FBS	Fetal bovine serum

HPLC	High-performance liquid chromatography
HCl	Hydrogen chloride
H_2SO_4	Sulfuric acid
HRMS	High-resolution mass spectrometry
^{1}H-NMR	Proton nuclear magnetic resonance
IC_{50}	Half maximal inhibitory concentration
ICO1686	*N*-(3-{[2-({4-[4-acetylpiperazin-1-yl]-2-methoxyphenyl}amino)-5-(trifluoromethyl)pyrimidin-4-yl]amino}-5-iodophenyl)acrylamide
KI	Potassium iodide
K_2CO_3	Potassium carbonate
L858R	Leucine-858 to arginine
Met790	Methionine-790
NSCLC	Non-small cell lung cancer
NaI	Sodium iodide
$NaNO_2$	Sodium nitrite
NaOH	Sodium hydroxide
NBS	*N*-bromosuccinimide
NCS	*N*-chlorosuccinimide
$NaHCO_3$	Sodium hydrogen carbonate
Na_2SO_4	Sodium sulfate
PET	Photon emission tomography
$POCl_3$	Phosphoryl chloride
PB	Phosphate buffer

PBS	Phosphate buffered saline
Pd/C	Palladium on carbon
$PdCl_2(PPh_3)_2$	Palladium(II)bis(triphenylphosphine) dichloride
RP-HPLC	Reversed-phase high-performance liquid chromatography
SPECT	Single photon emission computed tomography
SD	Standard deviation
$SnCl_2 \cdot 2H_2O$	Tin (II) chloride dihydrate
TK	Tyrosine kinase
TKIs	Tyrosine kinase inhibitors
T790M	Threonine-790 to methionine
TFA	Trifluoro acetic acid
TLC	Thin layer chromatography
WST-8	2-(2-methoxy-4-nitrophenyl)-3-(4-nitrophenyl)-5-(2,4-disulfophenyl)-2H tetrazolium monosodium salt
keV	Kilo-electron-Volts
kBq	Kilo becquerel
MBq	Mega becquerel
nM	Nanomolar
µg	Microgram
mL	Millilitre
%ID/g	Percent injected dose per gram
i.v.	Intravenous

Summary

Despite the continuous development of cancer treatments, lung cancer remains a deadly disease worldwide, which approximately 30% of cancer-related deaths. Non-small cell lung cancer (NSCLC) is the most prevalent type, accounting for over 80% of all lung cancers. The mutation of exons 18-21 in the kinase domain of epidermal growth factor receptor (EGFR) has been associated with NSCLC. The single mutation EGFR L858R and 19 deletion are the frequent occurring mutation.

Currently, the treatment of NSCLC patients by EGFR targeting agents has shown impressive therapeutic outcomes in clinical. The first-generation EGFR-tyrosine kinase inhibitors (TKIs), such as gefitinib and erlotinib, successfully prolonged the overall survival of NSCLC patients with the EGFR L858R mutation or exon 19 deletion. However, almost all patients acquire drug resistant after long treatment by the first-generation TKIs. The mutation T790M in exon 20 was identified as the most frequent cause of the resistance. Therefore, some third-generation TKIs, such as osimertinib (Tagrisso™) and rociletinib (CO-1686), were developed to overcome the drug resistance.

Monitoring of tumor malignancies by nuclear medicine imaging has been a prestigious invention in clinical diagnosis due to the ability to estimate the expression level of the target molecule as well as the efficacy of inhibitors by modalities such as positron emission tomography (PET) and single photon emission computed tomography (SPECT). This technique is a complement to the biopsy method which is unable to describe the whole tumor profile, and repeated biopsies are invasive and a significant burden on patients.

Radiotracers based on third generation EGFR-TKIs, such as [^{11}C]-osimertinib, [^{11}C]-AZD3759, and [^{11}C]-rociletinib those have high affinity toward EGFR with T790M mutation were developed. These tracers were applied to detect the brain penetration in the NSCLC with brain metastases animal model in the preclinical setting. Nevertheless, imaging probes for the

monitoring of the EGFR L858R/T790M mutation have not been reported. Consequently, I aimed to develop the imaging probes toward EGFR L858R/T790M.

Here, I describe synthesis and evaluation of novel radiotracers based on a third generation EGFR CO-1686 derivative that has selective binding ability to EGFR with L858R/T790M mutation. This manuscript is divided into two chapters. **Chapter 1** describes the synthesis and preclinical evaluation of a novel radioiodinated probe [^{125}I]ICO1686 for SPECT imaging lung cancer with L858R/T790M mutation of EGFR. Radioiodinated compound [^{125}I]ICO1686 was synthesized using a stannylated precursor under non-carrier added conditions with *N*-chlorosuccinimide (NCS) as an oxidizing agent. In this study, ^{125}I was used as an alternative radionuclide instead of ^{123}I, which is a radionuclide for SPECT. **Chapter 2** describes the [^{77}Br]BrCO1686: Preclinical evaluation as a PET probe for lung cancer with L858R/T790M mutation of EGFR. ^{77}Br was used as an alternative radionuclide instead of ^{76}Br, which is a radionuclide for PET.

Chapter 1

Synthesis and preclinical evaluation of a novel radioiodinated probe [^{125}I]ICO1686 for imaging lung cancer with L858R/T790M mutation of epidermal growth factor receptor (EGFR)

Abstract

Rociletinib (CO-1686) is one of the third-generation EGFR-TKIs, which is selective toward epidermal growth factor receptor (EGFR) L858R/T790M, and consequently radiolabeled CO-1686 is expected to work in monitoring EGFR L858R/T790M mutation. In this study, I aimed to provide a novel radiolabeled probe, *N*-{3-[(2-{[4-(4-acetylpiperazin-1-yl)-2-methoxyphenyl]amino}-5-(trifluoromethyl)pyrimidine-4-yl] amino}-5-([^{125}I]iodophenyl) acrylamide ([^{125}I]ICO1686) to determine the EGFR L858R/T790M mutation for selection of sensitive patients to third generation EGFR-tyrosine kinase inhibitors (TKIs). The precursor was synthesized by tributylstannylation of nonradioactive ICO1686. [^{125}I]ICO1686 was prepared by iododestannylation of a corresponding tributylstannyl precursor with [^{125}I]NaI and *N*-chlorosuccinimide (NCS) with high radiochemical yield (77%) and purity (> 99%). I evaluated biological potency of [^{125}I]ICO1686 as a molecular probe for detecting EGFR L858R/T790M using three human NSCLC cell lines: H1975 (dual mutation EGFR L858R/T790M), H3255 (EGFR L858R active mutant), and H441 (wild-type EGFR). ICO1686 exhibited high cytotoxicity toward H1975 (IC_{50} 0.20 ± 0.05 μM) and H3255 (IC_{50} 0.50 ± 0.21 μM), which is comparable to CO-1686. In contrast, the cytotoxicity of ICO1686 toward H441 was 10-fold lower than that toward H1975. In the in vitro cell uptake studies, the uptake of [^{125}I]ICO1686 in H1975 was 101.52% dose/mg, whereas the uptakes in H3255 and H441 were 33.52 and 8.95% dose/mg, respectively. The uptake of [^{125}I]ICO1686 in H1975 was greatly reduced by treatment with excess CO-1686 as a blocking agent. In vivo biodistribution study

exhibited that radioactivity accumulation in H1975 tumor (1.77 ± 0.43% ID/g) was comparable to that in H3255 tumor (1.63 ± 0.23% ID/g) and the accumulation in H1975 tumor was not reduced by pretreatment with an excess dose of CO-1686.

1.1. Introduction

Although research on cancer treatment has been continuously conducted, lung cancer remains the deadliest disease in the world, accounting for approximately 30% of cancer-related deaths. The mutation of exons 18-21 due to the overexpression of epidermal growth factor receptor (EGFR) and tyrosine kinase (TK) has been associated with lung cancer [1-4], and non-small cell lung cancer (NSCLC) is the most prevalent type with 80–85% of all cases [5-7]. The single mutation EGFR L858R and 19 deletion are the frequent occurring mutation [1-3].

The mutation of exon 20 in codon 790 by changing the threonine-790 to methionine (T790M) of the EGFR gene has been reported in approximately 50% of all patients who acquired resistance to EGFR tyrosine kinase inhibitors (TKIs) therapy [8]. This mutation is supposed to be obtained during treatment by first- and second-generation EGFR-TKIs which eventually develop drug resistance. The T790M mutation has been identified as the most frequent mechanism in resistance of such NSCLC patients [9, 10].

Rociletinib (CO-1686) is a third generation EGFR-TKI, which specifically binds to the EGFR adenosine triphosphate (ATP) binding site with T790M mutation. The complex of CO-1686 with T790M EGFR by X-ray crystal structure analysis shows that the anilinopyrimidine framework of ligand dovetails to the methionine gatekeeper. The affinity of CO-1686 towards T790M EGFR is enhanced because of the hydrophobic interaction between the trifluoromethyl moiety of the CO-1686 and the Met790 side-chain [10]. The preclinical studies with human NSCLC also confirmed excellent activity as well as selectivity to the T790M EGFR over wild type EGFR [11-13]. Therefore, CO-1686 is a prominent EGFR-TKI as a base structure to develop molecular probes for active mutant T790M EGFR. In this study, I aimed to provide a novel radioiodine labeled CO-1686 to determine the EGFR L858R/T790M mutation for selection of sensitive patients to third generation EGFR-TKIs.

I synthesized and evaluated of a non-radioactive iodinated, *N*-(3-{[2-({4-[4-acetylpiperazin-1-yl]-2-methoxyphenyl}amino)-5-(trifluoromethyl)pyrimidin-4-yl]amino}-5-iodophenyl)acrylamide (ICO1686, **Scheme 1**, **10**) and a radioactive iodinated **10** ([^{125}I]ICO1686, **Scheme 2**, [^{125}I]**10**), and evaluated it using three types of human NSCLC cell lines H1975 (dual mutations EGFR L858R/T790M), H3255 (EGFR L858R active mutant) and H441 (wild-type EGFR) for use in selecting patients with NSCLC and predicting treatment strength of third-generation EGFR-TKIs. In this study, although I aimed at developing a SPECT imaging probe with ^{123}I ($t_{1/2}$ = 13 h) to determine the EGFR L858R/T790M mutation for selection of sensitive patient to the therapy, ^{125}I ($t_{1/2}$ = 59 d) was used as an alternative radionuclide for initial fundamental studies because of its longer half-life.

1.2. Experimental Section

1.2.1. Materials and methods

All chemical reagents and solvents were purchased commercially from Tokyo Chemical Industry, Co., Ltd., (Tokyo, Japan), Merck (Darmstadt, Germany), Nacalai Tesque, Inc., (Kyoto, Japan), Fujifilm Wako Pure Chemical Corporation (Osaka, Japan), and Kanto Chemical, Co., Inc. (Tokyo, Japan). [^{125}I]Sodium iodide (644 GBq/mg) was purchased from Perkin Elmer (Waltham, MA, USA). The radioactivity was measured by an Auto Gamma System ARC-7010B (Hitachi, Ltd., Tokyo, Japan). Reactions were performed and monitored by thin-layer chromatography (TLC) on silica plates 60 F_{254} (Merck, Darmstadt, Germany).

DMEM/Ham's F-12 and RPMI-1640 medium, penicillin-streptomycin, phosphate-buffered saline (PBS) and trypsin–EDTA (0.25%) were obtained from Nacalai Tesque, Inc., (Kyoto, Japan). Fetal bovine serum (FBS) was obtained from Biowest (Nuaillé, France). Bicinchoninic Acid (BCA) Protein Assay Kit and Cell Counting Kit (CCK) were purchased from Nacalai Tesque, Inc. and Dojindo (Kumamoto, Japan), respectively.

Nuclear magnetic resonance (NMR) spectroscopy was obtained on JEOL JNM-ECS 400

(JEOL Ltd, Tokyo, Japan). Direct analysis in real time mass spectra (DART-MS) was obtained on JEOL JMS-T100TD. Fast atom bombardment mass spectra (FAB-MS) was obtained on JEOL JMS-T700 (JEOL Ltd). Analytical high-performance liquid chromatography (HPLC) system was obtained on the Shimadzu SPD-20A system (Shimadzu Corp., Kyoto, Japan). The optical density was obtained on Infinite® F200 Pro microplate reader (TECAN, Männedorf, Switzerland).

1.2.2. Synthesis of non-radioactive compound

Intermediate compounds were synthesized according to previous studies, with a slight modification [14-17]. Detailed procedures and analyses were shown in **Scheme 1** and Supporting Information (**Figure S1-S11**).

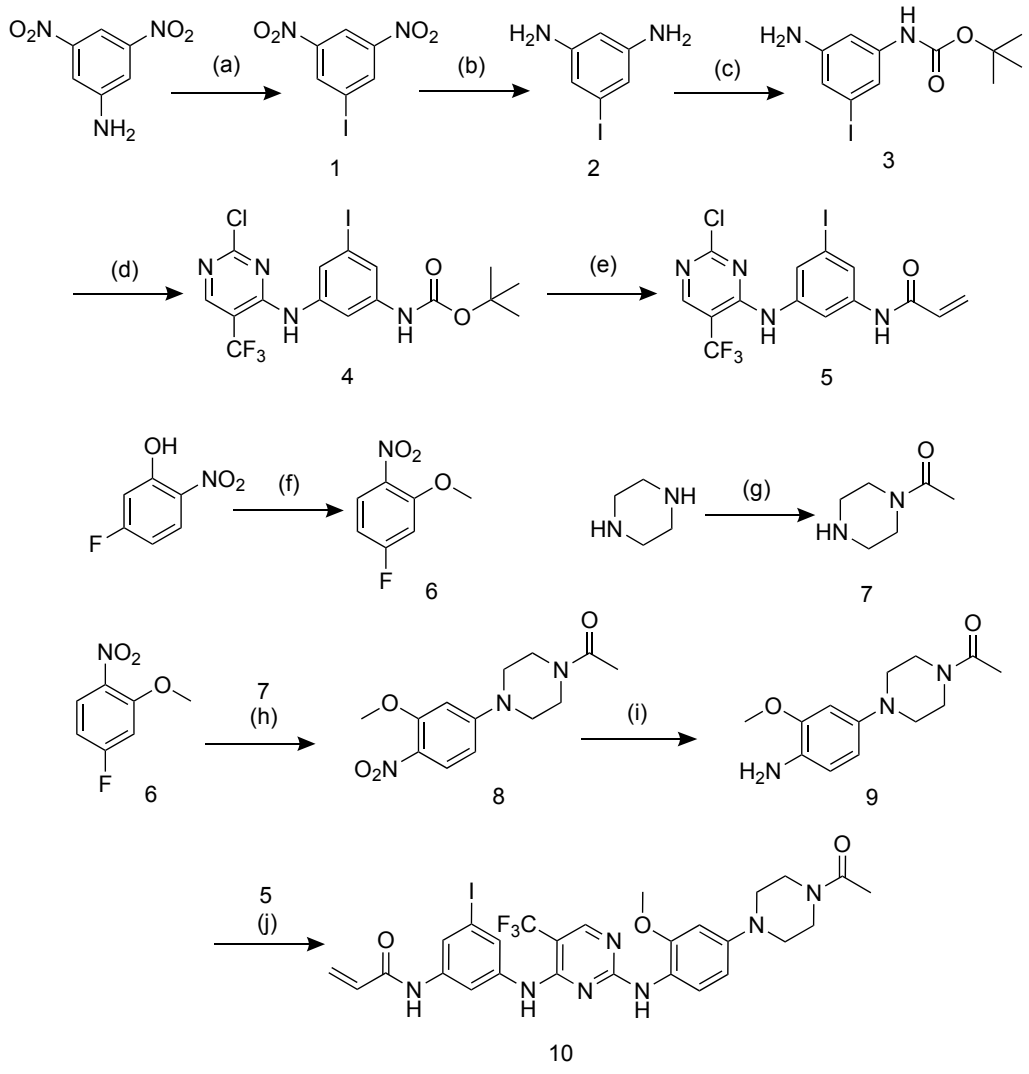

Scheme 1. Synthesis of non-radioactive iodinated Rociletinib. Reagent: (a) H_2SO_4, $NaNO_2$, KI, 0 °C, rt, 3 h; (b) Ethanol, $SnCl_2 \cdot 2H_2O$, 45 °C, 1 h; (c) Acetonitrile, Boc_2O, rt, 2 h; (d) *n*-Butanol, 2,4-dichloro-5(trifluoromethyl) pyrimidine, DIPEA, 0 °C, 1 h, rt, 4 h; (e) HCl/ethyl acetate, rt, 1 h, dichloromethane, acryloyl chloride, DIPEA, −30 °C, rt, 1 h; (f) Acetone, K_2CO_3, CH_3I, 0 °C, 5 h; (g) Dichloromethane, acetic anhydride, 0 °C, 5 h; (h) Dimethylacetamide, DIPEA, 90 °C, overnight; (i) Pd/C 10%, H_2, rt, 5 h; (j) Dioxane, TFA, 60 °C, 3 h.

*Synthesis of 1-iodo-3,5-dinitrobenzene (**1**)*

To a stirred mixture of 3,5-dinitroaniline ($C_6H_5N_3O_4$) (0.70 g, 3.82 mmol, 1.0 eq.) and sulfuric acid (H_2SO_4) (0.60 mL, 11.46 mmol, 3.0 eq.), sodium nitrite ($NaNO_2$) (0.40 g, 5.73 mmol, 1.5 eq.) was added at 0 °C. After the formation of the diazonium salt was confirmed by TLC, potassium iodide (KI) (1.60 g, 9.55 mmol, 2.5 eq.) was added to the mixture and the mixture was stirred at room temperature for 3 h. After the reaction was completed, pH was adjusted to neutral using saturated aqueous sodium bicarbonate ($NaHCO_3$). Then the reaction mixture was extracted with ethyl acetate. The organic layer was separated, dried over sodium sulfate (Na_2SO_4), filtered and concentrated under reduced pressure to afford **1** (1.1 g, 97%) as a brown crystal. ^{1}H–NMR (400 MHz, $CDCl_3$): δ 8.88 (2H, d, J = 1.6 Hz), 9.02 (1H, t, J = 2.0 Hz). ^{13}C–NMR (100 MHz, $CDCl_3$): δ 93.5, 118.5, 137.8, 148.5. HRMS (FAB+) calculated for $C_6H_3IN_2O_4$ $[M + H]^+$: m/z = 294.9216, found 294.9225.

*Synthesis of 5-iodobenzene-1,3-diamine (**2**)*

To a stirred mixture of **1** (1.10 g, 3.74 mmol, 1.0 eq.) and ethanol (20 mL), tin (II) chloride dihydrate ($SnCl_2 \cdot 2H_2O$) (4.22 g, 18.70 mmol, 5.0 eq.) was added at 45 °C and the mixture was stirred for 1 h under nitrogen atmosphere. After the reaction was completed, the pH was adjusted to neutral using saturated aqueous $NaHCO_3$. The reaction mixture was extracted with ethyl acetate. The organic layer was separated, dried over Na_2SO_4, filtered and concentrated under reduced pressure to afford **2** (0.62 g, 71%) as a brown solid. ^{1}H–NMR (400 MHz, $CDCl_3$): δ 3.57 (4H, s), 5.95 (1H, t, J = 2.0 Hz), 6.48 (2H, d, J = 2.0 Hz). ^{13}C–NMR (100 MHz, $CDCl_3$): δ 95.5, 101.0, 114.8, 148.5. HRMS (FAB+) calculated for $C_6H_7IN_2$ $[M + H]^+$: m/z = 233.9654, found 233.9645.

*Synthesis of tert-butyl (3-amino-5-iodophenyl)carbamate (**3**)*

To a stirred mixture of **2** (0.62 g, 2.65 mmol, 1.0 eq.) and acetonitrile (5.0 mL), di-*tert*-butyl dicarbonate (Boc_2O) (0.60 g, 2.65 mmol, 1.0 eq.) was added at room temperature and the mixture was stirred for 2 h under nitrogen atmosphere. After the reaction was completed, the product was purified by column chromatography on silica gel (hexane/ethyl acetate = 7/3) and concentrated under reduced pressure to afford **3** (0.28 g, 32%) as an orange crystal. ^{1}H–NMR (400 MHz, $CDCl_3$): δ 1.50 (9H, s), 3.68 (2H, s), 6.34 (1H, s), 6.71 (1H, t, J = 1.6 Hz), 6.86 (1H, s), 6.96 (1H, t, J = 1.6 Hz). ^{13}C–NMR (100 MHz, $CDCl_3$): δ 28.5 (3C), 80.9, 94.8, 104.0, 117.2, 118.7, 140.3, 148.3, 152.5. HRMS (FAB+) calculated for $C_{11}H_{15}IN_2O_2$ $[M + H]^+$: m/z = 334.0178, found 334.0168.

*Synthesis of tert-Butyl (3-{[2-chloro-5-(trifluoromethyl)pyrimidin-4-yl]amino}-5-iodophenyl) carbamate (**4**)*

To a stirred mixture of **3** (0.28 g, 0.85 mmol, 1.0 eq.) and *n*-butanol (2.6 mL), 2,4-dichloro-5(trifluoromethyl)pyrimidine (115 μL, 0.85 mmol, 1.0 eq.), *N*,*N*-diisopropylethylamine (DIPEA) (296 μL, 1.70 mmol, 2.0 eq.) were added at 0 °C and stirred for 1 h. The stirring was continued at room temperature for 4 h. After the reaction was completed, the crude product was purified using column chromatography on silica gel (dichloromethane) and concentrated under reduced pressure to afford **4** (0.29 g, 66%) as a colorless solid. ^{1}H–NMR (400 MHz, $CDCl_3$): δ 1.53 (9H, s), 6.68 (1H, s), 7.00 (1H, s), 7.58 (1H, t, J = 1.6 Hz), 7.61 (1H, t, J = 1.6 Hz), 7.72 (1H, t, J = 1.6 Hz), 8.46 (1H, s). ^{13}C–NMR (100 MHz, $CDCl_3$): δ 28.2 (3C), 81.4, 93.8, 106.7 (q, J_{CF} = 31.4 Hz), 111.6, 123.0 (q, J_{CF} = 270 Hz), 124.2, 125.4, 137.6, 140.1, 152.2, 156.1 (q, J_{CF} = 4.7 Hz), 157.0, 163.5. HRMS (FAB+) calculated for $C_{16}H_{15}ClF_3IN_4O_2$ $[M + H]^+$: m/z = 513.9880, found 513.9875.

*Synthesis of N-(3-{[2-chloro-5-(trifluoromethyl)pyrimidin-4-yl]amino}-5-iodophenyl) acrylamide (**5**)*

The mixture of compound **4** (1.0 g, 1.94 mmol, 1.0 eq.) and 4.0 M HCl/ethyl acetate (1.0 mL) was stirred at room temperature for 1 h. The reaction was monitored by TLC (hexane/ethyl acetate = 7/3) after the reaction was completed, the solvent was removed by nitrogen gassing and the residue was dried under reduced pressure to afford a colorless solid (0.81 g). The crude material was used to the next step without further purification. To a stirred mixture of the crude material (0.81 g), DIPEA (1.0 mL, 5.85 mmol, 3.0 eq.) and dichloromethane (20 mL), acryloyl chloride (237 μL, 2.93 mmol, 1.5 eq.) were added at –30 °C and stirred at room temperature for 1 h. The crude product was dissolved in ethyl acetate and washed with 1.0 M HCl, saturated aqueous $NaHCO_3$ and brine successively. The organic layer was separated, dried over Na_2SO_4, filtered and concentrated under reduced pressure. The crude product was purified using column chromatography on silica gel (hexane/ethyl acetate = 7/3) and concentrated under reduced pressure to afford **5** (380 mg, 43%) as a colorless solid. ^{1}H NMR (400 MHz, $(CD_3)_2SO$): δ 5.79 (1H, dd, J = 10.0, 2.0 Hz), 6.27 (1H, dd, J = 16.8, 2.0 Hz), 6.40 (1H, dd, J = 16.4, 10.0 Hz), 7.56 (1H, d, J = 2.0 Hz), 7.77 (1H, d, J = 2.0 Hz), 7.99 (1H, d, J = 2.0 Hz), 8.62 (1H, s), 9.57 (1H, s), 10.31 (1H, s). ^{13}C NMR (150 MHz, $(CD_3)_2SO$): δ 93.6, 106.1 (q, J_{CF} = 30.2 Hz), 115.8, 123.0 (q, J_{CF} = 270 Hz), 125.0, 127.7, 128.9, 131.4, 138.4, 140.4, 156.9 (q, J_{CF} = 4.4 Hz), 157.5, 162.3, 163.4. HRMS (FAB+) calculated for $C_{14}H_9ClF_3IN_4O$ $[M + H]^+$: m/z = 468.9461, found 468.9559.

*Synthesis of 4-fluoro-2-methoxy-1-nitrobenzene (**6**)*

To a stirred mixture of 5-fluoro-2-nitrophenol ($C_6H_4FNO_3$) (1.0 g, 6.43 mmol, 1.0 eq.) and acetone (15 mL), potassium carbonate (K_2CO_3) (1.77 g, 12.80 mmol, 2.0 eq.) and iodomethane (CH_3I) (0.80 mL, 12.80 mmol, 2.0 eq.) were added. The mixture was stirred at 0 °C for 5 h. After the reaction was completed, ethyl acetate and water (1:1) were added to the

mixture. The organic layer was separated, dried over Na_2SO_4, filtered and concentrated under reduced pressure to afford **6** (1.1 g, 100%) as an orange crystal. ^{1}H–NMR (400 MHz, $CDCl_3$): δ 3.97 (3H, s), 6.74 (1H, dt, *J* = 8.4, 2.0 Hz), 6.80 (1H, dd, *J* = 10.4, 2.4 Hz), 7.96 (1H, dd, *J* = 8.4, 6.4 Hz). ^{13}C–NMR (100 MHz, $(CD_3)_2SO$): δ 56.7, 101.5, 107.0, 128.0, 155.3, 164.3, 167.0. HRMS (DART+) calculated for $C_7H_6FNO_3$ $[M + H]^+$: *m/z* = 172.0331, found 172.0345.

*Synthesis of 1-(piperazine-1-yl)ethan-1-one (**7**)*

To a stirred mixture of piperazine ($C_4H_{10}N_2$) (1.70 g, 19.70 mmol, 2.0 eq.) and dichloromethane (50 mL), acetic anhydride ($C_4H_6O_3$) (0.94 mL, 9.90 mmol, 1.0 eq.) was added at 0 °C and the mixture was stirred for 5 h. After the reaction was completed, the reaction mixture was quenched with water (15 mL) and extracted with dichloromethane, the organic layer then dried over Na_2SO_4, filtered and concentrated under reduced pressure to afford **7** (0.26 g, 20%) as a colorless solid. ^{1}H–NMR (400 MHz, $CDCl_3$): δ 2.13 (3H, s), 3.40–3.70 (8H, m). ^{13}C–NMR (100 MHz, $CDCl_3$): δ 21.3, 41.2 (2C), 45.7 (2C), 169.1. HRMS (FAB+) calculated for $C_6H_{12}N_2O$ $[M + H]^+$: *m/z* = 129.0949, found 129.1031.

*Synthesis of 1-(4-{3-Methoxy-4-nitrophenyl}piperazine-1-yl)ethan-1-one (**8**)*

To a stirred mixture of **7** (1.90 g, 11.0 mmol, 1.0 eq.) and dimethylacetamide (6.0 mL), **6** (1.40 g, 11.0 mmol, 1.0 eq.) and DIPEA (2.0 mL) were added at 90 °C. The mixture was stirred overnight under nitrogen atmosphere with a reflux condenser. After the reaction was completed, the reaction mixture was quenched with water and extracted with ethyl acetate. The organic layer was dried over Na_2SO_4, filtered and concentrated under reduced pressure. The crude product was purified using column chromatography on silica gel (chloroform/methanol = 150/1) to afford **8** (2.61 g, 83%) as a pale brown solid. ^{1}H–NMR (400 MHz, $CDCl_3$): δ 2.16 (3H, s), 3.40–3.50 (4H, m), 3.67 (2H, t, *J* = 4.0 Hz), 3.81 (2H, t, *J* = 4.0 Hz), 3.97 (3H, s), 6.33 (1H, d, *J* = 1.6 Hz), 6.42 (1H, dd, *J* = 6.0, 1.6 Hz), 8.02 (1H, d, *J* = 6.4 Hz). ^{13}C–NMR (100

MHz, $CDCl_3$): δ, 21.2, 40.5, 45.2, 46.5, 46.6, 56.0, 97.0, 105.1, 128.4, 129.5, 155.0, 156.0, 169.0. HRMS (FAB+) calculated for $C_{13}H_{17}N_3O_4$ $[M + H]^+$: *m/z* = 280.1219, found 280.1295.

*Synthesis of 1-(4-{4-Amino-3-methoxyphenyl}piperazine-1-yl)ethan-1-one (**9**)*

To a stirred mixture of **8** (100 mg, 0.35 mmol, 1.0 eq.) and ethanol (3.50 mL) under a nitrogen atmosphere, palladium on carbon (Pd/C 10%) (20 mg) was added at room temperature. The mixture then stirred under a hydrogen atmosphere for 5 h. After the reaction was completed, the catalyst was removed by filtration through a pad of Celite®; the filtrate was concentrated under reduced pressure to afford **9** (98 mg, 100%) as a purple solid. This compound was so unstable that it was used in the following reaction without further purification right after characterization by ^1H NMR and MS analyses. ^1H–NMR (400 MHz, $CDCl_3$): δ 2.13 (3H, s), 2.95–3.08 (4H, m), 3.62 (2H, t, *J* = 5.6 Hz), 3.77 (2H, t, *J* = 5.2 Hz), 3.85 (3H, s), 6.42 (1H, dd, *J* = 8.8, 2.8 Hz), 6.52 (1H, s), 6.66 (1H, d, *J* = 8.4 Hz). HRMS (FAB+) calculated for $C_{13}H_{19}N_3O_2$ $[M + H]^+$: *m/z* = 249.1477, found 249.1464.

*Synthesis of N-(3-{[2-({4-[4-acetylpiperazin-1-yl]-2-methoxyphenyl}amino)-5-(trifluoromethyl)pyrimidin-4-yl]amino}-5-iodophenyl)acrylamide (**10**)*

To a stirred mixture of compound **5** (25 mg, 0.05 mmol, 1.0 eq.) and 2.0 M trifluoroacetic acid (TFA)/dioxane, compound **9** was added (17 mg, 0.068 mmol, 1.36 eq.) and the mixture was stirred at 60 °C for 3 h. After the reaction was completed, the pH was adjusted to neutral using saturated aqueous $NaHCO_3$. The reaction mixture was extracted with ethyl acetate. The organic layer was separated, dried over Na_2SO_4, filtered and concentrated under reduced pressure. The crude product was purified by HPLC with mobile phase system ethyl acetate/methanol = 97/3, using a Cosmosil® 5SL-II (20 ID × 250 mm) column, a flow rate 9.5 mL/min. The column temperature was maintained at 40 °C. The pure product was concentrated under reduced pressure to afford **10** (30 mg, 73%) as a colorless solid. ^1H–NMR (400 MHz,

$(CD_3)_2SO$): δ 2.05 (3H, s), 3.10 (2H, t, J = 4.8 Hz), 3.16 (2H, t, J = 4.4 Hz), 3.53–3.63 (4H, m), 3.82 (3H, s), 5.77 (1H, dd, J = 10.0, 2.0 Hz), 6.25 (1H, dd, J = 16.8, 2.0 Hz), 6.41 (1H, dd, J = 16.8, 10.0 Hz), 6.49 (1H, dd, J = 8.8, 2.0 Hz), 6.71 (1H, s), 7.74 (1H, s), 7.77 (2H, s), 7.82 (1H, s), 7.86 (1H, s), 8.35 (1H, s), 9.79 (1H, s), 10.14 (1H, s). ^{13}C–NMR (100 MHz, $(CD_3)_2SO$): δ 21.0, 40.8, 45.4, 48.7, 49.0, 56.0, 94.1, 98.3 (q, J_{CF} = 30.5 Hz), 100.8, 107.5, 110.9, 119.1, 122.2, 124.1, 124.5, 124.8 (q, J_{CF} = 270 Hz), 127.4, 131.6, 140.1, 141.2, 149.0, 151.8, 155.2 (q, J_{CF} = 4.8 Hz), 156.8, 160.8, 163.2, 168.3. HRMS (FAB+) calculated for $C_{27}H_{27}F_3IN_7O_3$ [M + H]$^+$: m/z = 681.1172, found 681.1186.

*Synthesis of N-(3-{[2-({4-[4-acetylpiperazin-1-yl]-2-methoxyphenyl}amino)-5-(trifluoromethyl)pyrimidin-4-yl]amino}-5-{tributylstannyl}phenyl)acrylamide (**11**)*

To a stirred mixture of compound **10** (35 mg, 51.40 μmol, 1.0 eq.) and dry dioxane (5 mL), hexabutyldistannane (519 μL, 1.03 mmol, 20 eq.) and palladium(II)bis(triphenylphosphine) dichloride ($PdCl_2(PPh_3)_2$) (15 mg, 21 μmol, 0.4 eq.) were added, the mixture was stirred at 60 °C for 18 h under nitrogen atmosphere. After the reaction was completed, the catalysis was removed by filtration through a pad of Celite®; the filtrate was concentrated under reduced pressure. The crude product was purified by HPLC with mobile phase system ethyl acetate/methanol = 97/3, using a Cosmosil® 5SL-II (20 ID × 250 mm) column, a flow rate 9.5 mL/min. The column temperature was maintained at 40 °C. The pure product was concentrated under reduced pressure to afford **11** (4 mg, 10%) as a white solid. ^{1}H–NMR (400 MHz, $(CDCl_3)$: δ 0.88 (9H, t, J = 7.6 Hz), 1.06 (6H, t, J = 8.0 Hz), 1.33 (6H, sex, J = 7.6 Hz), 1.54 (6H, quin, J = 7.6 Hz), 2.14 (3H, s), 3.10–3.20 (4H, m), 3.62 (2H, t, J = 5.6 Hz), 3.78 (2H, t, J = 5.6 Hz), 3.91 (3H, s), 5.75 (1H, d, J = 11.2 Hz), 6.23 (1H, dd, J = 17.2, 10.8 Hz), 6.43 (1H, d, J = 1.6 Hz), 6.48 (1H, dd, J = 7.6, 2.0 Hz), 6.54 (1H, d, J = 2.4 Hz), 7.68 (1H, s) 7.06 (1H, s), 7.14 (1H, s), 7.20 (1H, s), 7.44 (1H, s), 7.97 (1H, s), 8.16 (1H, d, J = 8.4 Hz), 8.29 (1H, s). HRMS (FAB+) calculated for $C_{39}H_{54}F_3N_7O_3Sn$ [M + H]$^+$: m/z =

845.3267 found 845.3262.

1.2.3. Cell viability assays

The half maximal inhibitory concentration (IC_{50}) of **10**, CO-1686 or gefitinib to NSCLC cell lines was performed by 2-(2-methoxy-4-nitrophenyl)-3-(4-nitrophenyl)-5-(2,4-disulfophenyl)-2H tetrazolium monosodium salt (WST-8) assay. The NSCLC cell lines H1975, H441 and H3255 were kindly supplied by Dr. Juri G. Gelovani, formerly of the Department of Experimental Diagnostic Imaging, at the University of Texas, MD Anderson Cancer Center, Houston, TX, USA. H1975 (2.5×10^3 cells/well), H441 (2.5×10^3 cells/well) and H3255 (1×10^4 cells/well) were seeded in 96-well tissue culture plates and cultured in medium supplemented with 10% fetal bovine serum (FBS) and penicillin (100 IU/mL) streptomycin (100 mg/mL) at 37 °C in a humidified atmosphere with 5% CO_2. After incubation for 24 h, cells were treated with various concentrations (0.01–100 μM) of **10**, CO-1686 or gefitinib for 48 h and cell viability was assessed using the Cell Counting Kit-8 (Dojindo, Kumamoto, Japan) following the manufacturer's protocol. All data were analyzed using GraphPad Prism 5.0 software (GraphPad Software, San Diego, CA., USA) and presented as mean ± standard deviation (SD).

*1.2.4. Radiosynthesis of [^{125}I]ICO1686 ([^{125}I]**10**)*

Radiosynthesis [^{125}I]**10** was performed by an iododestannylation reaction of the corresponding precursor **11** (**Scheme 2**). A solution of [^{125}I]NaI in NaOH aqueous solution (2.5 MBq, 1 μL) was charged into a sealed vial containing **11** (1 mg/mL, 10 μL) in ethanol, acetic acid (5%, 30 μL) and *N*-chlorosuccinimide (NCS) (20 mg/mL, 10 μL). The mixture was vortexed 5 min and shaken 15 min at 37 °C. The product was quenched by the addition of aqueous sodium hydrogen sulfite (5 mg/mL, 10 μL) and was analyzed by reversed-phase (RP)-HPLC with mobile phase system water (A) and methanol (B), B: 70–100%, 20 min using a

Cosmosil® 5C_{18} MSII (4.6 ID × 150 mm) column, a flow rate 1 mL/min. The column temperature was maintained at 40 °C.

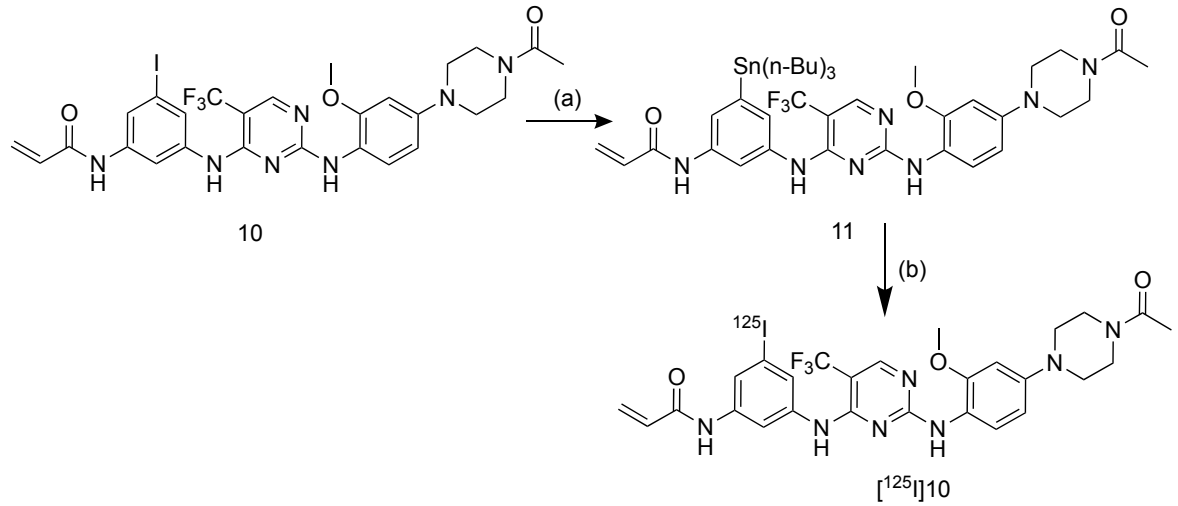

Scheme 2. Synthesis of a stannylated radiolabeling precursor **11** and radioiodinated compound [^{125}I]**10**. (a) Dry dioxane, hexabutyldistannane, $PdCl_2(PPh_3)_2$, 60 °C, 18 h; (b) [^{125}I]NaI, acetic acid, ethanol, NCS, 37 °C, 15 min.

1.2.5. Determination of partition coefficient

The partition coefficient of [^{125}I]**10** was measured, as previously reported with a slight modification [18]. Briefly, [^{125}I]**10** was added to the mixture of *n*-octanol (3 mL) and 0.1 M pH 7.4 phosphate buffer (3 mL) in a test tube. The test tube was vortexed for 1 min, left at room temperature for 10 min and centrifuged at 3,000× *g* and 4 °C for 5 min. The *n*-octanol layer (2 mL) was transferred into a new test tube followed by adding 1 mL of new *n*-octanol and 3 mL of phosphate buffer. The radioactivity of each 1 mL layer, *n*-octanol and phosphate buffer was measured using an auto well gamma counter (n = 4). The log *P* value was calculated by the logarithm of the ratio of radioactivity per milliliter (cpm/mL) in *n*-octanol to that in phosphate buffer and represents mean ± SD.

1.2.6. In vitro stability experiments

The in vitro stability of [^{125}I]**10** was examined in phosphate buffered saline (PBS) and mouse plasma. Briefly, [^{125}I]**10** solution (50 μL) in a sealed tube containing 0.1 M PBS pH 7.4

(450 μL) was incubated at 37 °C for 1 and 24 h. After incubation, the purities of radiotracers were analyzed by RP-HPLC with mobile phase system water (A) and methanol (B), B: 70–100%, 20 min using a Cosmosil® $5C_{18}$ MSII (4.6 ID × 150 mm) column, a flow rate 1 mL/min. The column temperature was kept at 40 °C.

The plasma was prepared by centrifugation of murine blood at 4 °C for 20 min at 100 rpm. The reaction was started by the addition of [^{125}I]**10** (20 μL) in the plasma (180 μL). The mixture was incubated in a shaker at 300 rpm at 37 °C. Samples (100 μL) were taken at 0, 1 and 24 h, and then acetonitrile (100 μL) was added for deproteinization of the plasma. The samples were left in the fridge for 15 min and then centrifuged at 4 °C for 15 min at 150 rpm. The supernatant was filtered through a pore size of 0.45 μm, then analyzed by RP-HPLC with a mobile phase gradient system water (A) and methanol (B), B: 70–100%, for 20 min using a Cosmosil® $5C_{18}$ MSII (4.6 ID × 150 mm) column at a flow rate of 1 mL/min. The column temperature was maintained at 40 °C. Radioactivity was measured by an auto well gamma counter.

1.2.7. Cellular uptake studies

The NSCLC cell lines H1975 (1×10^5 cells/well), H441 (1×10^5 cells/well) and H3255 (2×10^5 cells/well) were grown in medium supplemented with 10% FBS and penicillin (100 IU/mL) streptomycin (100 mg/mL) on 6-well culture plates at 37 °C in a humidified atmosphere with 5% CO_2 for 24 h. Then, the cell culture was incubated in a serum-free medium containing [^{125}I]**10** (3.7 kBq/well) for 4 h. The medium from each well was removed and the cells were washed with 1 mL of ice-cold PBS. Finally, all cell fractions were lysed twice with 0.5 mL of 1 M NaOH aqueous solution. The radioactivity of every fraction was determined by an auto well gamma counter. Total cell protein was determined using the Bicinchoninic Acid (BCA) Protein Assay Kit (Nacalai) protocol, which uses bovine serum albumin as a standard reference. In blocking experiments, inhibitors (CO-1686 and gefitinib with a final

concentration of 100 μM) were combined with radiotracer and assessed using the same method mentioned above. All data were expressed as percent dose per milligram of protein (% dose/mg protein) ± SD.

1.2.8. Animals

Male ddY mice (27–30 g, 6 weeks old) and female BALB/c nu/nu mice (12–17 g, 4 weeks old) were purchased from Japan SLC Inc. (Hamamatsu, Japan). The mice were housed in a cage with free access to food and water maintained at a constant temperature (23–25 °C) with a 12 h light/dark cycle. To prepare tumor-bearing mice, female BALB/c nu/nu mice were implanted subcutaneously, with H1975 (5×10^6 cells/100 μL) and H3255 (1×10^7 cells/100 μL) in the left and right shoulder, respectively. The tumor reached palpable size 2- and 3-weeks post-inoculation. Animal experiments were conducted in accordance with laboratory guidelines for the care and use of animals of Kanazawa University. The animal handling protocol was approved by the Kanazawa University Animal Care Committee (approval number: AP-163766).

1.2.9. Biodistribution studies

Mice were injected intravenously via the lateral tail vein with a saline solution of [^{125}I]**10** (25 kBq, 100 μL) containing 1% tween-80 and 10% ethanol. The ddY mice were sacrificed at 10 min, 1, 4 and 24 h; meanwhile, the tumor-bearing mice were sacrificed at 1 and 4 h post injection. The selected tissues and organs were collected and weighed, and their radioactivity was measured using an auto well gamma counter. In blocking experiments, female BALB/c *nu/nu* mice were intraperitoneally injected with CO-1686 (30 mg/kg) as a blocking agent 1 h prior to intravenous injection of [^{125}I]**10** (25 kBq, 100 μL). The mice were sacrificed 1 h after the administration of radiotracer. The biodistribution data are expressed as percent injected dose per gram of tissue (% ID/g) along with the SD.

1.2.10. Statistical analysis

All data were analyzed using GraphPad Prism 5.0. All values are presented as mean ± SD. Differences between groups were analyzed either by one-way ANOVA followed by a Tukey's multiple-comparison test or Dunnett's multiple-comparison test or two-tailed unpaired Student's *t*-test. The level of statistical significance was set to a $p < 0.05$.

1.3. Results

1.3.1. Synthesis of non-radioactive compound

The non-radioactive iodinated compound **10**, a derivative of CO-1686, was synthesized according to the reported synthetic procedure of CO-1686 starting from 5-iodo-*m*-phenylenediamine instead of *m*-phenylenediamine. 5-iodo-*m*-phenylenediamine was synthesized by 2 steps from commercially available 1,3-dinitroaniline. A stannylated radiolabeling precursor **11** was prepared by palladium catalyzed stannylation reaction of **10** in 10% yield after purification using HPLC.

1.3.2. Cell viability assays

In order to evaluate the cytotoxicity of **10**, CO-1686, and gefitinib toward NSCLC cells, WST-assay was performed. Three types of NSCLC cells with various mutation statuses were cultured in the presence of various concentration (0.01–100 μM) of **10**, CO-1686, or gefitinib. As displayed in **Table 1**, the cytotoxicity of **10** toward H1975 was similar to that of CO-1686 whereas the cytotoxicity of **10** toward H3255 and H441 was weaker than non-iodinated CO-1686.

Table 1. The IC_{50} of **10**, CO-1686 and gefitinib toward NSCLC cell lines by WST-8 assay.

Cell Lines	Mutation Status	IC_{50} (μM)		
		10	CO-1686	Gefitinib
H1975	L858R/T790M	0.20 ± 0.05	0.14 ± 0.05	> 10
H3255	L858R	0.50 ± 0.21	0.15 ± 0.02	0.02 ± 0.02
H441	Wild-type	1.84 ± 0.44	0.26 ± 0.04	> 10

Data represent the mean ± SD of three separate experiments.

*1.3.3. Radiosynthesis of [^{125}I]ICO1686 ([^{125}I]**10**)*

As provided in **Scheme 2,** [^{125}I]**10** was synthesized by an iododestannylation reaction with the corresponding tributyltin precursor **11**. This radiotracer was synthesized using NCS as an oxidizing agent in an acidic solution at 37 °C in high radiochemical yield (77%). Radiochemical purity was over 99% after purification using RP-HPLC. The identity of [^{125}I]**10** was confirmed by comparing the retention times of the radioiodinated compound and nonradioactive **10** in the HPLC analyses. These peaks were shown at the same retention time in the chromatograms (**Figure S12**).

1.3.4. Determination of partition coefficient

The shake-flask method by phase separation resulting in the log *P* value for [^{125}I]**10** was 1.84 ± 0.01.

1.3.5. In vitro stability experiments

The stability profile of [^{125}I]**10** in phosphate-buffered saline (PBS) and murine plasma is shown in the Supporting Information (**Figure S13)**. Until 1 h, [^{125}I]**10** slightly decomposed in either the PBS or plasma and its purity decreased gradually after 24 h incubation.

1.3.6. Cellular uptake studies

The in vitro cell uptake experiments of [^{125}I]**10** was performed using three types of NSCLC cell lines: L858R/T790M active mutant EGFR H1975, L858R active mutant EGFR H3255, and the wild-type EGFR H441. As shown in **Figure 1**, H1975 cells exhibited a high accumulation of [^{125}I]**10,** at 101.5% dose/mg protein at 4 h incubation. The accumulation was significantly higher than that in H3255 and H441 cells at 33.52 and 8.95% dose/mg protein, respectively. The presence of the T790M activating mutation in the EGFR kinase domain accounts for the greater accumulation of [^{125}I]**10** in H1975 cells.

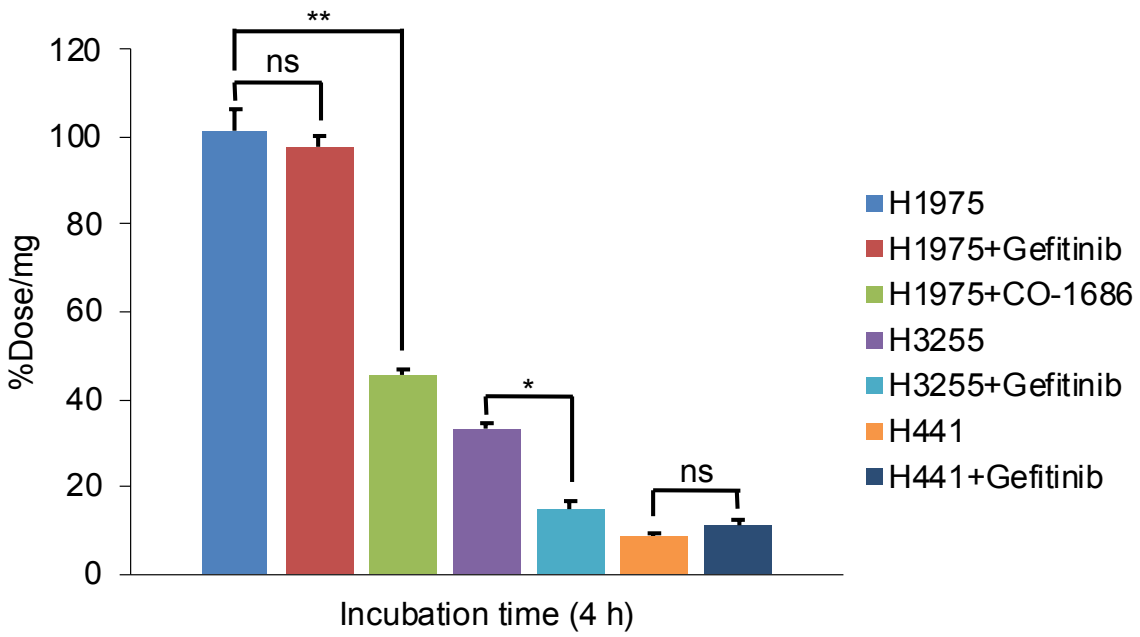

Figure 1. The cell uptake of radiolabeled compound [^{125}I]**10** to the H1975, H3255 and H441 cell lines. Significance was determined using Dunnett's multiple-comparison test or unpaired Student's *t*-test (*p < 0.001; **p < 0.0001) ns: not significant.

1.3.7. Biodistribution studies

In order to determine the in vivo accumulation of [^{125}I]**10** in tissues, a biodistribution experiment was performed. The biodistribution data in normal mice is summarized in **Table 2**. The highest accumulation was observed in the three different organs at different time points. Liver, small intestine, and large intestine exhibited highest uptake at 10 min, 1 h, and 4 h, respectively. At 4 h postinjection, all the organs except large intestine exhibited decrease of the accumulation. The biodistribution data in tumor-bearing mice inoculated with H1975 and H3255 cells is summarized in **Table 3**. The tumor uptake at 1 h postinjection showed low accumulation for both H1975 and H3255 tumor with the ratio of tumor to blood 1 and the value was similar to the ratio in the 4 h postinjection. **Table 3** also shows the tumor accumulation of [^{125}I]**10** at 1 h after treatment with an excess amount of CO-1686. The results indicated that the accumulation of [^{125}I]**10** in the tumor was slightly decreased upon co-injection with a blocking dose.

Table 2. Biodistribution of [^{125}I]**10** at 10 min, 1, 4, and 24 h after i.v. injection in ddY mice.

Tissues	Time after Injection			
	10 min	1 h	4 h	24 h
Blood	1.06 (0.19)	0.49 (0.05)	0.33 (0.07)	0.05 (0.01)
Liver	26.69 (0.81)	18.57 (2.72)	7.85 (0.92)	0.80 (0.10)
Kidney	7.48 (1.55)	3.76 (0.40)	2.37 (0.17)	0.25 (0.01)
Small intestine	9.46 (2.19)	23.96 (2.18)	9.81 (1.03)	0.10 (0.01)
Large intestine	0.57 (0.04)	0.53 (0.08)	53.44 (6.73)	0.34 (0.08)
Spleen	2.14 (0.50)	0.90 (0.17)	0.58 (0.11)	0.08 (0.04)
Pancreas	1.93 (0.37)	0.99 (0.26)	0.41 (0.03)	0.10 (0.11)
Lung	4.47 (1.39)	1.33 (0.08)	0.86 (0.10)	0.26 (0.03)
Heart	3.11 (0.64)	0.79 (0.13)	0.35 (0.09)	0.09 (0.05)
Stomach ‡	3.52 (2.70)	5.10 (1.18)	1.38 (0.56)	0.08 (0.02)
Bone	1.16 (0.21)	0.50 (0.22)	0.29 (0.11)	0.07 (0.05)
Muscle	1.40 (0.16)	0.44 (0.05)	0.13 (0.03)	0.04 (0.04)
Brain	0.11 (0.02)	0.05 (0.02)	0.03 (0.01)	0.01 (0.01)
Urine	–	–	–	4.07 (0.83)
Feces	–	–	–	69.93 (15.71)

Data were presented as % ID/g tissue. Each value represents mean ± SD for four mice.
‡Presented as % ID/organ.

Table 3. Biodistribution of [^{125}I]**10** at 1 and 4 h after i.v. injection in tumor-bearing mice.

Tissues	Time after Injection		
	1 h	4 h	Blocking (1 h)
Blood	1.74 (0.18)	0.77 (0.07)	1.79 (0.21)
Liver	28.12 (5.43)	12.40 (1.06)	21.77 (2.83)
Kidney	5.26 (1.50)	1.62 (0.26)	4.19 (1.28)
Small intestine	85.58 (7.68)	9.82 (3.17)	60.68 (6.67)
Large intestine	18.65 (19.88)	144.21 (10.97)	8.96 (7.48)
Spleen	3.20 (0.62)	0.71 (0.19)	2.81 (0.77)
Pancreas	1.99 (0.52)	0.49 (0.12)	3.87 (0.87)
Lung	4.67 (0.85)	1.02 (0.28)	3.40 (0.93)
Heart	1.46 (0.31)	0.60 (0.67)	1.53 (0.58)
Stomach ‡	1.04 (0.36)	0.48 (0.19)	1.44 (0.57)
Bone	0.50 (0.40)	0.24 (0.20)	1.07 (0.36)
Muscle	0.86 (0.21)	0.27 (0.08)	1.09 (0.42)
Brain	0.11 (0.08)	0.04 (0.02)	0.10 (0.02)
H1975	1.77 (0.43)	0.43 (0.08)	1.65 (0.64)
H3255	1.63 (0.23)	0.70 (0.13)	1.47 (0.71)

Data were presented as % ID/g tissue. Each value represents mean ± SD for four mice.
‡ Presented as % ID/organ.

1.4. Discussion

Overexpression of EGFR or mutation in the tyrosine kinase domain were highly associated with lung cancer, particularly NSCLC [6]. EGFR mutations have been treated with various specific inhibitors depending on its type. During treatment using EGFR TKIs, mutations develop and cause resistance to TKIs. T790M is the most common EGFR TKI residence mutation after getting treatment with first generation EGFR TKIs. Therefore, monitoring the mutational malignancies is necessary to improve the therapeutic effect.

Biopsy for monitoring the development of mutations through gene sequencing is providing new perspectives to the field of diagnostic. However, the analysis of biopsy specimens does not necessarily reflect complete tumor mutation status because tumor tissues are heterogenous and the tiny fraction of them in a biopsy may not be representative of the whole tumor profile [19]. Additionally, repeated biopsies are invasive and a significant burden on patients [20]. SPECT imaging modality plays an important role in precision medicine. This technique is noninvasive, and quantitative information of biological processes *in vivo* with high sensitivity. It assesses not only the current status of mutation and stratification of cancer but also optimizes the therapy by monitoring the efficacy of the treatment [21].

Here, I designed and synthesized a novel radiotracer *N*-(3-{[2-({4-[4-acetylpiperazin-1-yl]-2-methoxyphenyl}amino)-5-(trifluoromethyl)pyrimidin-4-yl]amino}-5-([^{125}I]iodophenyl) acrylamide ([^{125}I]ICO1686, **Scheme 2**, [^{125}I]**10**). The synthesis of the tracer was achieved via a one-step radioiodination using NCS as an oxidizing agent with excellent radiochemical yield (77%) and high radiochemical purity (>99%). While **10** was based on CO-1686, the cell viability assay by WST-8 protocol showed that the IC_{50} of **10** (0.20 ± 0.05 μM) was comparable to that of CO-1686 (0.14 ± 0.05 μM) toward H1975 cells (**Table 1**). This data demonstrated that the iodine substituent on **10** did not significantly affect activity toward H1975 cells. Besides, the introduction of iodine reduced the cytotoxicity of **10** toward H441 cells; however, this was unimportant because CO-1686 is indeed less potent against wild-type than L858R/T790M mutations [11, 22]. Hence, [^{125}I]**10** would be promising imaging probe to determine L858R/T790M EGFR mutations in preclinical study.

The cellular uptake experiment showed that [^{125}I]**10** uptake was significantly higher in H1975 (101.52% dose/mg protein) than H3255 (33.52% dose/mg protein) or H441 (8.95% dose/mg protein), revealing that the probe selectivity binds to the EGFR with T790M mutation. The methoxyl group contributes to the selectivity of CO-1686 for EGFR. In addition, the

trifluoromethyl substituent of CO-1686 is conducive to forming hydrophobic interactions with Met790 as the mutant gatekeeper residue. This hydrophobicity is only accorded by Met790 which is not accorded by wild-type gatekeeper residue (Thr790). This explains why [^{125}I]**10** prefers to accumulate in H1975 expressing EGFR L858R/T790M mutations [10]. Furthermore, with its high specificity, [^{125}I]**10** has suitable characteristics for observing the EGFR mutation status during therapy by EGFR-TKIs in vitro.

In the blocking studies, the uptakes of [^{125}I]**10** in H1975 were significantly reduced to 45.61% dose/mg protein by pretreatment with an excess of CO-1686, indicating that [^{125}I]**10** bound competitively, versus CO-1686, to EGFR-TK with L858R/T790M double mutations. However, the degree of the blocking effects was lower than I expected. It means that the nonspecific binding of [^{125}I]**10** on or inside H1975 cells may be not low. Although H1975 cells harbor the L858R EGFR mutation, gefitinib did not reduce the accumulation of [^{125}I]**10** in in vitro blocking experiments. This was due to the T790M mutation, which interferes with the binding of gefitinib to the tyrosine kinase domain of EGFR, thereby conferring resistance to gefitinib [22]. In contrast, the radiotracer accumulation of [^{125}I]**10** in H3255 was dramatically reduced (over 50%) by pretreatment with a dose of gefitinib, which is attributable to the high affinity for gefitinib of H3255 cells carrying the L858R mutation [23, 24].

The biodistribution data in normal mice are summarized in **Table 2**. The high radioactivity rapidly accumulated in liver after the injection of [^{125}I]**10**. This was considered to have been caused by the relatively hydrophobic structure of [^{125}I]**10** (Log *P* 1.84 ± 0.01). Liver activity decreased gradually and [^{125}I]**10** was transferred to the small intestine via bile excretion [25] and then to large intestine as time passed; as a result, the large intestine exhibited high uptake of the radiotracer (53.44 ± 6.73% ID/g) at 4 h post injection. Finally, almost 70% of the radiotracer was excreted in feces 24 h after injection. Namely, [^{125}I]**10** was mainly eliminated through hepatobiliary clearance. Meanwhile, Ballard *et al*. reported a PET image of [^{11}C]CO-

1686 in a monkey. In the PET image using average data from 0 to 123 min, [^{11}C]CO-1686 showed high accumulation in the intestine and moderate accumulation in the liver. Moreover, [^{11}C]CO-1686 hardly accumulated in the brain [26]. These results seem to be similar to the biodistribution pattern of [^{125}I]**10**.

Table 3 summarizes the biodistribution data in tumor-bearing mice inoculated with H1975 and H3255 cells. The accumulation of [^{125}I]**10** in H1975 tumors (1.77 ± 0.43% ID/g) was comparable to that in H3255 tumors (1.63 ± 0.23% ID/g). These data indicate that the in vivo uptake in mouse xenografts did not correlate with the in vitro uptake of [^{125}I]**10** toward EGFR double mutations. Moreover, accumulation in H1975 tumors was not inhibited by pretreatment with an excess dose of CO-1686. Zhang *et al*. reported that gefitinib did not sufficiently block the uptake of [^{11}C]gefitinib [27]. In this case, it may have been due to high nonspecific binding in tumor regions.

As above-mentioned, the purpose of my study is the development of probes for SPECT imaging using ^{123}I. However, it must be difficult to visualize the tumor for [^{123}]**10,** even if the imaging would be performed using tumor-bearing mice because tumor/blood ratio was approximately 1. Moreover, tumor/lung ratio is also important for imaging of NSCLC patients in clinical. Therefore, an increase of tumor uptake and/or decrease of non-target tissue uptake to be background, such as lung and blood, are necessary.

Lack of specific tumor uptake of [^{125}I]**10** was likely not caused by metabolic instability in blood, as I found that [^{125}I]**10** hardly decomposed in the plasma until 1 h in the in vitro stability experiment. The high level of nonspecific uptake in normal tissues and the high hepatobiliary excretion are the possible reasons why tumor uptake was suboptimal [27]. The high lipophilicity was related to the hepatobiliary excretion of [^{125}I]**10**, resulting in very high elimination of radiotracer, which might have influenced the intratumoral uptake of [^{125}I]**10** [28]. Improving water solubility may be necessary to improve the accumulation of [^{125}I]**10** in

tumors. Structural modification by a short-chain polyethylene glycol in the linker phenyl group may be an alternative for reducing nonspecific accumulation without a significant reduction of the affinity for EGFR L858R/T790M [10, 15].

1.5. Conclusions

In this study, I successfully synthesized ^{125}I labeled CO1686 in high radiochemical yield and radiochemical purity. In vitro evaluation in the mutant EGFR NSCLC demonstrated that [^{125}I]**10** has high specificity to EGFR L858R/T790M mutation. The in vivo study showed inadequate tumor uptake, resulting in a low tumor-to-blood ratio. To optimize the intra-tumoral uptake, reducing the lipophilicity by replacement of radioiodine with radiobromine [^{77}Br] would be possible approach.

Chapter 2

Radiobrominated probe [^{77}Br]BrCO1686 for imaging lung cancer with L858R/T790M mutations of EGFR

Abstract

Radiobrominated rociletinib (CO-1686) could be an imaging agent for monitoring tumors activating L858R/T790M mutation by positron emission tomography (PET). Therefore, I reported the synthesis of a ^{77}Br-labeled derivative of CO-1686 and its evaluation as epidermal growth factor receptor (EGFR) imaging probes. The non-radioactive compound bromo-CO-1686 (BrCO1686) was synthesized by condensation of *N*-(3-{[2-chloro-5-(trifluoromethyl)pyrimidin-4-yl]amino}-5-bromophenyl) acrylamide with the corresponding substituted 1-(4-{4-amino-3-methoxyphenyl}piperazine-1-yl)ethan-1-one. [^{77}Br]BrCO1686 was prepared through stannylation of the corresponding tributylstannyl precursor with [^{77}Br] in moderate radiochemical yield 45% and high radiochemical purity over 99%. Nonradioactive BrCO1686 showed a high affinity toward H1975 with IC_{50} 0.18 ± 0.06 μM. In vitro uptake study of double tracers, [^{77}Br]BrCO1686 and [^{125}I]ICO1686, showed that accumulation of the both radiotracers in H1975 (L858R/T790M active mutant EGFR) on 4 h incubation was significantly higher than that of H3255 (L858R active mutant EGFR) and H441 (wild-type EGFR). The radioactivity accumulation of [^{77}Br]BrCO1686 (136.3%dose/mg protein) and [^{125}I]ICO1686 (151.3%dose/mg protein) were significantly reduced to 56.9 and 67.7 %dose/mg protein, respectively, by the pretreatment of an excess CO-1686 as blocking agent. Although the radioactivity accumulation of [^{77}Br]BrCO1686 and [^{125}I]ICO1686 in H1975 tumor (4.51 ± 0.17 and 0.68 ± 0.11% ID/g, respectively) was higher than that of H441 tumor (3.71 ± 0.13 and 0.44 ± 0.06% ID/g, respectively) on 1 h post-injection, the tumor-to-blood ratio needs to be increased to provide a clear contrast.

2.1. Introduction

PET modality offers higher spatial resolution over conventional SPECT and also allows quantification of radioactivity with high accuracy. The radionuclides such as ^{11}C ($t_{1/2}$ = 20 min), ^{13}N ($t_{1/2}$ = 10 min), and ^{15}O ($t_{1/2}$ = 2 min) are isotopes of natural elements that are part of most biochemicals and drugs. Developing PET imaging probes by these isotopes could minimize the alteration biological properties and pharmacokinetics of the biomolecule. However, the short half-lives of these three PET radionuclides are not ideal for developing commercial PET radiopharmaceuticals for routine clinical use [29].

The halogens radioisotopes such as ^{18}F, ^{76}Br, and ^{124}I are available for developing radiopharmaceuticals for PET. Although ^{124}I has been an interesting radionuclide for clinical and experimental PET due to its half-life ($t_{1/2}$ = 4.2 day), the decay properties are not ideal since the positron abundance is only 24% [29]. In the halogen elements, ^{76}Br is potentially useful positron emitter. ^{76}Br has a fairly high abundance (56%) compared to ^{124}I (24%). The half-life of 16.2 h also makes ^{76}Br one of the most attractive radionuclides for PET imaging [30]. The long half-life of ^{76}Br makes it possible to deliver the radiopharmaceuticals to distant places and to take delayed PET imaging, such as at 1-day postinjection, which is impossible for ^{18}F-labeled probes [31]. In this study, I aimed to provide a novel radiobromine-labeled CO-1686 for monitoring tumors activating L858R/T790M mutations by PET.

Here, I describe synthesis and pharmacological evaluation of a non-radioactive brominated *N*-(3-{[2-({4-[4-acetylpiperazin-1-yl]-2-methoxyphenyl}amino)-5-(trifluoromethyl) pyrimidin-4-yl]amino}-5-bromophenyl)acrylamide (BrCO1686, **Scheme 3**, **17**) and a novel radiotracer *N*-(3-{[2-({4-[4-acetylpiperazin-1-yl]-2-methoxyphenyl}amino)-5-(trifluoromethyl)pyrimidin-4-yl]amino}-5-[^{77}Br]bromophenyl)acrylamide ([^{77}Br]BrCO1686, **Scheme 4,** [^{77}Br]**17**) for PET imaging the EGFR T790M ATP binding site. Although I am interested in developing ^{76}Br-labeled probes for PET, in these initial studies,

^{77}Br was used because of its longer half-life ($t_{1/2}$ = 57.0 h).

2.2. Experimental Section

2.2.1. Materials

The chemical and instrumental analysis used as mentioned in Chapter 1. The radionuclide ^{77}Br was produced in University of Fukui [32] and was delivered to Kanazawa University.

2.2.2. Synthesis of non-radioactive compound

Design and synthesis procedures were shown in **Schemes 3** and **4**. Intermediate compounds were synthesized according to the previous studies, with a slight modification [16, 17, 28, 33]. NMR spectra are provided in the Supporting Information (**Figures S14-S19**).

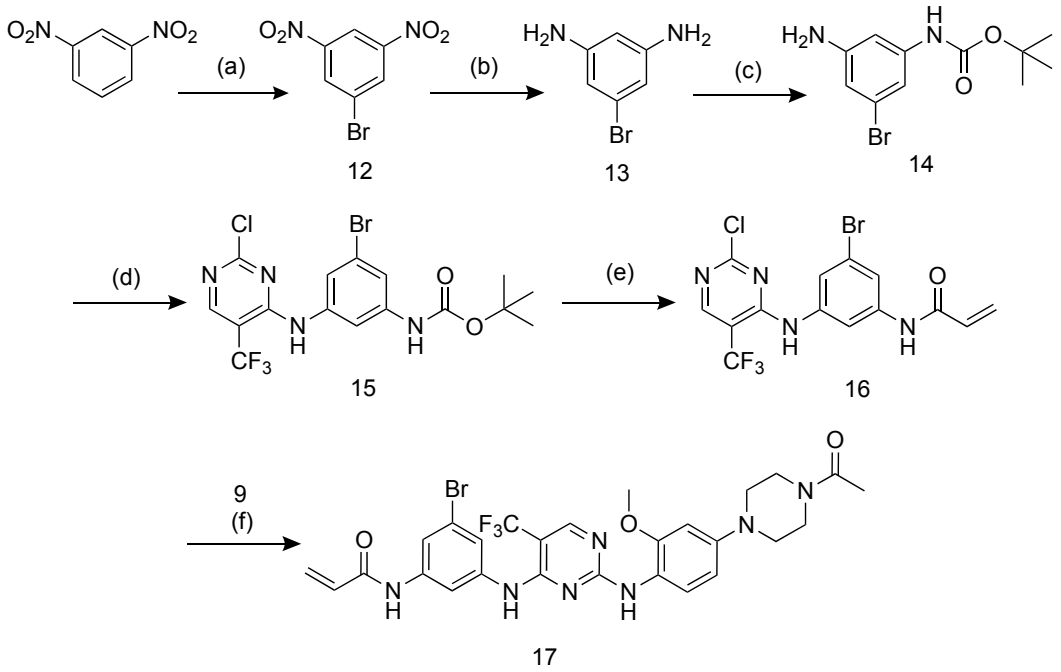

Scheme 3. Synthesis of non-radioactive brominated compound. (a) H_2SO_4, NBS, 80 °C; (b) $SnCl_2.2H_2O$, rt; (c) Boc_2O, 50 °C; (d) 2,4-Dichloro-5(trifluoromethyl) pyrimidine, DIPEA, 0 °C, rt; (e) Acryloyl chloride, DIPEA, -30 °C, rt; (f) TFA, 60 °C.

*Synthesis of 1-bromo-3,5-dinitrobenzene (**12**)*

To a stirred mixture of 1,3-dinitrobenzene ($C_6H_4N_2O_4$) (5.0 g, 29.74 mmol, 1.0 eq.) and H_2SO_4 (30 mL) at 80 °C, *N*-bromosuccinimide (NBS) (7.41 g, 41.63 mmol, 1.4 eq.) was added to the reaction mixture in nine portions over 1.5 h (one addition every10 min). The temperature

of the mixture was kept at 80-90 °C during the addition. After the reaction was completed (30 min), the reaction mixture was quenched with water and extracted with ethyl acetate. The organic layer then dried with sodium sulfate, filtered, and concentrated under reduced pressure to afford **12** (7.0 g, 70%) as a pale-yellow solid. ^{1}H NMR (400 MHz, $CDCl_3$): δ 8.72 (2H, d, *J* = 1.6 Hz), 9.01 (1H, t, *J* = 1.6 Hz). ^{13}C NMR (100 MHz, $CDCl_3$): δ 117.7, 123.8, 132.2, 149.1. HRMS (FAB+) calculated for $C_6H_3BrN_2O_4$ $[M+H]^+$: *m/z* = 245.9298, found 245.9276.

*Synthesis of 5-bromobenzene-1,3-diamine (**13**)*

To a stirred mixture of **12** (7.0 g, 28.34 mmol, 1.0 eq.) and ethanol (150 mL), $SnCl_2 \cdot 2H_2O$ (51.16 g, 226.72 mmol, 8 eq.) was added at room temperature and the mixture was stirred for 3 h under nitrogen atmosphere. After the reaction was completed, the pH was adjusted to neutral using saturated aqueous $NaHCO_3$, the reaction mixture was extracted with ethyl acetate. The organic layer then dried with sodium sulfate, filtered, and concentrated under reduced pressure to afford **13** (5.26 g, 99%) as a pale-yellow solid. ^{1}H NMR (400 MHz, $CDCl_3$): δ 3.60 (4H, br s), 5.91 (1H, s), 6.25 (2H, d, *J* = 2.0 Hz). ^{13}C NMR (100 MHz, $CDCl_3$): δ 100.1, 108.8, 123.7, 148.5. HRMS (FAB+) calculated for $C_6H_7BrN_2$ $[M+H]^+$: *m/z* = 185.9777, found 185.9793.

*Synthesis of tert-butyl (3-amino-5-bromophenyl)carbamate (**14**)*

To a stirred mixture of **13** (5.26 g, 28.13 mmol, 1.0 eq.) and acetonitrile (50 mL), Boc_2O (6.14 g, 28.13 mmol, 1 eq.) was added at 50 °C and the mixture was stirred for overnight under nitrogen atmosphere. After the reaction was completed, the product was purified by column chromatography on silica gel (hexane/ethyl acetate = 7/3) and concentrated under reduced pressure to afford **14** (4.45 g, 55%) as a crystal orange. ^{1}H NMR (400 MHz, $CDCl_3$): δ 1.51 (9H, s), 3.73 (2H, s), 6.42 (1H, s), 6.50 (1H, s), 6.79 (2H, s). ^{13}C NMR (100 MHz, $CDCl_3$): δ 28.2, 80.8, 103.3, 111.3, 112.6, 123.1, 140.5, 148.3, 152.5. HRMS (FAB+) calculated for

$C_{11}H_{15}BrN_2O_2$ [M+ H]$^+$: *m/z* = 286.0300, found 286.0317.

*Synthesis of tert-butyl (3-{[2-chloro-5-(trifluoromethyl)pyrimidin-4-yl]amino}-5-bromophenyl)carbamate (**15**)*

To a stirred mixture of **14** (4.45 g, 15.50 mmol, 1.0 eq.) and *n*-butanol (31 mL), 2,4-dichloro-5(trifluoromethyl) pyrimidine (2 mL, 1 eq.), DIPEA (5 mL, 2 eq.) were added at 0 °C and stirred for 2 h. The stirring was continued at room temperature for 4 h. The stirring was continued at room temperature for 4 h. After the reaction was completed, the crude product was purified using column chromatography on silica gel (hexane/ethyl acetate = 7/3) and concentrated under reduced pressure to afford **15** (4.1 g, 85%) as pale-yellow solid. ^{1}H NMR (400 MHz, $CDCl_3$): δ 1.54 (9H, s), 6.59 (1H, s), 7.00 (1H, s), 7.39 (1H, s), 7.48 (1H, s), 7.66 (1H, s), 8.46 (1H, s). ^{13}C NMR (100 MHz, $CDCl_3$): δ 28.2, 81.7, 106.8 (q, J_{CF} = 30.5 Hz), 110.6, 118.6, 119.6, 122.8, 123.4 (q, J_{CF} = 271.8 Hz), 137.8, 140.2, 152.3, 156.1 (q, J_{CF} = 4.8 Hz), 157.1, 163.6. HRMS (FAB+) calculated for $C_{16}H_{15}BrClF_3N_4O_2$ [M+ H]$^+$: *m/z* = 465.9854, found 465.9842.

*Synthesis of N-(3-{[2-chloro-5-(trifluoromethyl)pyrimidin-4-yl]amino}-5-bromophenyl) acrylamide (**16**)*

The mixture of compound **15** (4.1 g, 8.77 mmol, 1.0 eq.) and 4.0 M HCl/ethyl acetate (1.0 mL) was stirred at room temperature for 1 h. The reaction was monitored by TLC (hexane/ethyl acetate = 7/3), after the reaction was completed, the solvent was removed by nitrogen gassing, and the residue was dried under reduced pressure to afford a colorless solid (4 g). The crude material was used to the next step without further purification. To a stirred mixture of the crude material (3 g), DIPEA (4.3 mL, 24.48 mmol, 3 eq.) and dichloromethane (81 mL), acryloyl chloride (1 mL, 12.24 mmol, 1.5 eq.) was added at -30 °C and stirred at room temperature for 2 h. The crude product was dissolved in ethyl acetate then washed with 1 M

HCl, the organic layer then neutralized using saturated aqueous $NaHCO_3$ and washed with brine. The crude product was purified using column chromatography on silica gel (dichloromethane/methanol = 200/1), crystalized by chloroform/hexane and concentrated under reduced pressure to afford **16** (200 mg, 10%) as a white solid. ^{1}H NMR (400 MHz, $CDCl_3$): δ 5.84 (2H, d, J = 7.2 Hz), 6.24 (1H, dd, J = 11.2, 6.8 Hz), 6.47 (1H, d, J = 11.2 Hz), 7.43 (1H, s), 7.50 (1H, s), 7.66 (1H, s), 7.98 (1H, s), 8.63 (1H, s). ^{13}C NMR (100 MHz, $(CD_3)_2SO$): δ 101.3 (q, J_{CF} = 70.5 Hz), 109.8, 116.2, 117.6, 121.6, 123.9 (q, J_{CF} = 270.8 Hz), 127.8, 131.8, 140.8, 141.5, 157.0 (q, J_{CF} = 4.8 Hz), 161.3, 163.7, 166.2. HRMS (FAB+) calculated for $C_{14}H_9BrClF_3N_4O$ $[M+H]^+$: m/z = 419.9702, found 419.9600.

*Synthesis of N-(3-{[2-({4-[4-acetylpiperazin-1-yl]-2-methoxyphenyl}amino)-5-(trifluoromethyl)pyrimidin-4-yl]amino}-5-bromophenyl)acrylamide (**17**)*

To a stirred mixture of compound **16** (120 mg, 0.28 mmol, 1.0 eq.) and TFA in dioxane (0.6 mL, 2 M), compound **9** was added (70 mg, 0.28 mmol, 1 eq.), the mixture was stirred at 60 °C for 3 h. After the reaction was completed, the pH was adjusted to neutral using saturated aqueous $NaHCO_3$, the reaction mixture was extracted with ethyl acetate. The crude product was purified using HPLC (ethyl acetate/methanol = 97/3) and concentrated under reduced pressure to afford **17** (80 mg, 45%) as a white solid. ^{1}H NMR (400 MHz, $CDCl_3$): δ 2.16 (3H, s), 3.12–3.20 (4H, m), 3.64 (2H, t, J = 4.4 Hz), 3.79 (2H, t, J = 4.8 Hz), 3.91 (3H, s), 5.80 (1H, d, J = 10.8 Hz), 6.21 (1H, dd, J = 15.2, 10.4 Hz), 6.44 (1H, d, J = 15.6 Hz), 6.54–6.60 (2H, m), 7.11 (1H, s), 7.25 (1H, s), 7.43 (1H, s), 7.56 (1H, s), 7.66 (1H, s), 7.74 (1H, s), 8.07 (1H, d, J = 8.8 Hz), 8.30 (1H, s). ^{13}C NMR (100 MHz, $(CD_3)_2SO$): δ 16.9, 41.2, 47.3, 51.0, 51.5, 60.2, 113.0 (q, J_{CF} = 40.5 Hz), 116.2, 124.5, 127.4, 135.3, 136.9, 138.9, 142.1, 146.4 (q, J_{CF} = 334.9 Hz), 147.1, 149.6, 154.8, 165.5, 167.1, 177.1, 180.9, 184.2 (q, J_{CF} = 6.0 Hz), 186.8, 191.2, 194.4, 200.7. HRMS (FAB+) calculated for $C_{27}H_{27}BrF_3N_7O_3$ $[M+H]^+$: m/z = 633.1324, found 633.1311.

2.2.3. Cell viability assays

The cell viability assays of [^{77}Br]**17** were performed as **Chapter 1** mentioned.

*2.2.4. Radiosynthesis of [^{77}Br]BrCO1686 ([^{77}Br]**17**)*

Radiotracers, [^{77}Br]**17** was synthesized by a bromodestannylation reaction of the corresponding tributylstannyl precursors (**Scheme 4**). A solution of [^{77}Br]Br (2.5 MBq, 1 μL) was charged into a sealed vial containing **11** (1 mg/mL, 10 μL) in ethanol, acetic acid (5%, 30 μL), and NCS (20 mg/mL, 10 μL). The mixture was vortexed 5 min and shaken 60 min at 80 °C. The product was quenched by addition of aqueous sodium hydrogensulfite (5 mg/mL, 10 μL) and was analyzed by RP-HPLC with mobile phase system water (A) and methanol (B), B: 60-100%, 20 min using a Cosmosil 5C_{18} MSII (4.6ID × 150 mm) column, a flow rate 1 mL/min. The column temperature was maintained at 40 °C. The identity of [^{77}Br]**17** was confirmed by comparing its retention time with that of the corresponding nonradioactive **17** in the HPLC analyses.

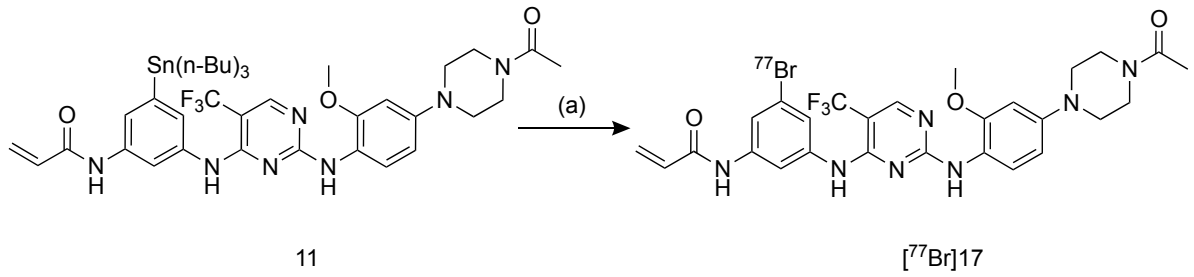

Scheme 4. Synthesis of radiobrominated compound [^{77}Br]**17**. (a) [^{77}Br]Br, acetic acid, ethanol, NCS, 80 °C, 60 min.

2.2.5. Determination of partition coefficient

The partition coefficient determination of [^{77}Br]**17** was performed as **Chapter 1** mentioned.

2.2.6. In vitro stability experiments

The stability assays of [^{77}Br]**17** were performed as **Chapter 1** mentioned.

2.2.7. Cellular uptake studies

The cells were prepared as **Chapter 1** mentioned. The cell culture then incubated in FBS-free medium containing double tracers [^{77}Br]**17** and [^{125}I]**10** (3.7 kBq/well, respectively) for 4 h. A window from 16 to 71 keV was used for counting ^{125}I and a window from 100 to 600 keV was used for counting for ^{77}Br. When the radioactivity of ^{77}Br was measured, the crossover of ^{125}I activity into the ^{77}Br channel was negligible. More than one month after the experiments, ^{125}I activity was determined because the radioactivity of ^{77}Br was negligible at that time. The protein concentration was measured as **Chapter 1** mentioned.

2.2.8. Animals

The animal experiments were conducted as **Chapter 1** mentioned with slight modification. H1975 cells (5×10^6 cells) were implanted in the right shoulder, and H441 cells (3×10^6 cells) were implanted in the left shoulder. The tumor reached palpable size after post-inoculation 12 and 9 days for H1975 and H441, respectively.

2.2.9. Biodistribution studies

The biodistribution studies were conducted as **Chapter 1** mentioned with slight modification. [^{77}Br]**17** (10 kBq) and [^{125}I]**10** (25 kBq) in 100 μL of saline solution containing 1% tween-80 and 10% ethanol were co-injected into the mice. The radioactivity of ^{77}Br was measured at the time of experiment. One month later, ^{125}I activity was determined. The biodistribution data are expressed as percent injected dose per gram tissue (%ID/g) along with the SD. The same procedure was applied to perform biodistribution of [^{77}Br]Br (111 kBq).

2.2.10. Statistical analysis

The statistical analysis was conducted as **Chapter 1** mentioned

2.3. Results

2.3.1. Synthesis of non-radioactive compound

The derivative of CO-1686, brominated compounds **17**, was synthesized multi steps starting from commercially available 1,3-dinitrobenzene. Bromine atom was introduced in the diaminophenyl group of CO-1686 using NBS. The bromine was attached in this substituent because this would not so influence the affinity of CO-1686 toward EGFR L858R/T790M according the complex crystal structure of CO-1686 and T790M EGFR. The most important substituents and play a pivotal role for the binding of CO-1686 to EGFR L858R/T790M are the anilinopyrimidine core, methoxy, and trifluoromethyl groups [15].

2.3.2. Cell viability assays

The cytotoxicity effect of **17** toward H1975 and H3255 looks similar with CO-1686 as we can see in the **Table 4**. This can explain that the bromine substituent on **17** did not significantly influence the activity toward mutated EGFR both active mutant L858R EGFR and double mutation L858R/T790M EGFR. In opposite, the cytotoxicity of **17** toward H441 was significantly lower than non-brominated CO-1686.

Table 4. The IC_{50} of **17**, **10**, CO-1686, and gefitinib toward NSCLC cell lines by WST-8 assay.

Cell lines	Mutation status	IC_{50} (μM)			
		17	**10**	CO-1686	Gefitinib
H1975	L858R/T790M	0.18 ± 0.06	0.20 ± 0.05	0.14 ± 0.05	> 10
H3255	L858R	0.20 ± 0.01	0.50 ± 0.21	0.15 ± 0.02	0.02 ± 0.02
H441	Wild type	0.64 ± 0.04	1.84 ± 0.44	0.26 ± 0.04	> 10

Data represent the mean ± SD of three separate experiments.

*2.3.3. Radiosynthesis of [^{77}Br]BrCO1686 ([^{77}Br]**17**)*

The [^{77}Br]**17** was synthesized by a bromodestannylation reaction with the corresponding tributyltin precursor **11**, as provided in **Scheme 4**. This radiotracer was synthesized using NCS as an oxidizing agent in an acidic solution at 80°C in moderate radiochemical yield (45%). After purification using RP-HPLC, the radiochemical purity was over 99%. The identity of [^{77}Br]**17** was confirmed by comparing the retention times of the nonradioactive **17** in the HPLC

analyses. These peaks were shown at the same retention time in the chromatograms (**Figure S20**).

2.3.4. Determination of partition coefficient

The log *P* value for [^{77}Br]**17** was 1.72 ± 0.21 revealed an appropriate lipophilic property to penetrate the cell membrane passively.

2.3.5. In vitro stability experiments

The stability profile of [^{77}Br]**17** in PBS and murine plasma is presented in Supporting Information (**Figure S21)**. [^{77}Br]**17** was stable in the PBS and murine plasma at 37°C, with >80% of intact parent compound after 1 h incubation. Its purity decreased gradually after 24 h incubation.

2.3.6. Cellular uptake studies

Measurement of double tracers [^{77}Br]**17** and [^{125}I]**10** in vitro uptake preference in three types of NSCLC cell lines confirmed that both radiotracers accumulation in H1975 (L858R/T790M active mutant EGFR) on 4 h incubation was significantly higher than that of H3255 (L858R active mutant EGFR) and H441 (wild-type EGFR) (**Figure 2**). In the in vitro blocking experiment toward H1975 cells, the radioactivity accumulation of [^{77}Br]**17** (136.3%dose/mg protein) and [^{125}I]**10** (151.3%dose/mg protein) was significantly reduced to 56.9 and 67.7 %dose/mg protein, respectively, by the pretreatment of an excess CO-1686. Meanwhile, the pretreatment of an excess gefitinib toward H1975 was meaningless but significantly reduce the accumulation of both radiotracers toward H3255 cells.

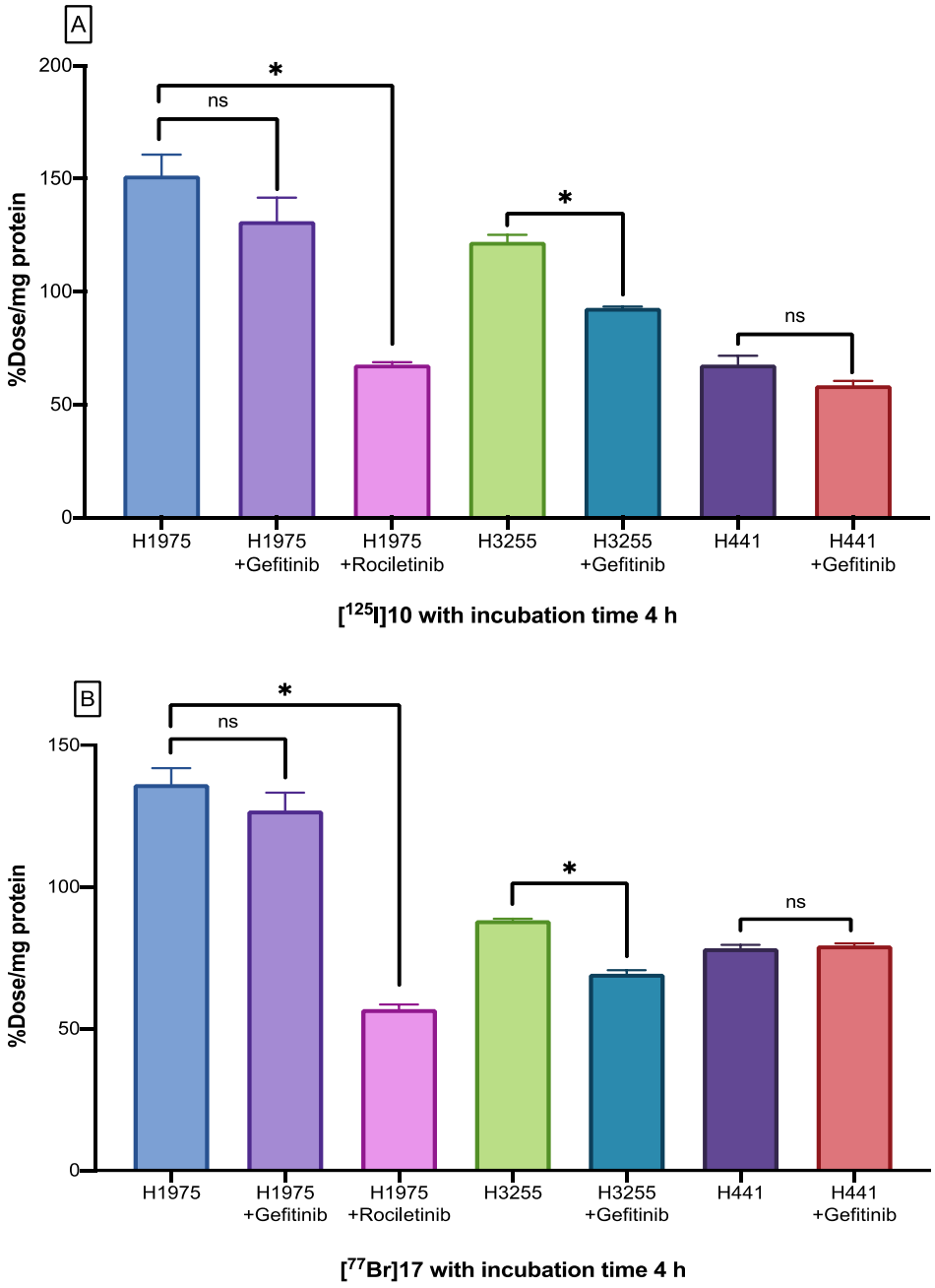

Figure 2. The cell uptake of (A) [^{125}I]**10** and (B) [^{77}Br]**17** to the H1975, H3255, and H441 cell lines at 4 h incubation. Significance was determined using Dunnet's multiple-comparison test or unpaired Student's *t*-test (*$P < 0.05$) ns: not significant.

2.3.7. Biodistribution studies

Biodistributions of [^{77}Br]**17** and [^{125}I]**10** in normal mice and tumor-bearing mice are summarized in **Table 5** and **Table 6**, respectively. Activity distribution patterns were similar between [^{77}Br]**17** and [^{125}I]**10**, with the highest uptake in the intestine and liver. Meanwhile, the accumulation of [^{77}Br]**17** in almost all tissues containing H1975 and H441 tumors at 1 h

and 4 h post injection was higher than that of [^{125}I]**10**. Biodistribution of [^{77}Br]Br in normal mice is summarized in **Table 7**.

Table 5. Biodistribution of [^{77}Br]**17** and [^{125}I]**10** at 10 min, 1, 4, and 24 h after i.v. injection in ddY mice.

Tissues	Time after injection			
	10 min	1 h	4 h	24 h
[^{77}Br]**17**				
Blood	3.57 (0.21)	3.24 (0.30)	3.19 (0.18)	1.99 (0.28)
Liver	11.04 (0.55)	3.83 (0.38)	3.72 (0.30)	1.04 (0.21)
Kidney	11.68 (0.94)	4.21 (0.67)	2.81 (1.17)	1.33 (0.25)
Small intestine	25.38 (5.45)	26.49 (2.77)	5.23 (1.06)	1.00 (0.15)
Large intestine	2.83 (0.57)	3.18 (0.19)	47.73 (7.88)	0.98 (0.11)
Spleen	5.11 (3.46)	4.83 (1.82)	2.92 (2.02	1.14 (0.46)
Pancreas	3.78 (2.53)	3.58 (0.10)	3.04 (0.28)	1.13 (0.09)
Lung	8.72 (1.25)	4.97 (1.97)	5.08 (0.28)	1.62 (0.22)
Heart	4.57 (0.89)	2.93 (0.24)	1.87 (1.25)	0.80 (0.21)
Stomach‡	6.17 (1.45)	7.00 (0.58)	6.68 (1.02)	2.21 (0.33)
Bone	2.76 (0.83)	1.66 (1.18)	1.54 (0.62)	0.89 (0.93)
Muscle	3.18 (0.55)	2.02 (0.55)	1.13 (0.78)	0.47 (0.20)
Brain	0.45 (0.30)	0.95 (0.14)	0.74 (0.50)	0.42 (0.09)
Urine	–	–	–	13.48 (1.28)
Feces	–	–	–	35.01 (6.85)
[^{125}I]**10**				
Blood	1.41 (0.38)	0.17 (0.02)	0.06 (0.01)	0.13 (0.06)
Liver	19.21 (2.04)	7.40 (1.01)	6.45 (1.21)	1.40 (0.17)
Kidney	9.66 (1.19)	2.40 (0.56)	0.75 (0.18)	0.54 (0.10)
Small intestine	36.32 (12.00)	40.99 (4.13)	6.08 (1.99)	0.30 (0.11)
Large intestine	0.94 (0.18)	1.65 (0.34)	81.54 (10.19)	0.52 (0.55)
Spleen	2.73 (0.56)	0.55 (0.09)	0.20 (0.07)	0.13 (0.04)
Pancreas	2.03 (0.20)	0.86 (0.15)	0.12 (0.04)	0.05 (0.01)
Lung	3.61 (0.40)	0.59 (0.25)	0.16 (0.03)	0.14 (0.02)
Heart	2.24 (0.49)	0.30 (0.08)	0.08 (0.04)	0.20 (0.25)
Stomach‡	2.60 (1.23)	1.64 (0.71)	0.76 (0.61)	0.05 (0.02)
Bone	0.74 (0.19)	0.16 (0.03)	0.05 (0.08)	0.09 (0.05)
Muscle	1.20 (0.14)	0.23 (0.09)	0.04 (0.01)	0.04 (0.02)
Brain	0.08 (0.01)	0.01 (0.01)	0.01 (0.00)	0.00 (0.00)
Urine	–	–	–	1.63 (0.24)
Feces	–	–	–	71.54 (6.53)

Data were presented as %ID/g tissue. Each value represents mean ± SD for four mice.
‡ Presented as %ID/organ.

Table 6. Biodistribution of double tracers [^{77}Br]**17** and [^{125}I]**10** at 1 and 6 h after i.v. injection in tumor-bearing mice.

Tissues	Time after injection							
	1 h		6 h		1 h		6 h	
	[^{77}Br]**17**				[^{125}I]**10**			
Blood	5.64	(0.19)	5.35	(0.99)	0.50	(0.20)	0.17	(0.03)
Liver	15.89	(0.72)	6.76	(1.78)	30.32	(2.78)	10.16	(3.50)
Kidney	7.75	(0.85)	4.91	(0.80)	2.64	(1.45)	1.05	(0.41)
Small intestine	64.52	(3.35)	12.46	(5.93)	86.29	(2.99)	11.72	(8.01)
Large intestine	24.33	(17.81)	59.40	(18.22)	27.65	(21.75)	95.22	(32.67)
Spleen	9.19	(2.12)	2.04	(2.36)	1.80	(0.75)	0.25	(0.07)
Pancreas	12.95	(5.14)	4.28	(0.91)	2.71	(0.87)	0.36	(0.22)
Lung	11.42	(1.52)	6.29	(0.52)	1.62	(0.67)	0.37	(0.15)
Heart	5.36	(1.07)	2.99	(1.05)	0.61	(0.20)	0.53	(0.86)
Stomach‡	1.31	(0.39)	1.27	(0.89)	1.49	(0.52)	1.17	(1.68)
Bone	1.93	(1.51)	1.95	(2.50)	0.42	(0.16)	0.22	(0.15)
Muscle	3.42	(1.19)	1.79	(0.30)	0.36	(0.18)	0.10	(0.05)
Brain	1.49	(0.16)	1.39	(0.17)	0.04	(0.01)	0.02	(0.03)
H1975	4.51	(0.17)	3.48	(0.50)	0.68	(0.11)	0.10	(0.02)
H441	3.71	(0.13)	3.30	(0.54)	0.44	(0.06)	0.19	(0.06)

Data were presented as %ID/g tissue. Each value represents mean ± SD for four mice.
‡ Presented as %ID/organ.

Table 7. Biodistribution of [^{77}Br]Br at 15 min, 1, 4, and 24 h after i.v. injection in ddY mice.

Tissues	Time after injection							
	15 min		1h		4h		24h	
[^{77}Br]Br$^-$								
Blood	6.96	(0.58)	6.98	(0.45)	6.42	(0.64)	3.48	(0.36)
Liver	2.45	(0.29)	2.61	(0.17)	2.35	(0.30)	1.18	(0.12)
Kidney	5.10	(0.83)	4.58	(0.21)	4.51	(0.58)	2.62	(0.34)
Small intestine	3.94	(0.24)	3.92	(0.16)	3.18	(0.29)	1.99	(0.22)
Large intestine	3.12	(0.44)	2.78	(0.22)	2.37	(0.30)	1.55	(0.16)
Spleen	4.74	(0.31)	4.30	(0.26)	3.75	(0.73)	2.25	(0.36)
Pancreas	5.09	(0.78)	4.38	(0.27)	3.80	(0.37)	2.22	(0.32)
Lung	8.02	(0.95)	7.12	(0.48)	5.81	(0.59)	3.62	(0.32)
Heart	3.72	(0.47)	3.23	(0.09)	2.41	(0.20)	1.50	(0.19)
Stomach‡	3.94	(0.54)	4.59	(1.18)	5.44	(1.23)	4.18	(1.00)
Bone	3.72	(0.44)	3.25	(0.24)	3.00	(0.38)	1.78	(0.30)
Muscle	2.28	(0.18)	1.92	(0.11)	1.63	(0.14)	0.98	(0.04)
Brain	1.08	(0.13)	1.49	(0.07)	1.45	(0.14)	0.84	(0.09)
Neck‡	2.45	(0.50)	3.02	(0.35)	2.46	(0.42)	1.27	(0.28)
Urine							20.74	(4.69)
Feces							1.33	(0.49)

Data were presented as %ID/g tissue. Each value represents mean ± SD for four mice.
‡ Presented as %ID/organ.

2.4. Discussion

Modulating EGFR expression has been used for targeted therapy due to its highly specific targeting capability. The therapeutic effect of EGFR-TKIs in NSCLC could be assessed by PET imaging of EGFR which can provide more accurate information to aid in the selection of patients for individualized therapy. Several PET probes based on the EGFR TKIs derivatives have been reported in recent years to provide highly specific radiotracer for detecting EGFR mutation or/and predicting treatment response in NSCLC [25, 34-36].

Since I found the high selectivity of [^{125}I]**10**, a CO-1686 analog, toward double mutation EGFR L858R/T790M in vitro, I am encouraged to carry out further research by designed and synthesized a radiobrominated [^{77}Br]**17** as a molecular imaging agent for EGFR L858R/T790M. Bromine could be bioisosters of iodine that allows a bioisosteric substitution of the iodine. Therefore, a bromine atom was introduced in the diaminophenyl group of CO-1686 as iodine introduced in the previous study. Introducing iodine on this position didn't affect significantly the affinity of CO-1686 toward EGFR L858R/T790M because it does not play a key role in the binding activity of CO-1686 toward EGFR L858R/T790M based on the complex crystal structure analysis. As expected, the IC_{50} of **17** toward H1975 was similar to that of the iodinated compound **10**.

Actually, CO-1686 has low affinity toward a human lung cancer cell line with a wild type EGFR [22, 37], but in this study CO-1686 exhibited moderate inhibitory activity toward H441 cell lines as a wild type EGFR. This result was in line with Walter *et al.* finding. They reported that although CO-1686 exhibited moderate cytotoxicity toward a cancer cell with the wild type EGFR, it does not correlate to the phosphorylation activity of wild type EGFR [37]. In this case, the cytotoxicity mechanism is unclear, it might be related to non-EGFR related drug activities of CO-1686 [38].

Concerning ^{77}Br labeling, radiobromination was achieved by the presence of an

oxidizing agent NCS with a moderate radiochemical yield. Radiobromine is directly introduced on the aromatic group by a destannylation reaction with a positively charged radiobromine generated [39]. I assumed that using the same method with the radioiodination will produce a high radiochemical yield of [^{77}Br]**17**. Contrary to my expectation, the radiochemical yields of [^{77}Br]**17** approximately 45% was lower than that of [^{125}I]**10** (77%).

The HPLC analyses showed that the retention time of [^{77}Br]**17** was a little shorter than [^{125}I]**10**. This result supported the log *P* value of [^{77}Br]**17** little lower than radioiodinated [^{125}I]**10**.

The pattern of [^{77}Br]**17** and [^{125}I]**10** showed preferential accumulation toward H1975 cells. In the in vitro blocking studies, both radiotracers showed high specificity toward double mutation EGFR H1975 cells. The methoxyl group contributes in the specificity of CO-1686 to EGFR and the trifluoromethyl substituent of CO-1686 is beneficial to form hydrophobic interaction with Met790 which is not afforded by wild-type gatekeeper residue with Thr790 [10]. The specificity of both radiotracers in H1975 was evaluated in two independent experiments using two blocking agents. As expected, the uptakes of [^{77}Br]**17** and [^{125}I]**10** in H1975 cells were significantly reduced by almost 60% with the pretreatment of blocking agent CO-1686, indicating that radiotracers competitively bound to EGFR-TK with L858R/T790M double mutations to CO-1686. Besides, gefitinib only reduced the radioactivity uptake in H3255 but not in H1975. Although H1975 cells carry the L858R active mutant EGFR, the presence of secondary mutation T790M interferes the binding of first-generation TKIs such as gefitinib to the ATP binding site [22, 40].

[^{77}Br]**17** and [^{125}I]**10** were co-injected into the mice to minimize the number of animals and increase the reliability of the data in the biodistribution study. At 4 h post-injection, the distribution patterns in normal organs were similar among groups, with the highest uptake in the intestine and liver. High uptake in the liver and small intestine indicates that radiotracers

were mainly eliminated through hepatobiliary clearance due to the relatively hydrophobic structure of both radiotracers. However, the clearance rate of [^{77}Br]**17** was slow and the radioactivity accumulation in the nontargeted tissues was retained. The [^{125}I]**10** was eliminated up to 70% into feces, while the [^{77}Br]**17** was eliminated only 35% after 24 h post-injection. It has been reported that the blood clearance of free bromide ion accumulates is slow [41-43]. Therefore, the radioactivity in the blood can be used as an index of debromination of radiobromine-labeled tracers in vivo. In this study, the radioactivity of [^{77}Br]**17** in the blood was higher than that of [^{125}I]**10**, which suggested that debromination occurred in vivo. The biodistribution studies of [^{77}Br]Br showed long-time retention in the blood and some organs (**Table 7**). Thus, in this context, I confirmed that radioactivity accumulation in the normal tissues in the biodistribution study of [^{77}Br]**17** should be caused by free bromide ions from debrominated [^{77}Br]**17**. Debromination also observed in some radiotracers, such as 4-[^{76}Br]-bromo-α-methyl-L-phenylalanine (4-[^{76}Br]BAMP) and 3-[^{76}Br]-bromo-α-methyl-L-tyrosine ([^{76}Br]BAMT). The both radiotracers were designed as PET imaging probe for monitoring colon adenocarcinoma [39, 44].

In the biodistribution experiments in tumor-bearing mice, although the radioactivity accumulation of [^{77}Br]**17** and [^{125}I]**10** in H1975 tumor (4.51 ± 0.17 and 0.68 ± 0.11% ID/g, respectively) was higher than that of H441 tumor (3.71 ± 0.13 and 0.44 ± 0.06% ID/g, respectively) on 1 h post-injection, the tumor-to-blood ratio needs to be increased to provide a clear contrast. Therefore, it is desirable to develop more stable and selective analogs that can be rapidly cleared from the body and high specificity intratumoral uptake. The structural modification by a short-chain polyethylene glycol in the linker phenyl group could be an alternative to improve the water solubility which might be required to optimize the tumor accumulation of [^{77}Br]**17**.

2.5. Conclusions

Radiobrominated [^{77}Br]**17** was synthesized successfully with high radiochemical purity. This radiotracer showed high in vitro specificity toward NSCLC cells with double mutation EGFR L858R/T790M compared to that in EGFR L858R and wild-type EGFR. However, the in vivo accumulation in the targeted tumor needs to be optimized by structural modification.

References

1. Bronte, G.; Rizzo, S.; La Paglia, L.; Adamo, V.; Siragusa, S.; Ficorella, C.; Santini, D.; Bazan, V.; Colucci, G.; Gebbia, N.; Russo, A., Driver mutations and differential sensitivity to targeted therapies: a new approach to the treatment of lung adenocarcinoma. *Cancer Treatment Reviews* **2010,** 36, S21-S29.
2. Yarden, Y.; Shilo, B.-Z., SnapShot: EGFR Signaling Pathway. *Cell* **2007,** 131, (5), 1018.e1-1018.e2.
3. Gazdar, A. F., Personalized medicine and inhibition of EGFR signaling in lung cancer. *N Engl J Med* **2009,** 361, (10), 1018-20.
4. Roskoski, R., The ErbB/HER family of protein-tyrosine kinases and cancer. *Pharmacological Research* **2014,** 79, 34-74.
5. Gately, K.; O'Flaherty, J.; Cappuzzo, F.; Pirker, R.; Kerr, K.; O'Byrne, K., The role of the molecular footprint of EGFR in tailoring treatment decisions in NSCLC. *Journal of Clinical Pathology* **2012,** 65, (1), 1-7.
6. Jorissen, R. N.; Walker, F.; Pouliot, N.; Garrett, T. P.; Ward, C. W.; Burgess, A. W., Epidermal growth factor receptor: mechanisms of activation and signalling. *Exp Cell Res* **2003,** 284, (1), 31-53.
7. Herbst, R. S.; Heymach, J. V.; Lippman, S. M., Lung Cancer. *New England Journal of Medicine* **2008,** 359, (13), 1367-1380.
8. Sullivan, I.; Planchard, D., Next-Generation EGFR Tyrosine Kinase Inhibitors for Treating EGFR-Mutant Lung Cancer beyond First Line. *Frontiers in Medicine* **2017,** 3, (76).
9. Pao, W.; Wang, T. Y.; Riely, G. J.; Miller, V. A.; Pan, Q.; Ladanyi, M.; Zakowski, M. F.; Heelan, R. T.; Kris, M. G.; Varmus, H. E., KRAS Mutations and Primary Resistance of Lung Adenocarcinomas to Gefitinib or Erlotinib. *PLOS Medicine* **2005,** 2, (1), e17.

10. Yan, X.-E.; Zhu, S.-J.; Liang, L.; Zhao, P.; Geun Choi, H.; Yun, C.-H., Structural basis of mutant-selectivity and drug-resistance related to CO-1686. *Oncotarget* **2017,** 8, (32).
11. Walter, A. O.; Sjin, R. T. T.; Haringsma, H. J.; Ohashi, K.; Sun, J.; Lee, K.; Dubrovskiy, A.; Labenski, M.; Zhu, Z.; Wang, Z.; Sheets, M.; St Martin, T.; Karp, R.; van Kalken, D.; Chaturvedi, P.; Niu, D.; Nacht, M.; Petter, R. C.; Westlin, W.; Lin, K.; Jaw-Tsai, S.; Raponi, M.; Van Dyke, T.; Etter, J.; Weaver, Z.; Pao, W.; Singh, J.; Simmons, A. D.; Harding, T. C.; Allen, A., Discovery of a Mutant-Selective Covalent Inhibitor of EGFR that Overcomes T790M-Mediated Resistance in NSCLC. *Cancer Discovery* **2013,** 3, (12), 1404-1415.
12. Cross, D. A. E.; Ashton, S. E.; Ghiorghiu, S.; Eberlein, C.; Nebhan, C. A.; Spitzler, P. J.; Orme, J. P.; Finlay, M. R. V.; Ward, R. A.; Mellor, M. J.; Hughes, G.; Rahi, A.; Jacobs, V. N.; Brewer, M. R.; Ichihara, E.; Sun, J.; Jin, H.; Ballard, P.; Al-Kadhimi, K.; Rowlinson, R.; Klinowska, T.; Richmond, G. H. P.; Cantarini, M.; Kim, D.-W.; Ranson, M. R.; Pao, W., AZD9291, an Irreversible EGFR TKI, Overcomes T790M-Mediated Resistance to EGFR Inhibitors in Lung Cancer. *Cancer Discovery* **2014,** 4, (9), 1046-1061.
13. Jänne, P. A.; Yang, J. C.-H.; Kim, D.-W.; Planchard, D.; Ohe, Y.; Ramalingam, S. S.; Ahn, M.-J.; Kim, S.-W.; Su, W.-C.; Horn, L.; Haggstrom, D.; Felip, E.; Kim, J.-H.; Frewer, P.; Cantarini, M.; Brown, K. H.; Dickinson, P. A.; Ghiorghiu, S.; Ranson, M., AZD9291 in EGFR Inhibitor–Resistant Non–Small-Cell Lung Cancer. *New England Journal of Medicine* **2015,** 372, (18), 1689-1699.
14. Gupta, R.; Dastane, A. M.; Forozan, F.; Riley-Portuguez, A.; Chung, F.; Lopategui, J.; Marchevsky, A. M., Evaluation of EGFR abnormalities in patients with pulmonary adenocarcinoma: the need to test neoplasms with more than one method. *Modern Pathology* **2009,** 22, (1), 128-133.

15. Song, Y.; Xiao, Z.; Wang, K.; Wang, X.; Zhang, C.; Fang, F.; Sun, X.; Shen, B., Development and Evaluation of ^{18}F-IRS for Molecular Imaging Mutant EGF Receptors in NSCLC. *Scientific Reports* **2017,** 7, (1), 3121.
16. Lux, J.; Chan, M.; Elst, L. V.; Schopf, E.; Mahmoud, E.; Laurent, S.; Almutairi, A., Metal Chelating Crosslinkers Form Nanogels with High Chelation Stability. *J Mater Chem B* **2013,** 1, (46), 6359-6364.
17. Zhou, W.; Ercan, D.; Chen, L.; Yun, C. H.; Li, D.; Capelletti, M.; Cortot, A. B.; Chirieac, L.; Iacob, R. E.; Padera, R.; Engen, J. R.; Wong, K. K.; Eck, M. J.; Gray, N. S.; Jänne, P. A., Novel mutant-selective EGFR kinase inhibitors against EGFR T790M. *Nature* **2009,** 462, (7276), 1070-4.
18. Ogawa, K.; Shiba, K.; Akhter, N.; Yoshimoto, M.; Washiyama, K.; Kinuya, S.; Kawai, K.; Mori, H., Evaluation of radioiodinated vesamicol analogs for sigma receptor imaging in tumor and radionuclide receptor therapy. *Cancer Science* **2009,** 100, (11), 2188-2192.
19. Zhang, J.; Späth, S. S.; Marjani, S. L.; Zhang, W.; Pan, X., Characterization of cancer genomic heterogeneity by next-generation sequencing advances precision medicine in cancer treatment. *Precis Clin Med* **2018,** 1, (1), 29-48.
20. Xiao, Z.; Song, Y.; Kai, W.; Sun, X.; Shen, B., Evaluation of ^{99m}Tc-HYNIC-MPG as a novel SPECT radiotracer to detect EGFR-activating mutations in NSCLC. *Oncotarget* **2017,** 8, (25), 40732-40740.
21. Ogawa, K.; Takeda, T.; Mishiro, K.; Toyoshima, A.; Shiba, K.; Yoshimura, T.; Shinohara, A.; Kinuya, S.; Odani, A., Radiotheranostics Coupled between an At-211-Labeled RGD Peptide and the Corresponding Radioiodine-Labeled RGD Peptide. *ACS Omega* **2019,** 4, (3), 4584-4591.
22. Su, H.; Seimbille, Y.; Ferl, G. Z.; Bodenstein, C.; Fueger, B.; Kim, K. J.; Hsu, Y. T.; Dubinett, S. M.; Phelps, M. E.; Czernin, J.; Weber, W. A., Evaluation of [^{18}F]gefitinib as

a molecular imaging probe for the assessment of the epidermal growth factor receptor status in malignant tumors. *Eur J Nucl Med Mol Imaging* **2008,** 35, (6), 1089-99.

23. Pal, A.; Balatoni, J. A.; Mukhopadhyay, U.; Ogawa, K.; Gonzalez-Lepera, C.; Shavrin, A.; Volgin, A.; Tong, W.; Alauddin, M. M.; Gelovani, J. G., Radiosynthesis and Initial In Vitro Evaluation of [^{18}F]F-PEG6-IPQA—A Novel PET Radiotracer for Imaging EGFR Expression-Activity in Lung Carcinomas. *Molecular Imaging and Biology* **2011,** 13, (5), 853-861.
24. Waaijer, S. J. H.; Kok, I. C.; Eisses, B.; Schröder, C. P.; Jalving, M.; Brouwers, A. H.; Lub-de Hooge, M. N.; de Vries, E. G. E., Molecular Imaging in Cancer Drug Development. *J Nucl Med* **2018,** 59, (5), 726-732.
25. Makino, A.; Miyazaki, A.; Tomoike, A.; Kimura, H.; Arimitsu, K.; Hirata, M.; Ohmomo, Y.; Nishii, R.; Okazawa, H.; Kiyono, Y.; Ono, M.; Saji, H., PET probe detecting non-small cell lung cancer susceptible to epidermal growth factor receptor tyrosine kinase inhibitor therapy. *Bioorg Med Chem* **2018,** 26, (8), 1609-1613.
26. Ballard, P.; Yates, J. W.; Yang, Z.; Kim, D. W.; Yang, J. C.; Cantarini, M.; Pickup, K.; Jordan, A.; Hickey, M.; Grist, M.; Box, M.; Johnström, P.; Varnäs, K.; Malmquist, J.; Thress, K. S.; Jänne, P. A.; Cross, D., Preclinical Comparison of Osimertinib with Other EGFR-TKIs in EGFR-Mutant NSCLC Brain Metastases Models, and Early Evidence of Clinical Brain Metastases Activity. *Clin Cancer Res* **2016,** 22, (20), 5130-5140.
27. Zhang, M.-R.; Kumata, K.; Hatori, A.; Takai, N.; Toyohara, J.; Yamasaki, T.; Yanamoto, K.; Yui, J.; Kawamura, K.; Koike, S.; Ando, K.; Suzuki, K., [^{11}C]Gefitinib ([^{11}C]Iressa): Radiosynthesis, In Vitro Uptake, and In Vivo Imaging of Intact Murine Fibrosarcoma. *Molecular Imaging and Biology* **2010,** 12, (2), 181-191.
28. Slobbe, P.; Windhorst, A. D.; Walsum, M. S.-v.; Schuit, R. C.; Smit, E. F.; Niessen, H. G.; Solca, F.; Stehle, G.; van Dongen, G. A. M. S.; Poot, A. J., Development of

[^{18}F]afatinib as new TKI-PET tracer for EGFR positive tumors. *Nuclear Medicine and Biology* **2014,** 41, (9), 749-757.

29. Vallabhajosula, S.; Solnes, L.; Vallabhajosula, B., A broad overview of positron emission tomography radiopharmaceuticals and clinical applications: what is new? *Semin Nucl Med* **2011,** 41, (4), 246-64.
30. Nayak, T. K.; Brechbiel, M. W., Radioimmunoimaging with longer-lived positron-emitting radionuclides: potentials and challenges. *Bioconjug Chem* **2009,** 20, (5), 825-841.
31. Zhou, D.; Kim, S. H.; Chu, W.; Voller, T.; Katzenellenbogen, J. A., Evaluation of aromatic radiobromination by nucleophilic substitution using diaryliodonium salt precursors. *J Labelled Comp Radiopharm* **2017,** 60, (9), 450-456.
32. Tolmachev, V.; Lövqvist, A.; Einarsson, L.; Schultz, J.; Lundqvist, H., Production of ^{76}Br by a low-energy cyclotron. *Applied Radiation and Isotopes* **1998,** 49, (12), 1537-1540.
33. Koura, M.; Yamaguchi, Y.; Kurobuchi, S.; Sumida, H.; Watanabe, Y.; Enomoto, T.; Matsuda, T.; Okuda, A.; Koshizawa, T.; Matsumoto, Y.; Shibuya, K., Discovery of a 2-hydroxyacetophenone derivative as an outstanding linker to enhance potency and β-selectivity of liver X receptor agonist. *Bioorganic & Medicinal Chemistry* **2016,** 24, (16), 3436-3446.
34. Bernard-Gauthier, V.; Bailey, J. J.; Berke, S.; Schirrmacher, R., Recent Advances in the Development and Application of Radiolabeled Kinase Inhibitors for PET Imaging. *Molecules (Basel, Switzerland)* **2015,** 20, (12), 22000-22027.
35. Shamni, O.; Grievink, H.; Itamar, B.; Mishani, E.; Abourbeh, G., Development of a Fluorinated Analogue of Erlotinib for PET Imaging of EGFR Mutation–Positive NSCLC. *Molecular Imaging and Biology* **2019,** 21, (4), 696-704.
36. Wei, W.; Ni, D.; Ehlerding, E. B.; Luo, Q.-Y.; Cai, W., PET Imaging of Receptor Tyrosine Kinases in Cancer. *Molecular Cancer Therapeutics* **2018,** 17, (8), 1625-1636.

37. Walter, A. O.; Sjin, R. T.; Haringsma, H. J.; Ohashi, K.; Sun, J.; Lee, K.; Dubrovskiy, A.; Labenski, M.; Zhu, Z.; Wang, Z.; Sheets, M.; St Martin, T.; Karp, R.; van Kalken, D.; Chaturvedi, P.; Niu, D.; Nacht, M.; Petter, R. C.; Westlin, W.; Lin, K.; Jaw-Tsai, S.; Raponi, M.; Van Dyke, T.; Etter, J.; Weaver, Z.; Pao, W.; Singh, J.; Simmons, A. D.; Harding, T. C.; Allen, A., Discovery of a mutant-selective covalent inhibitor of EGFR that overcomes T790M-mediated resistance in NSCLC. *Cancer Discov* **2013,** 3, (12), 1404-15.

38. Lu, X.; Yu, L.; Zhang, Z.; Ren, X.; Smaill, J. B.; Ding, K., Targeting EGFR(L858R/T790M) and EGFR(L858R/T790M/C797S) resistance mutations in NSCLC: Current developments in medicinal chemistry. *Med Res Rev* **2018,** 38, (5), 1550-1581.

39. Hanaoka, H.; Ohshima, Y.; Suzuki, Y.; Yamaguchi, A.; Watanabe, S.; Uehara, T.; Nagamori, S.; Kanai, Y.; Ishioka, N. S.; Tsushima, Y.; Endo, K.; Arano, Y., Development of a Widely Usable Amino Acid Tracer: ^{76}Br-α-Methyl-Phenylalanine for Tumor PET Imaging. *J Nucl Med* **2015,** 56, (5), 791-7.

40. Guo, A.; Villén, J.; Kornhauser, J.; Lee, K. A.; Stokes, M. P.; Rikova, K.; Possemato, A.; Nardone, J.; Innocenti, G.; Wetzel, R.; Wang, Y.; MacNeill, J.; Mitchell, J.; Gygi, S. P.; Rush, J.; Polakiewicz, R. D.; Comb, M. J., Signaling networks assembled by oncogenic EGFR and c-Met. *Proc Natl Acad Sci U S A* **2008,** 105, (2), 692-7.

41. Bruehlmeier, M.; Roelcke, U.; Bläuenstein, P.; Missimer, J.; Schubiger, P. A.; Locher, J. T.; Pellikka, R.; Ametamey, S. M., Measurement of the extracellular space in brain tumors using ^{76}Br-bromide and PET. *J Nucl Med* **2003,** 44, (8), 1210-8.

42. Rossin, R.; Berndorff, D.; Friebe, M.; Dinkelborg, L. M.; Welch, M. J., Small-animal PET of tumor angiogenesis using a ^{76}Br-labeled human recombinant antibody fragment to the ED-B domain of fibronectin. *J Nucl Med* **2007,** 48, (7), 1172-9.

43. Lee, H.; Finck, B. N.; Jones, L. A.; Welch, M. J.; Mach, R. H., Synthesis and evaluation of a bromine-76-labeled PPARgamma antagonist 2-bromo-5-nitro-N-phenylbenzamide. *Nucl Med Biol* **2006,** 33, (7), 847-54.

44. Ohshima, Y.; Hanaoka, H.; Watanabe, S.; Sugo, Y.; Watanabe, S.; Tominaga, H.; Oriuchi, N.; Endo, K.; Ishioka, N. S., Preparation and biological evaluation of 3-[^{76}Br]bromo-α-methyl-l-tyrosine, a novel tyrosine analog for positron emission tomography imaging of tumors. *Nuclear Medicine and Biology* **2011,** 38, (6), 857-865.

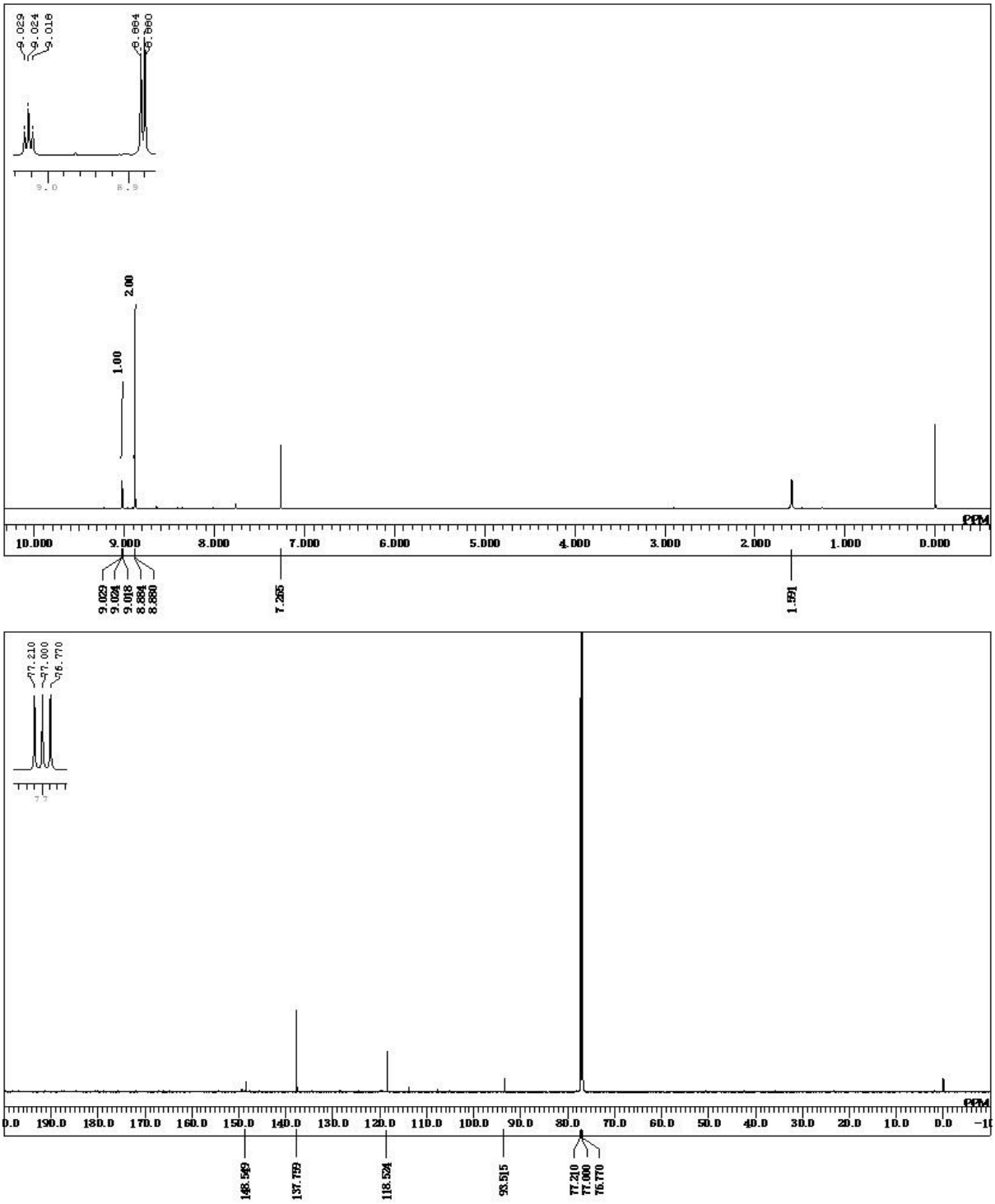

Figure S1. The NMR spectra of 1-iodo-3,5-dinitrobenzene (**1**). ^{1}H NMR (400 MHz, $CDCl_3$): δ 8.88 (2H, d, J = 1.6 Hz), 9.02 (1H, t, J = 2.0 Hz). ^{13}C NMR (100 MHz, $CDCl_3$): δ 93.5, 118.5, 137.8, 148.5. HRMS (FAB+) calculated for $C_6H_3IN_2O_4$ $[M+ H]^+$: m/z = 294.9216, found 294.9225.

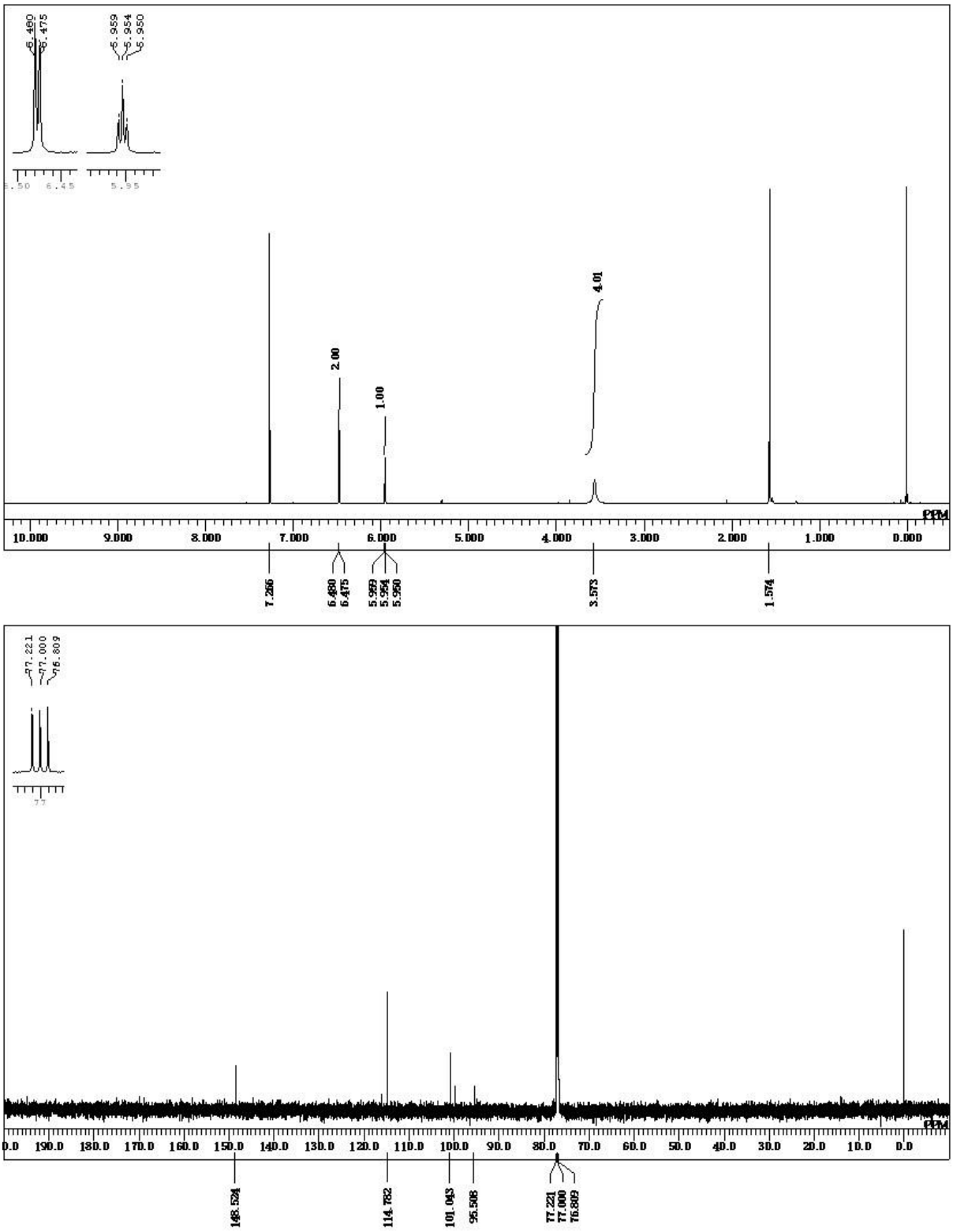

Figure S2. The NMR spectra of 5-iodobenzene-1,3-diamine (**2**). ^{1}H NMR (400 MHz, $CDCl_3$): δ 3.57 (4H, s), 5.95 (1H, t, J = 2.0 Hz), 6.48 (2H, d, J = 2.0 Hz). ^{13}C NMR (100 MHz, $CDCl_3$): δ 95.5, 101.0, 114.8, 148.5. HRMS (FAB+) calculated for $C_6H_7IN_2$ $[M+H]^+$: m/z = 233.9654, found 233.9645.

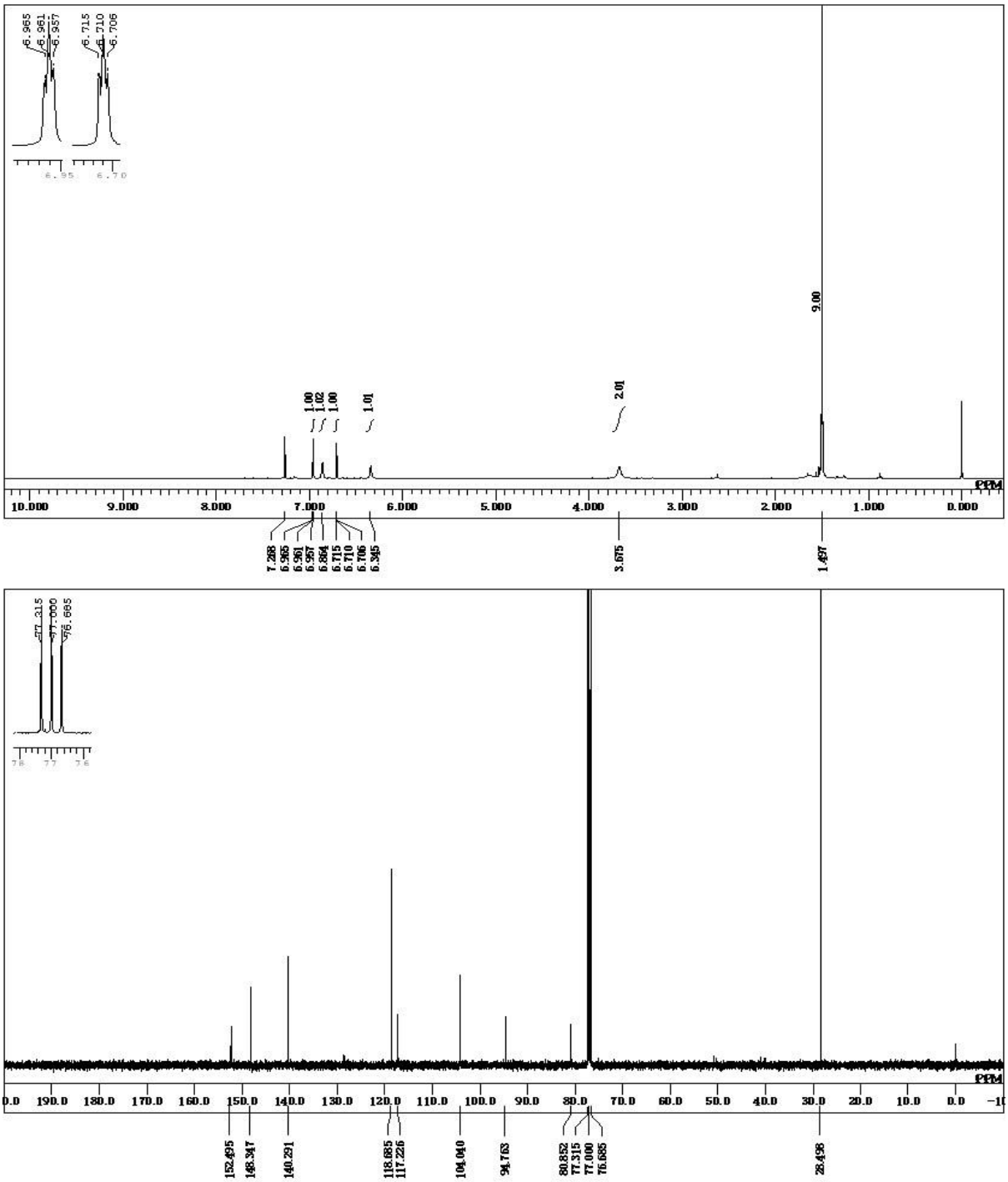

Figure S3. The NMR spectra of tert-butyl (3-amino-5-iodophenyl)carbamate (**3**). ^{1}H NMR (400 MHz, $CDCl_3$): δ 1.50 (9H, s), 3.68 (2H, s), 6.34 (1H, s), 6.71 (1H, t, J = 1.6 Hz), 6.86 (1H, s), 6.96 (1H, t, J = 1.6 Hz). ^{13}C NMR (100 MHz, $CDCl_3$): δ 28.5 (3C), 80.9, 94.8, 104.0, 117.2, 118.7, 140.3, 148.3, 152.5. HRMS (FAB+) calculated for $C_{11}H_{15}IN_2O_2$ $[M+H]^+$: *m/z* = 334.0178, found 334.0168.

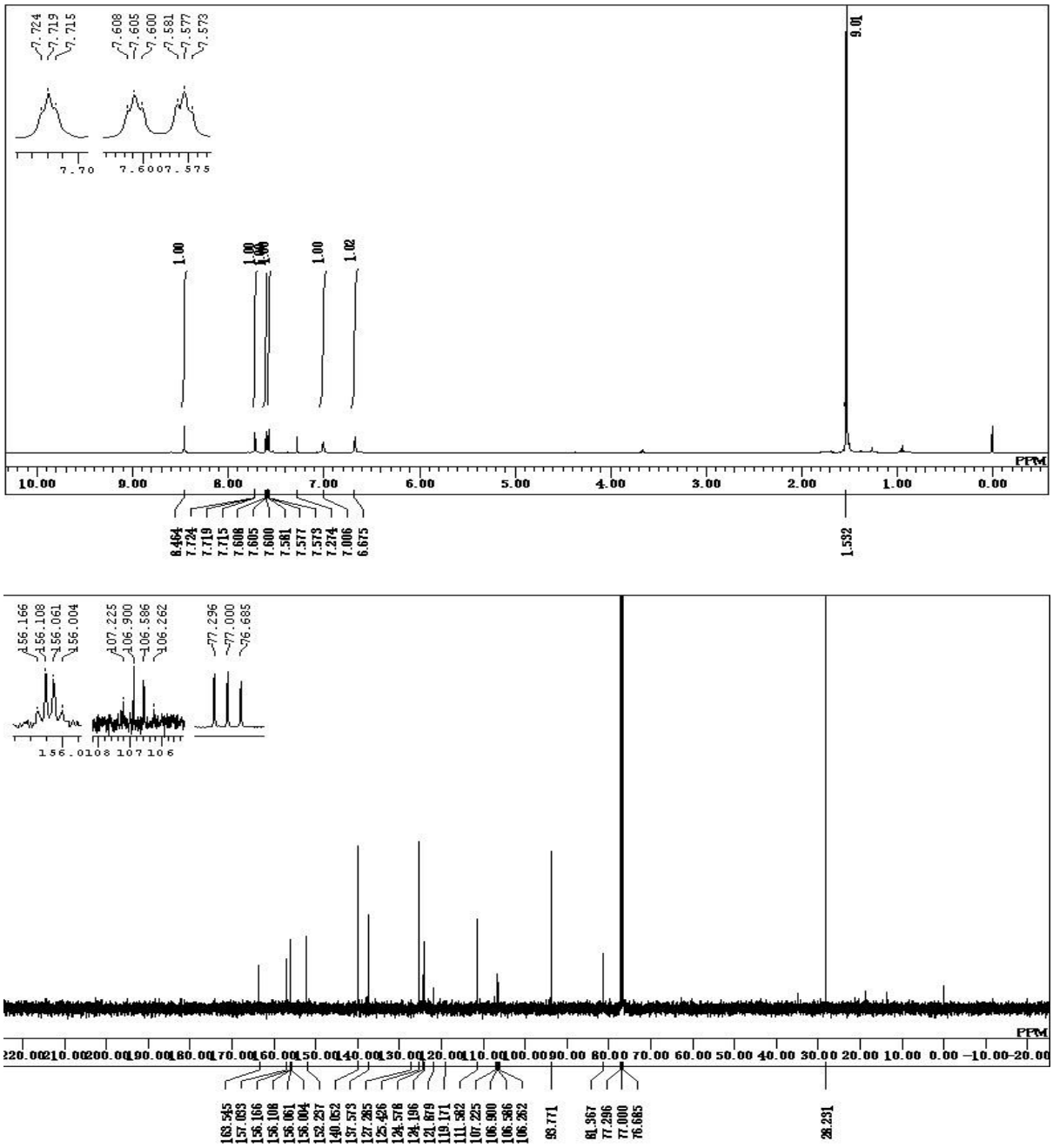

Figure S4. The NMR spectra of tert-butyl (3-((2-chloro-5-(trifluoromethyl)pyrimidin-4-yl)amino)-5-iodophenyl)carbamate (**4**). ^{1}H NMR (400 MHz, $CDCl_3$): δ 1.53 (9H, s), 6.68 (1H, s), 7.00 (1H, s), 7.58 (1H, t, J = 1.6 Hz), 7.61 (1H, t, J = 1.6 Hz), 7.72 (1H, t, J = 1.6 Hz), 8.46 (1H, s). ^{13}C NMR (100 MHz, $CDCl_3$): δ 28.2 (3C), 81.4, 93.8, 106.7 (q, J_{CF} = 31.4 Hz), 111.6, 123.0 (q, J_{CF} = 270 Hz), 124.2, 125.4, 137.6, 140.1, 152.2, 156.1 (q, J_{CF} = 4.7 Hz), 157.0, 163.5. HRMS (FAB+) calculated for $C_{16}H_{15}ClF_3IN_4O_2$ [M+ H]$^{+}$: m/z = 513.9880, found 513.9875.

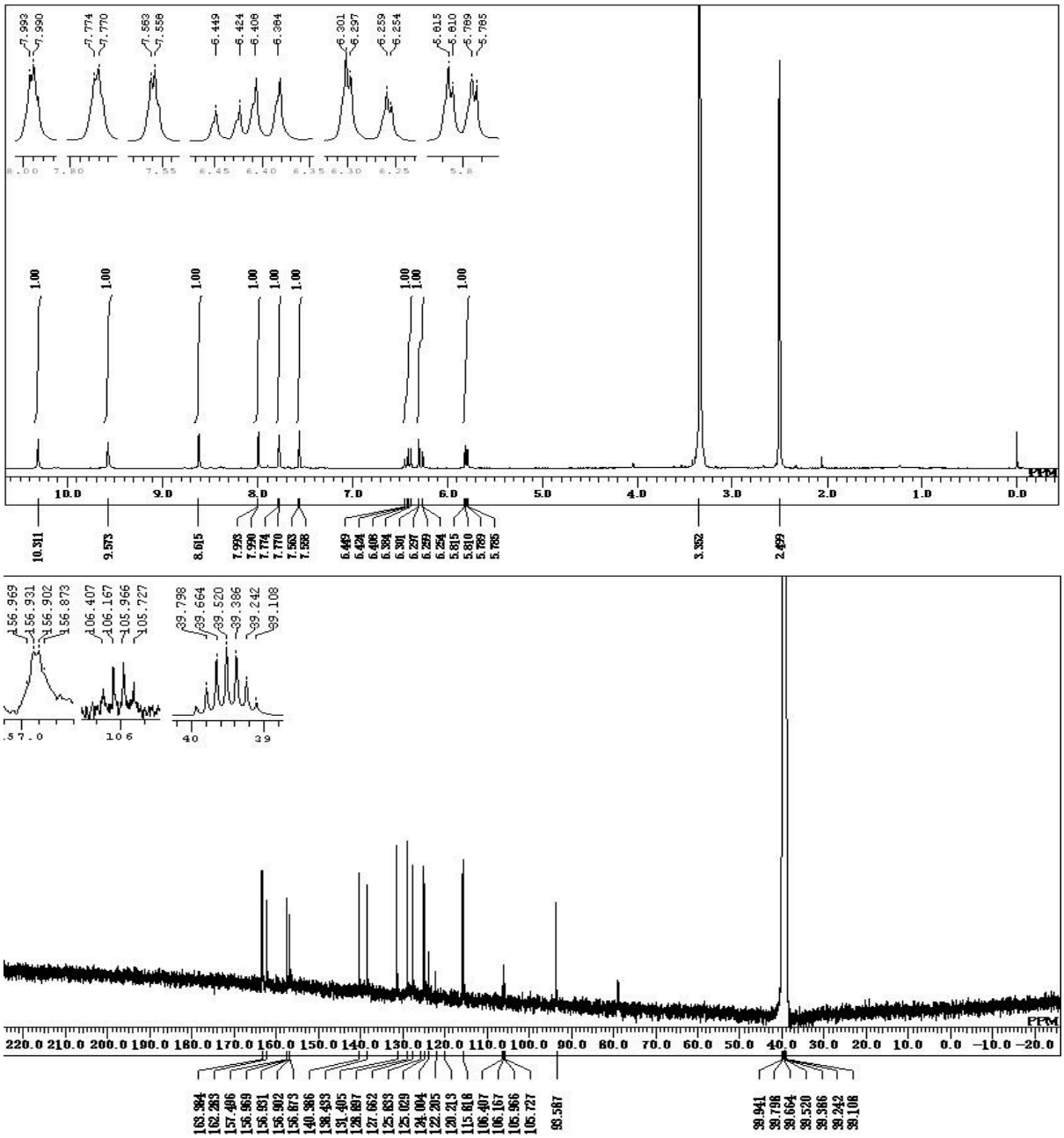

Figure S5. The NMR spectra of N-(3-((2-chloro-5-(trifluoromethyl)pyrimidin-4-yl)amino)-5-iodophenyl) acrylamide (**5**). ^{1}H NMR (400 MHz, $(CD_3)_2SO$): δ 5.79 (1H, dd, J = 10.0, 2.0 Hz), 6.27 (1H, dd, J = 16.8, 2.0 Hz), 6.40 (1H, dd, J = 16.4, 10.0 Hz), 7.56 (1H, d, J = 2.0 Hz), 7.77 (1H, d, J = 2.0 Hz), 7.99 (1H, d, J = 2.0 Hz), 8.62 (1H, s), 9.57 (1H, s), 10.31 (1H, s). ^{13}C NMR (150 MHz, $(CD_3)_2SO$): δ 93.6, 106.1 (q, J_{CF} = 30.2 Hz), 115.8, 123.0 (q, J_{CF} = 270 Hz), 125.0, 127.7, 128.9, 131.4, 138.4, 140.4, 156.9 (q, J_{CF} = 4.4 Hz), 157.5, 162.3, 163.4. HRMS (FAB+) calculated for $C_{14}H_9ClF_3IN_4O$ $[M+H]^+$: m/z = 468.9461, found 468.9559.

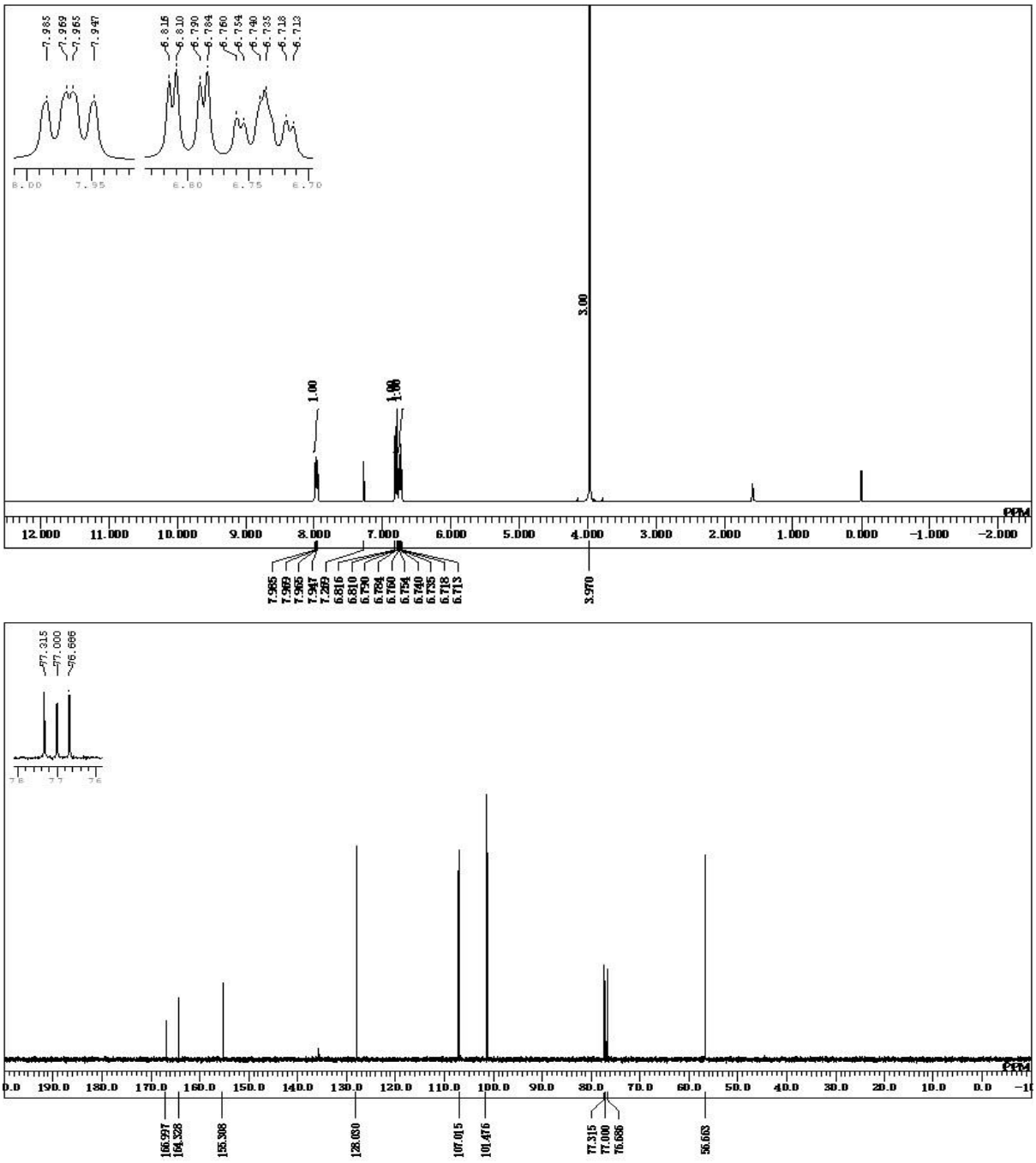

Figure S6. The NMR spectra of 4-fluoro-2-methoxy-1-nitrobenzene (**6**). ^{1}H NMR (400 MHz, $CDCl_3$): δ 3.97 (3H, s), 6.74 (1H, dt, *J* = 8.4, 2.0 Hz), 6.80 (1H, dd, *J* = 10.4, 2.4 Hz), 7.96 (1H, dd, *J* = 8.4, 6.4 Hz). ^{13}C NMR (100 MHz, $(CD_3)_2SO$): δ 56.7, 101.5, 107.0, 128.0, 155.3, 164.3, 167.0. HRMS (DART+) calculated for $C_7H_6FNO_3$ $[M+ H]^+$: *m/z* = 172.0331, found 172.0345.

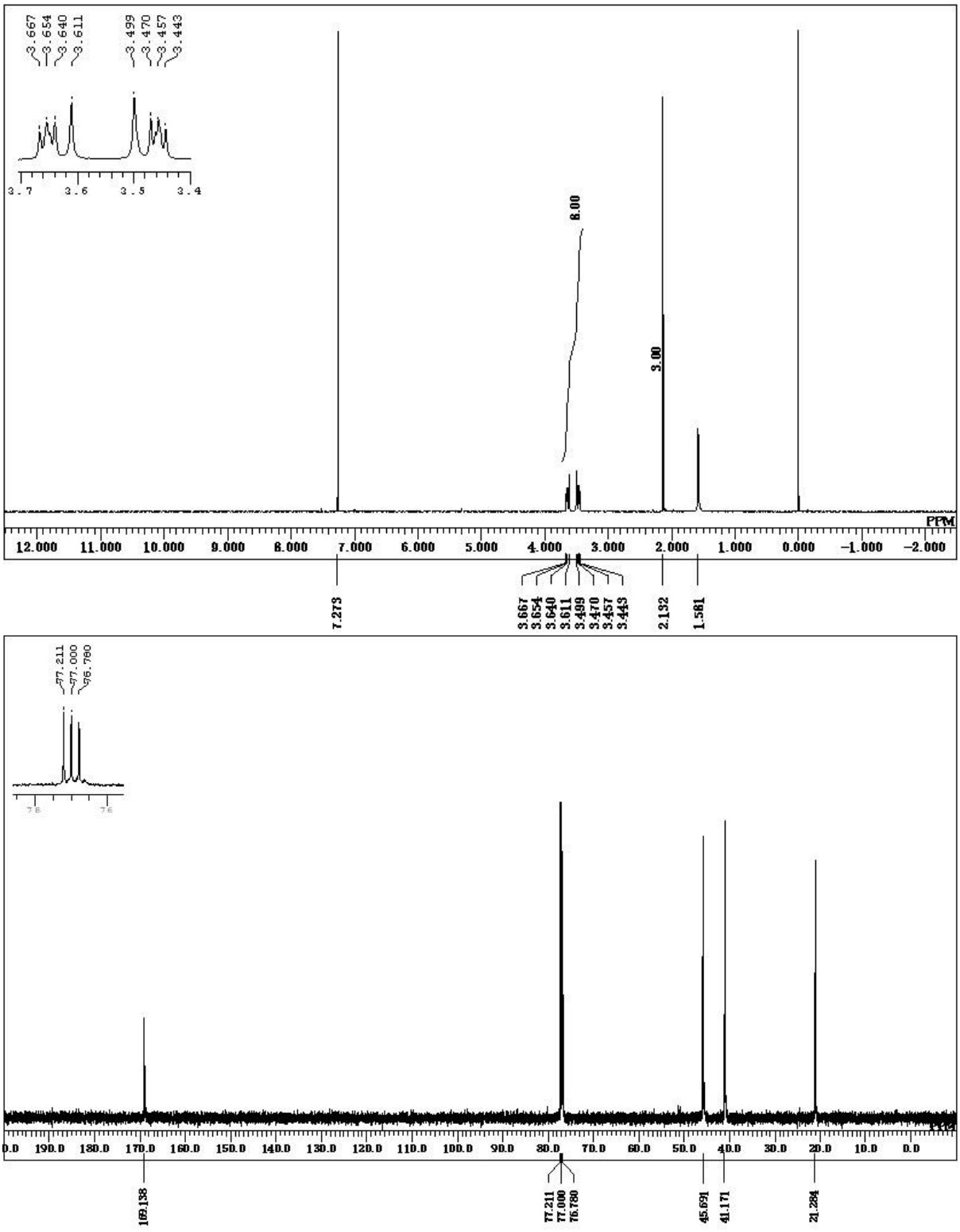

Figure S7. The NMR spectra of 1-(piperazine-1-yl)ethan-1-one (**7**). ^{1}H NMR (400 MHz, $CDCl_3$): δ 2.13 (3H, s), 3.40-3.70 (8H, m). ^{13}C NMR (100 MHz, $CDCl_3$): δ 21.3, 41.2 (2C), 45.7 (2C), 169.1. HRMS (FAB+) calculated for $C_6H_{12}N_2O$ $[M+ H]^+$: *m/z* = 129.0949, found 129.1031.

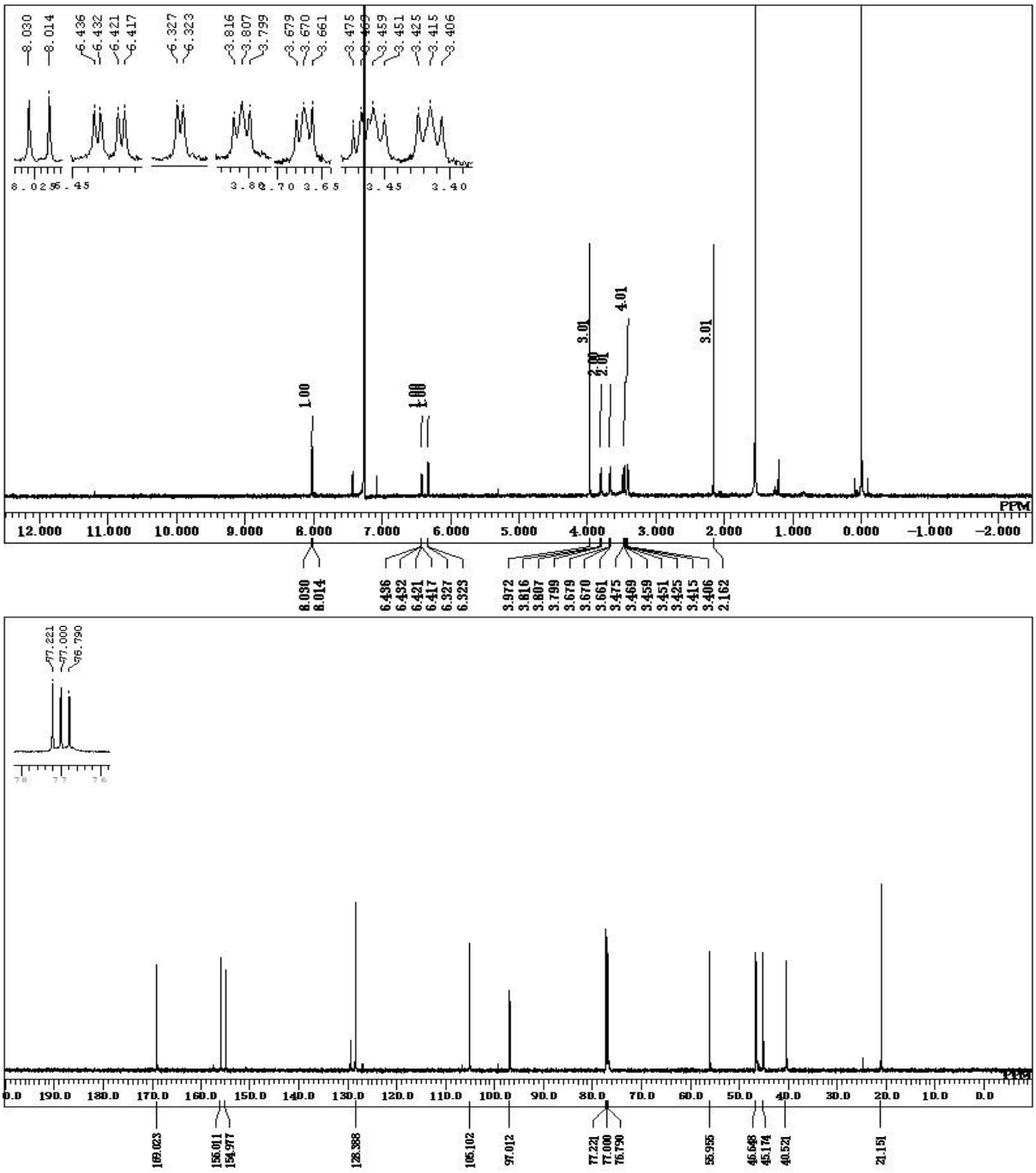

Figure S8. The NMR spectra of 1-(4-(3-methoxy-4-nitrophenyl)piperazine-1-yl)ethan-1-one (**8**). ^{1}H NMR (400 MHz, $CDCl_3$): δ 2.16 (3H, s), 3.40-3.50 (4H, m), 3.67 (2H, t, *J* = 4.0 Hz), 3.81 (2H, t, *J* = 4.0 Hz), 3.97 (3H, s), 6.33 (1H, d, *J* = 1.6 Hz), 6.42 (1H, dd, *J* = 6.0, 1.6 Hz), 8.02 (1H, d, *J* = 6.4 Hz). ^{13}C NMR (100 MHz, $CDCl_3$): δ, 21.2, 40.5, 45.2, 46.5, 46.6, 56.0, 97.0, 105.1, 128.4, 129.5, 155.0, 156.0, 169.0. HRMS (FAB+) calculated for $C_{13}H_{17}N_3O_4$ [M+H]$^{+}$: *m/z* = 280.1219, found 280.1295.

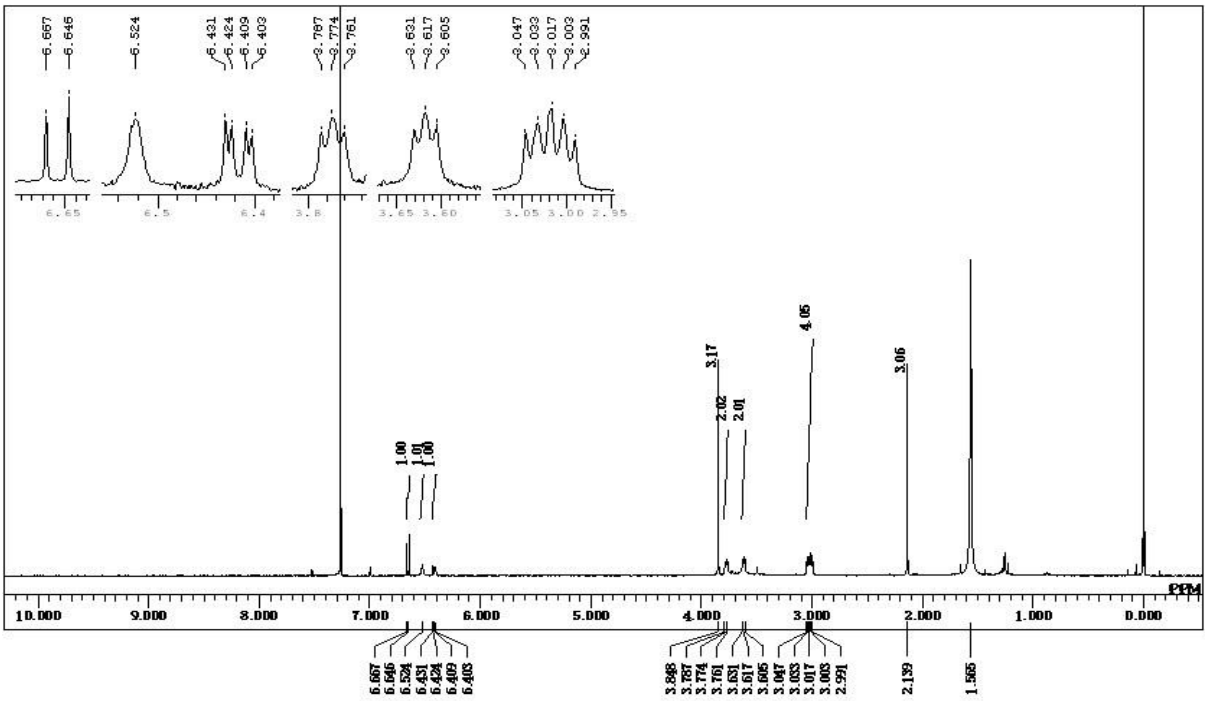

Figure S9. The proton NMR spectra of 1-(4-(4-amino-3-methoxyphenyl)piperazine-1-yl)ethan-1-one (**9**). ^{1}H NMR (400 MHz, $CDCl_3$): δ 2.13 (3H, s), 2.95-3.08 (4H, m), 3.62 (2H, t, *J* = 5.6 Hz), 3.77 (2H, t, *J* = 5.2 Hz), 3.85 (3H, s), 6.42 (1H, dd, *J* = 8.8, 2.8 Hz), 6.52 (1H, s), 6.66 (1H, d, *J* = 8.4 Hz). HRMS (FAB+) calculated for $C_{13}H_{19}N_3O_2$ $[M+H]^+$: *m/z* = 249.1477, found 249.1464.

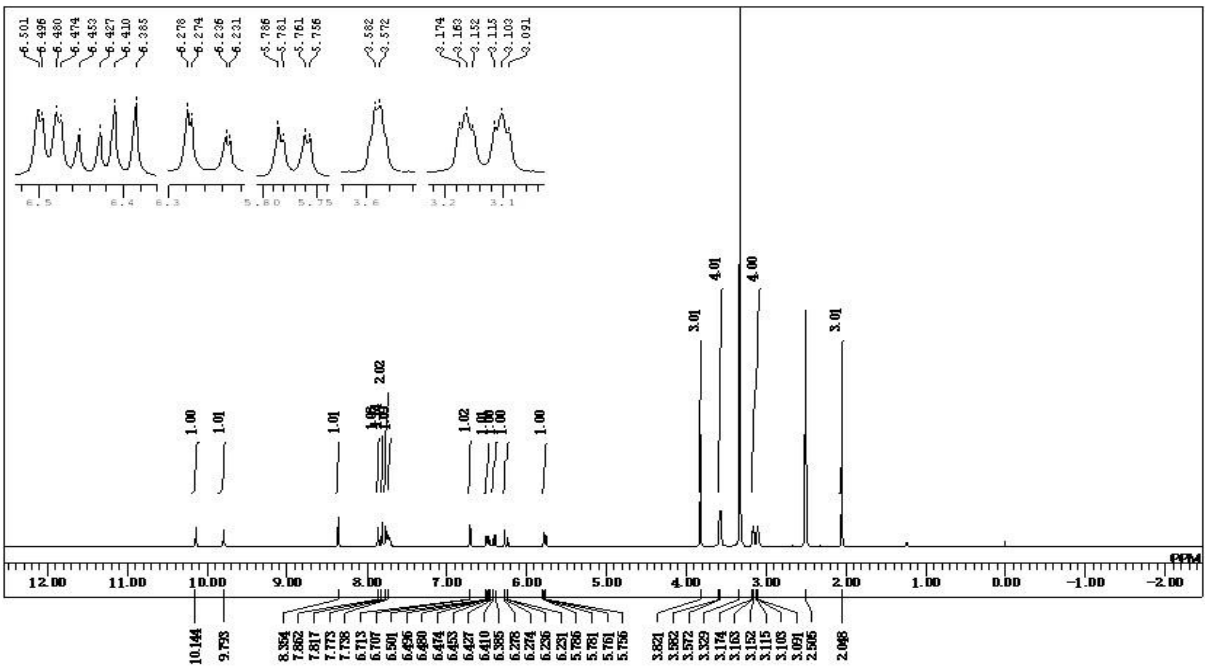

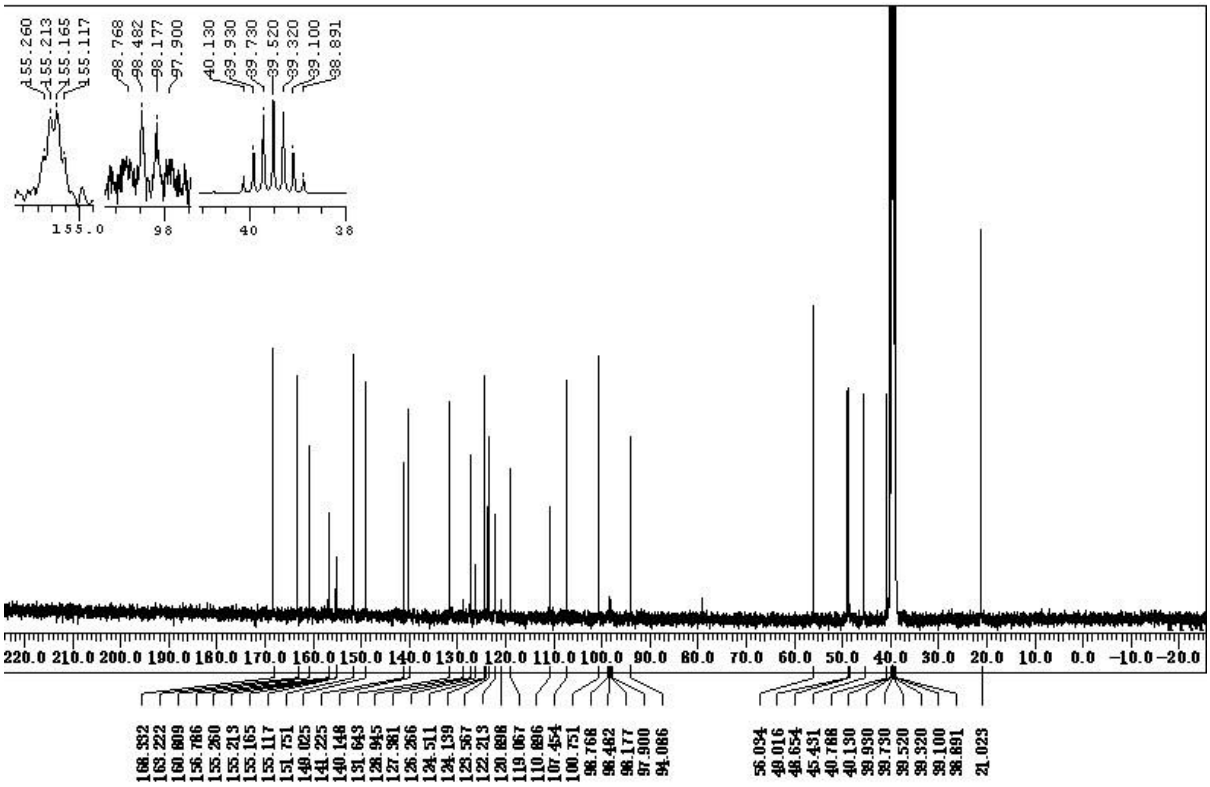

Figure S10. The NMR spectra of N-(3-((2-((4-(4-acetylpiperazin-1-yl)-2-methoxyphenyl)amino)-5-(trifluoromethyl)pyrimidin-4-yl)amino)-5-iodophenyl)acrylamide (**10**). ^{1}H NMR (400 MHz, $(CD_3)_2SO$): δ 2.05 (3H, s), 3.10 (2H, t, J = 4.8 Hz), 3.16 (2H, t, J = 4.4 Hz), 3.53-3.63 (4H, m), 3.82 (3H, s), 5.77 (1H, dd, J = 10.0, 2.0 Hz), 6.25 (1H, dd, J = 16.8, 2.0 Hz), 6.41 (1H, dd, J = 16.8, 10.0 Hz), 6.49 (1H, dd, J = 8.8, 2.0 Hz), 6.71 (1H, s), 7.74 (1H, s), 7.77 (2H, s), 7.82 (1H, s), 7.86 (1H, s), 8.35 (1H, s), 9.79 (1H, s), 10.14 (1H, s). ^{13}C NMR (100 MHz, $(CD_3)_2SO$): δ 21.0, 40.8, 45.4, 48.7, 49.0, 56.0, 94.1, 98.3 (q, J_{CF} = 30.5 Hz), 100.8, 107.5, 110.9, 119.1, 122.2, 124.1, 124.5, 124.8 (q, J_{CF} = 270 Hz), 127.4, 131.6, 140.1, 141.2, 149.0, 151.8, 155.2 (q, J_{CF} = 4.8 Hz), 156.8, 160.8, 163.2, 168.3. HRMS (FAB+) calculated for $C_{27}H_{27}F_3IN_7O_3$ $[M+H]^+$: m/z = 681.1172, found 681.1186.

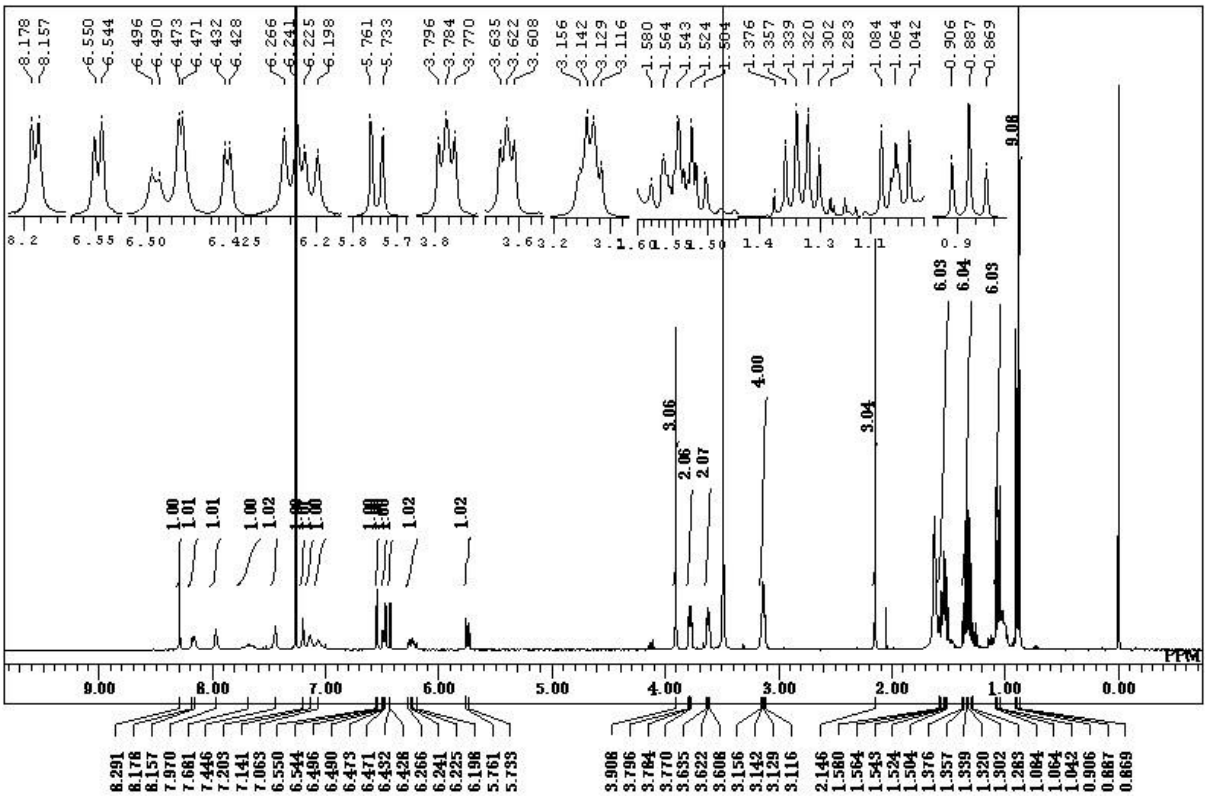

Figure S11. The proton NMR spectra of N-(3-((2-((4-(4-acetylpiperazin-1-yl)-2-methoxyphenyl)amino)-5-(trifluoromethyl)pyrimidin-4-yl)amino)-5-(tributylstannyl) phenyl) acrylamide (**11**). ^{1}H NMR (400 MHz, ($CDCl_3$): δ 0.88 (9H, t, *J* = 7.6 Hz), 1.06 (6H, t, *J* = 8.0 Hz), 1.33 (6H, sex, *J* = 7.6 Hz), 1.54 (6H, quin, *J* = 7.6 Hz), 2.14 (3H, s), 3.10-3.20 (4H, m), 3.62 (2H, t, *J* = 5.6 Hz), 3.78 (2H, t, *J* = 5.6 Hz), 3.91 (3H, s), 5.75 (1H, d, *J* = 11.2 Hz), 6.23 (1H, dd, *J* = 17.2, 10.8 Hz), 6.43 (1H, d, *J* = 1.6 Hz), 6.48 (1H, dd, *J* = 7.6, 2.0 Hz), 6.54 (1H, d, *J* = 2.4 Hz), 7.68 (1H, s) 7.06 (1H, s), 7.14 (1H, s), 7.20 (1H, s), 7.44 (1H, s), 7.97 (1H, s), 8.16 (1H, d, *J* = 8.4 Hz), 8.29 (1H, s). HRMS (FAB+) calculated for $C_{39}H_{54}F_3N_7O_3Sn$ $[M+H]^+$: *m/z* = 845.3267 found 845.3262.

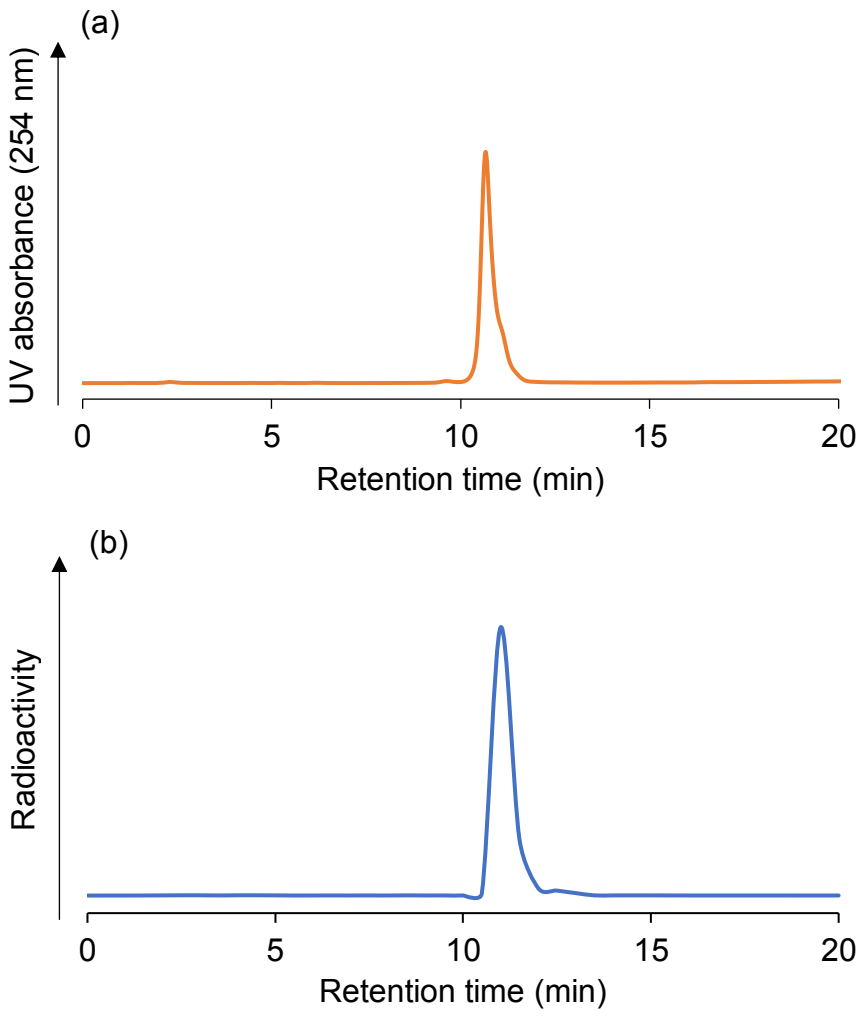

Figure S12. The chromatograms of (a) nonradioactive iodinated compound **10** (ICO1686) and (b) radioactive compound [^{125}I]**10** ([^{125}I]ICO1686).

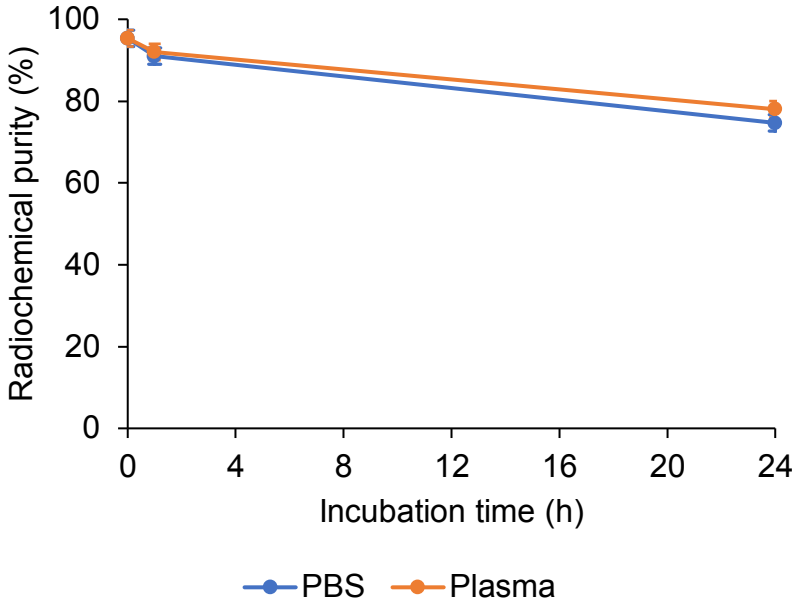

Figure S13. The stability of radiolabeled compound [^{125}I]**10** in PBS and plasma.

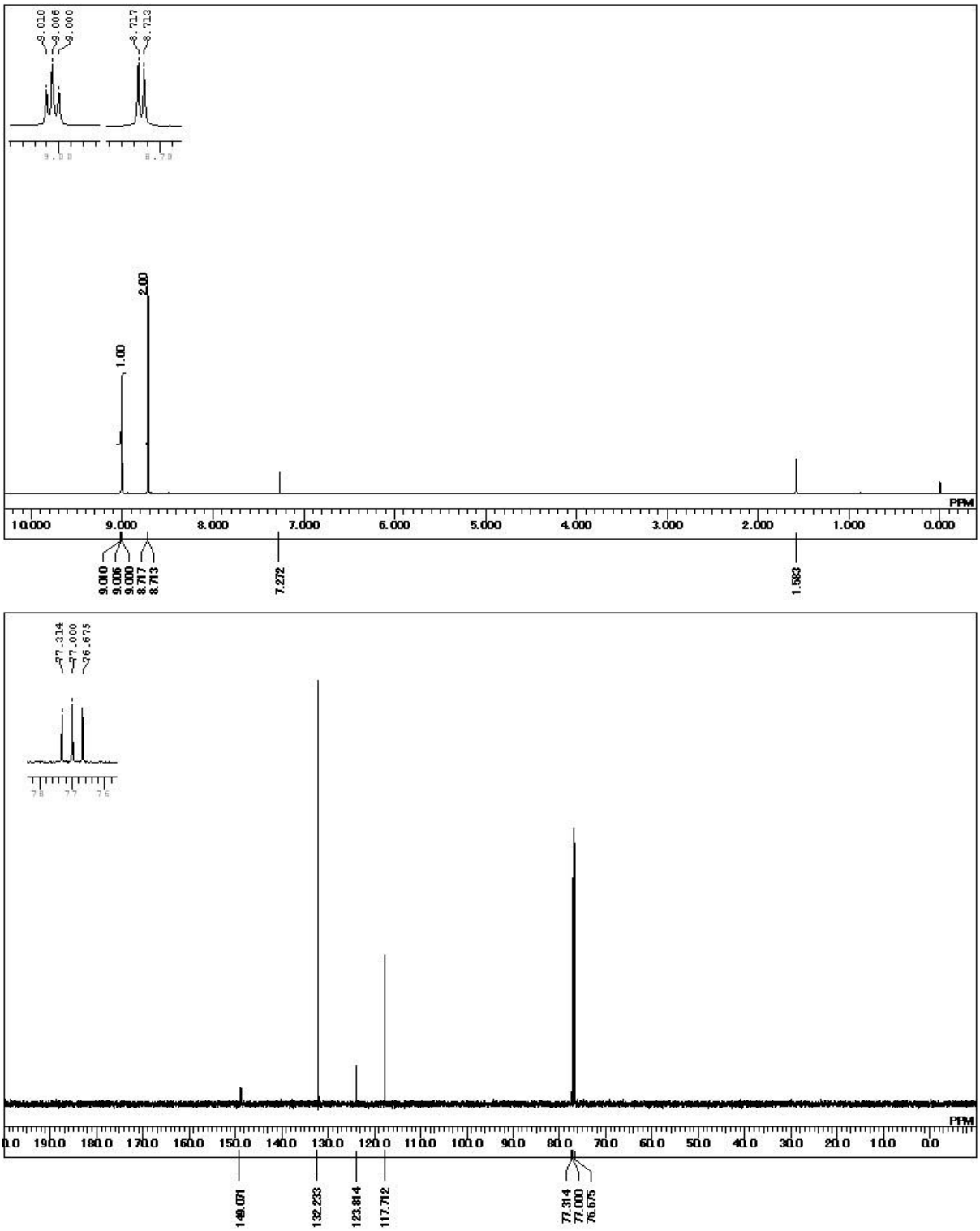

Figure S14. The NMR spectra of 1-bromo-3,5-dinitrobenzene (**12**). ^{1}H NMR (400 MHz, $CDCl_3$): δ 8.72 (2H, d, J = 1.6 Hz), 9.01 (1H, t, J = 1.6 Hz). ^{13}C NMR (100 MHz, $CDCl_3$): δ 117.7, 123.8, 132.2, 149.1. HRMS (FAB+) calculated for $C_6H_3BrN_2O_4$ $[M+H]^+$: *m/z* = 245.9298, found 245.9276.

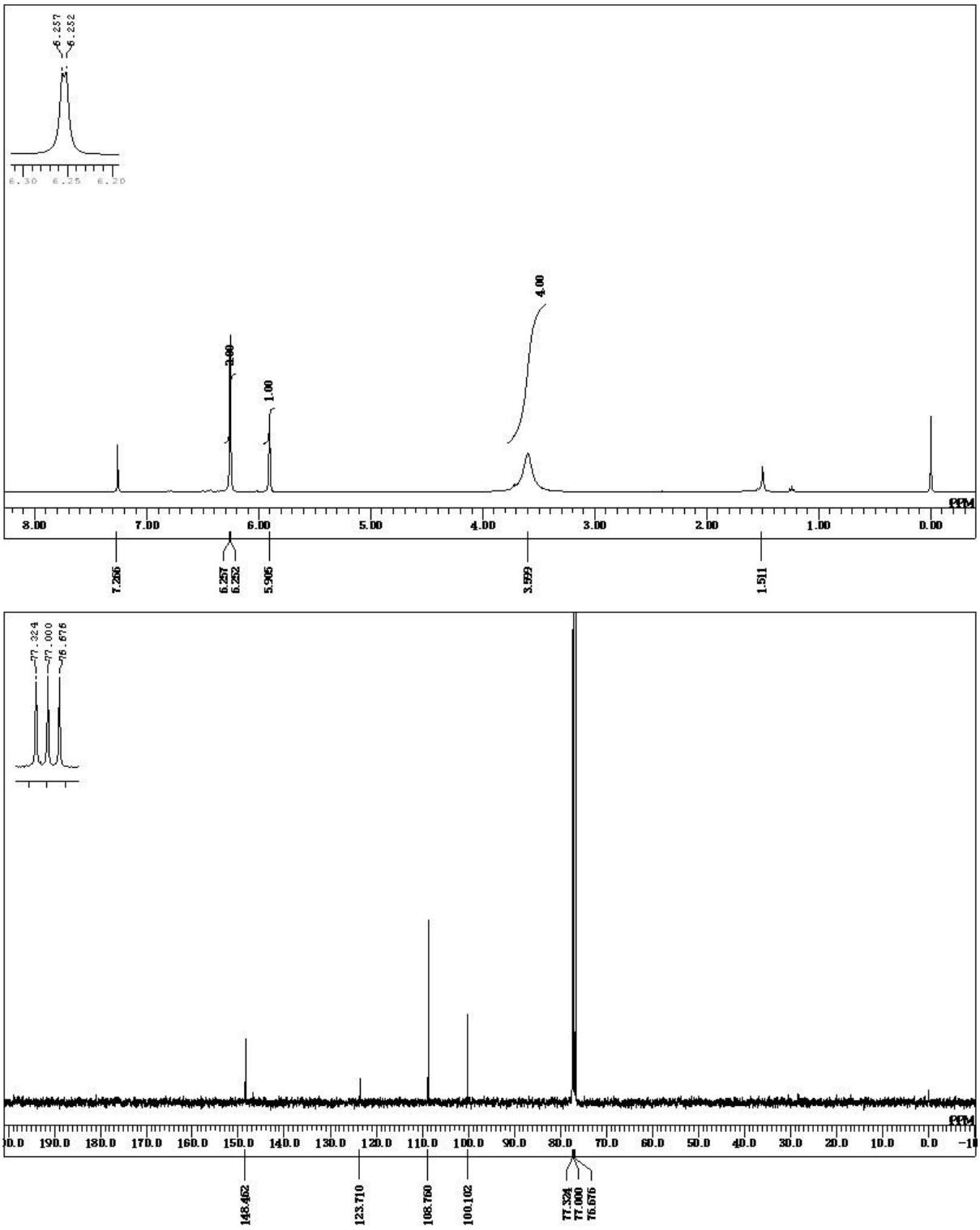

Figure S15. The NMR spectra of 5-bromobenzene-1,3-diamine (**13**). ^{1}H NMR (400 MHz, $CDCl_3$): δ 3.60 (4H, br s), 5.91 (1H, s), 6.25 (2H, d, J = 2.0 Hz). ^{13}C NMR (100 MHz, $CDCl_3$): δ 100.1, 108.8, 123.7, 148.5. HRMS (FAB+) calculated for $C_6H_7BrN_2$ $[M+H]^+$: *m/z* = 185.9777, found 185.9793.

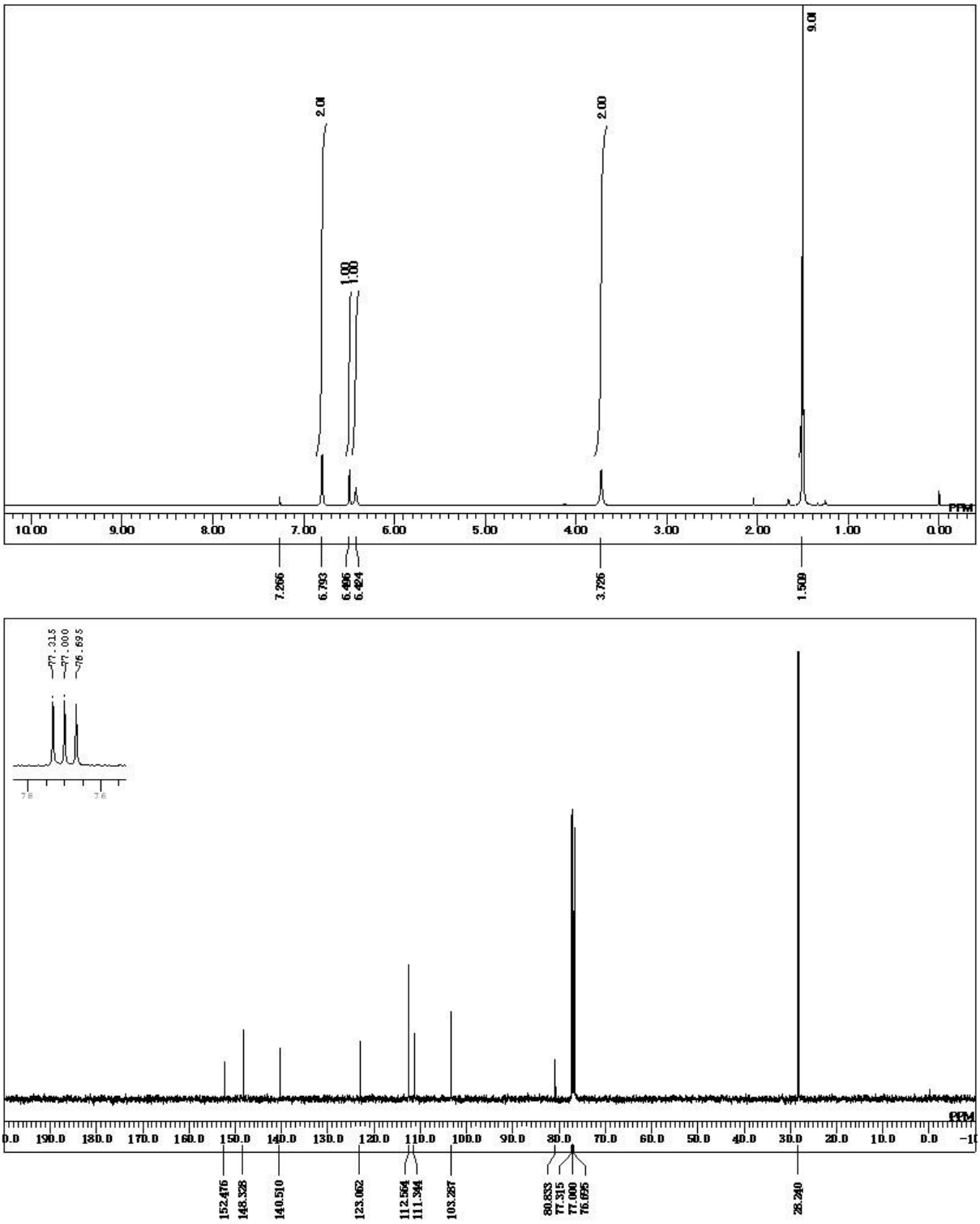

Figure S16. The NMR spectra of tert-butyl (3-amino-5-bromophenyl)carbamate (**14**). ^{1}H NMR (400 MHz, $CDCl_3$): δ 1.51 (9H, s), 3.73 (2H, s), 6.42 (1H, s), 6.50 (1H, s), 6.79 (2H, s). ^{13}C NMR (100 MHz, $CDCl_3$): δ 28.2, 80.8, 103.3, 111.3, 112.6, 123.1, 140.5, 148.3, 152.5. HRMS (FAB+) calculated for $C_{11}H_{15}BrN_2O_2$ $[M+H]^+$: *m/z* = 286.0300, found 286.0317.

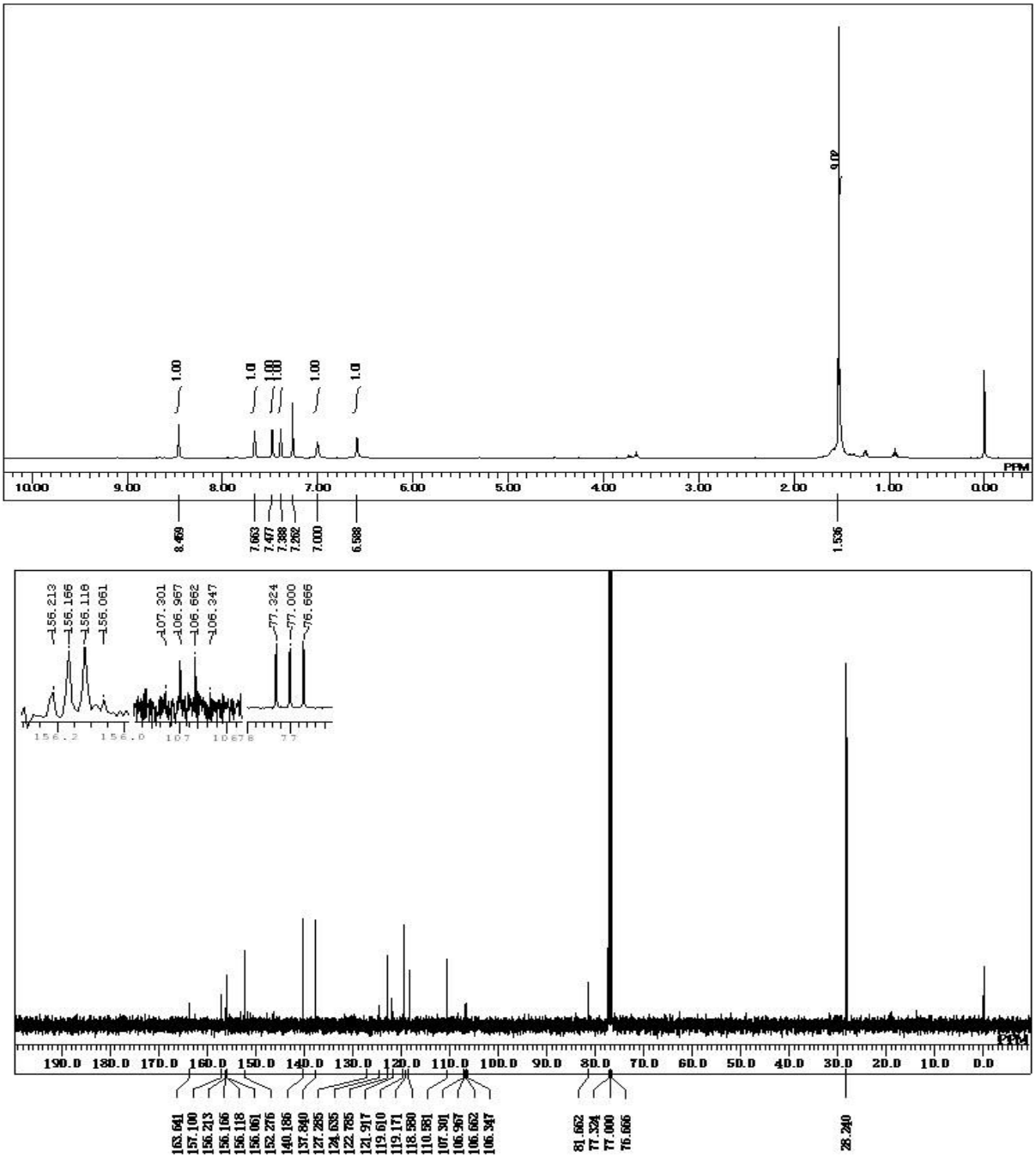

Figure S17. The NMR spectra of tert-butyl (3-{[2-chloro-5-(trifluoromethyl)pyrimidin-4-yl]amino}-5-bromophenyl)carbamate (**15**). ^{1}H NMR (400 MHz, $CDCl_3$): δ 1.54 (9H, s), 6.59 (1H, s), 7.00 (1H, s), 7.39 (1H, s), 7.48 (1H, s), 7.66 (1H, s), 8.46 (1H, s). ^{13}C NMR (100 MHz, $CDCl_3$): δ 28.2, 81.7, 106.8 (q, J_{CF} = 30.5 Hz), 110.6, 118.6, 119.6, 122.8, 123.4 (q, J_{CF} = 271.8

Hz), 137.8, 140.2, 152.3, 156.1 (q, J_{CF} = 4.8 Hz), 157.1, 163.6. HRMS (FAB+) calculated for $C_{16}H_{15}BrClF_3N_4O_2$ $[M+H]^+$: *m/z* = 465.9854, found 465.9842.

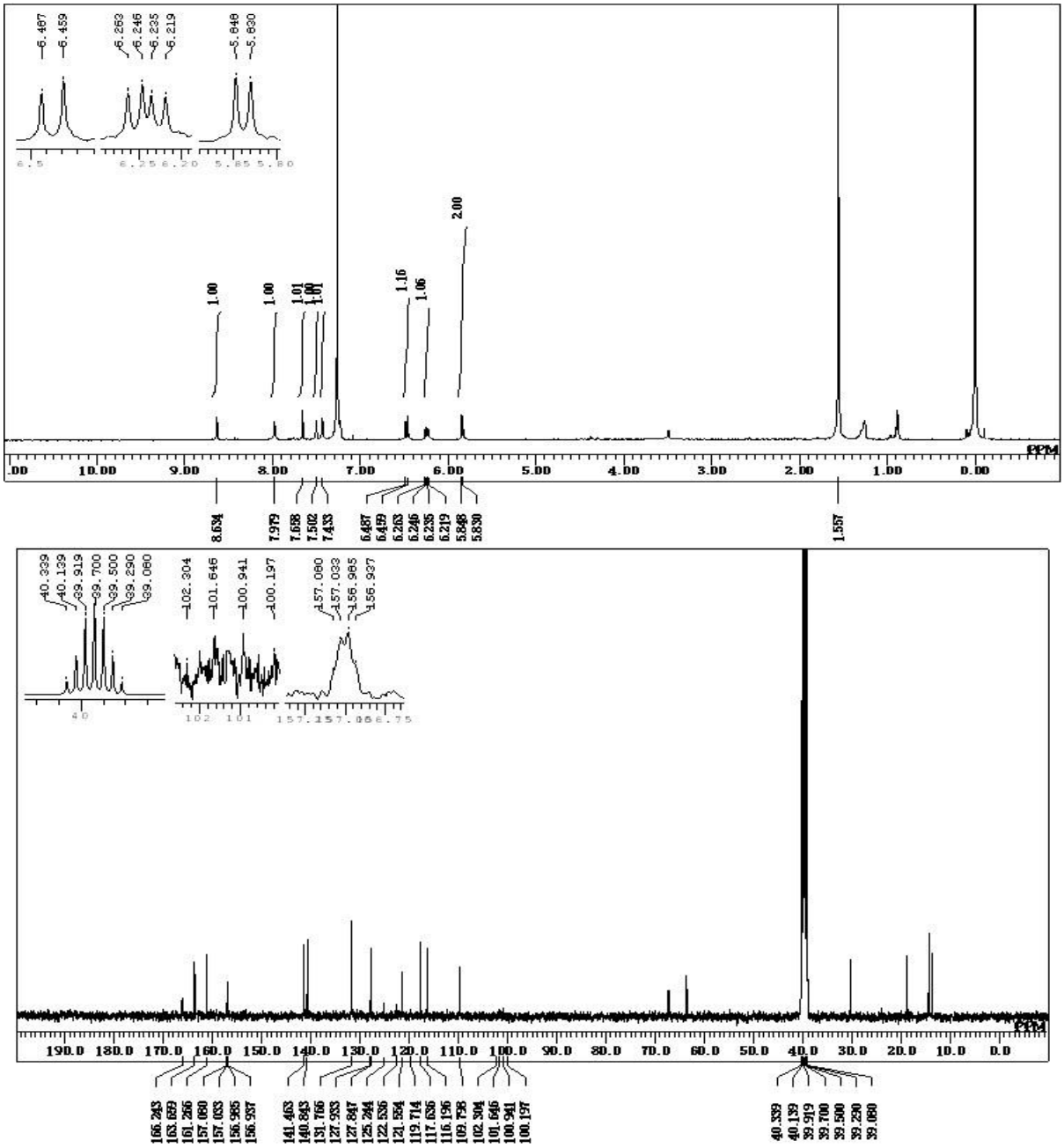

Figure S18. The NMR spectra of N-(3-{[2-chloro-5-(trifluoromethyl)pyrimidin-4-yl]amino}-5-bromophenyl) acrylamide (**16**). ^{1}H NMR (400 MHz, $CDCl_3$): δ 5.84 (2H, d, *J* = 7.2 Hz), 6.24 (1H, dd, *J* = 11.2, 6.8 Hz), 6.47 (1H, d, *J* = 11.2 Hz), 7.43 (1H, s), 7.50 (1H, s), 7.66 (1H, s), 7.98 (1H, s), 8.63 (1H, s). ^{13}C NMR (100 MHz, $(CD_3)_2SO$): δ 101.3 (q, J_{CF} = 70.5 Hz), 109.8, 116.2, 117.6, 121.6, 123.9 (q, J_{CF} = 270.8 Hz), 127.8, 131.8, 140.8, 141.5, 157.0 (q, J_{CF} = 4.8

Hz), 161.3, 163.7, 166.2. HRMS (FAB+) calculated for $C_{14}H_9BrClF_3N_4O$ [M+ H]$^+$: *m/z* = 419.9702, found 419.9600.

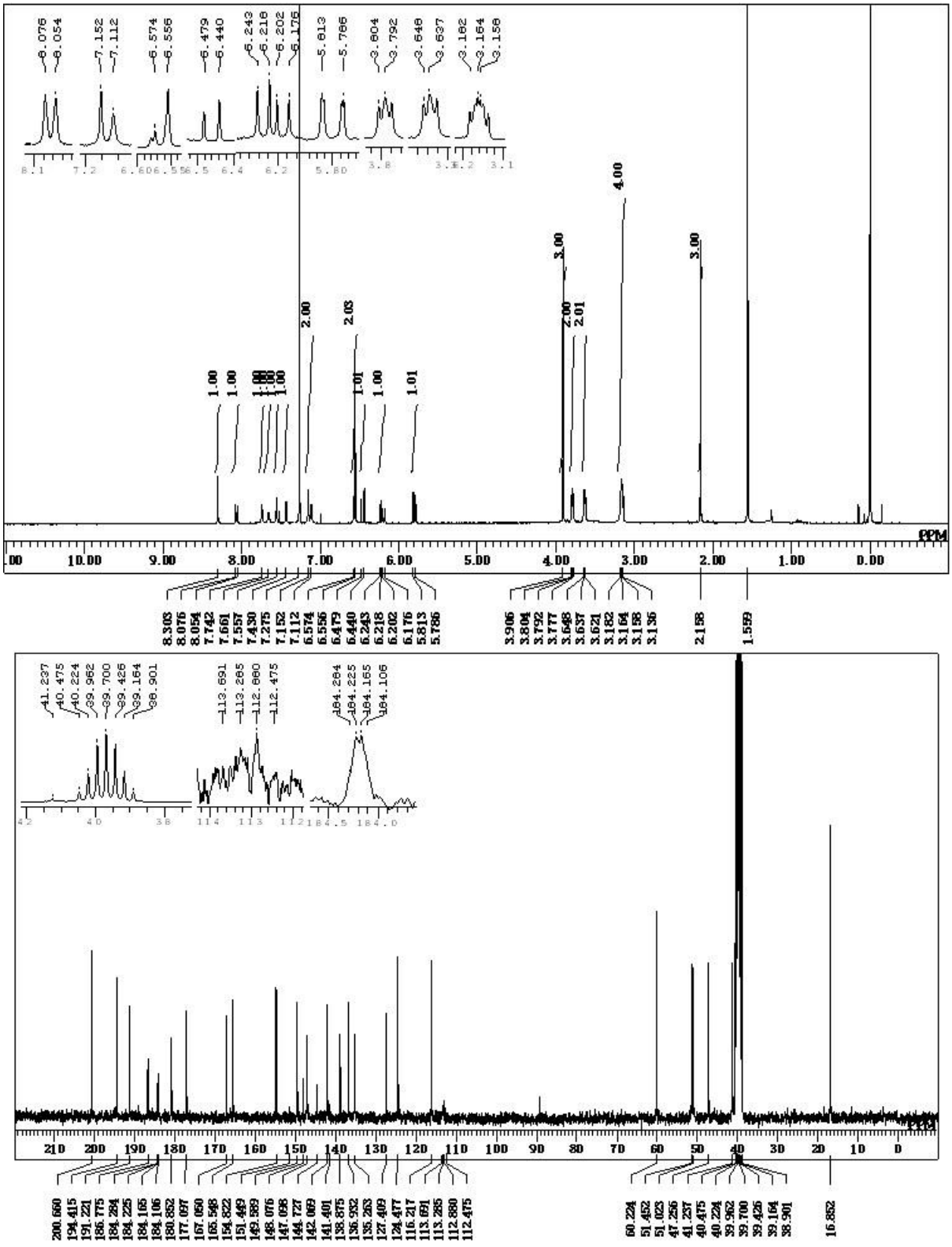

Figure S19. The NMR spectra of N-(3-{[2-({4-[4-acetylpiperazin-1-yl]-2-methoxyphenyl}amino)-5-(trifluoromethyl)pyrimidin-4-yl]amino}-5-bromophenyl)acrylamide (**17**). ^{1}H NMR (400 MHz, $CDCl_3$): δ 2.16 (3H, s), 3.12–3.20 (4H, m), 3.64 (2H, t, J = 4.4 Hz), 3.79 (2H, t, J = 4.8 Hz), 3.91 (3H, s), 5.80 (1H, d, J = 10.8 Hz), 6.21 (1H, dd, J = 15.2, 10.4 Hz), 6.44 (1H, d, J = 15.6 Hz), 6.54–6.60 (2H, m), 7.11 (1H, s), 7.25 (1H, s), 7.43 (1H, s), 7.56 (1H, s), 7.66 (1H, s), 7.74 (1H, s), 8.07 (1H, d, J = 8.8 Hz), 8.30 (1H, s). ^{13}C NMR (100 MHz, $(CD_3)_2SO$): δ 16.9, 41.2, 47.3, 51.0, 51.5, 60.2, 113.0 (q, J_{CF} = 40.5 Hz), 116.2, 124.5, 127.4, 135.3, 136.9, 138.9, 142.1, 146.4 (q, J_{CF} = 334.9 Hz), 147.1, 149.6, 154.8, 165.5, 167.1, 177.1, 180.9, 184.2 (q, J_{CF} = 6.0 Hz), 186.8, 191.2, 194.4, 200.7. HRMS (FAB+) calculated for $C_{27}H_{27}BrF_3N_7O_3$ $[M+H]^+$: m/z = 633.1324, found 633.1311.

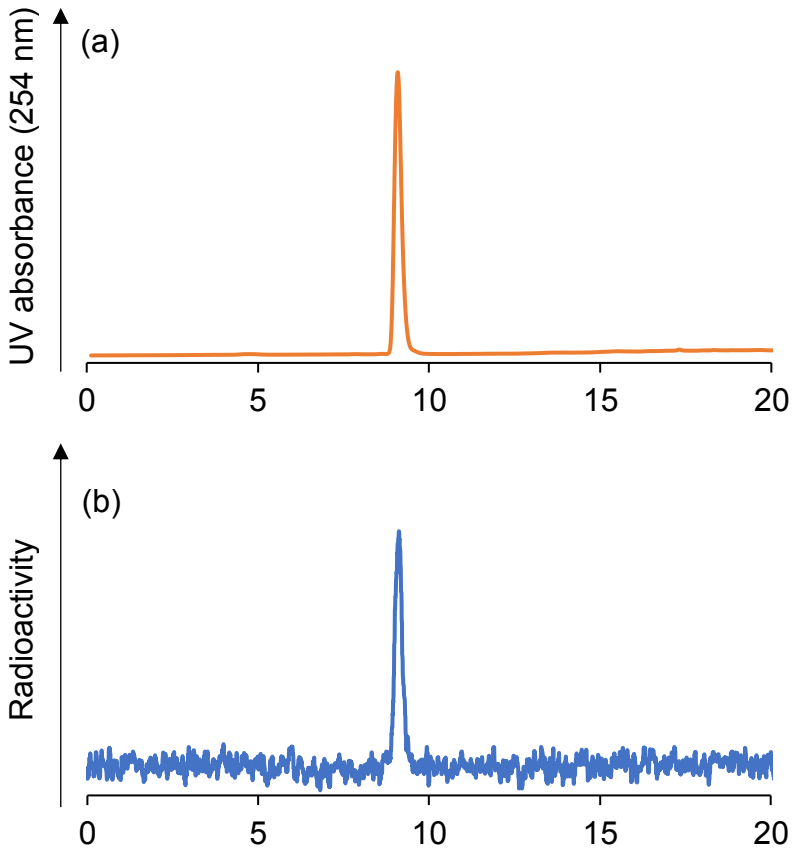

Figure S20. The chromatograms of (a) nonradioactive brominated compound **17** (BrCO1686) and (b) radioactive compound [^{77}Br]**17** ([^{77}Br]BrCO1686).

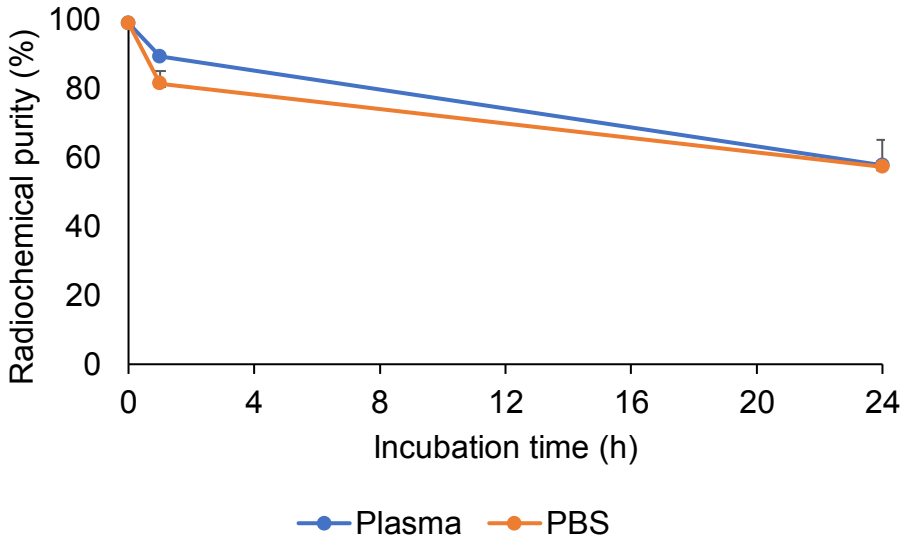

Figure S21. The stability of radiolabeled compound [^{77}Br]**17** in PBS and plasma.

Acknowledgments

This dissertation has been produced under the supervision of Professor Kazuma Ogawa at the Graduate School of Medical, Pharmaceutical and Health Sciences, Kanazawa University. My Ph.D. study was financed by Indonesia Endowment Fund for Education (LPDP) Scholarship. Undertaking this Ph.D. has been a truly life-changing experience for me, and all supports and guidance from many people have been encourage me to finish my study.

I am forever grateful to Professor Kazuma Ogawa for having accepted to be my supervisor and all the encouragement he gave me during the long term of my study. This field of study is new for me, but he assists me very well with his patience, guidance, charisma, and effort to improve my skills. In fact, he is not only my supervisor, but also like my father in this country. There are a lot of help and sacrifices that have been poured out for me, not only in my academic but also non-academic matters.

I express my sincere gratitude to emeritus Professor Akira Odani for his assistance in early I enrolled my study and his instructive discussion for two years later here. Also, heartfelt gratitude goes to Assistant Professor Kenji Mishiro for his help during my study period. The encouragement, assistance and training that I have received from him has contributed to develop my independent thinking and skills as a researcher. I extend my sincere thanks to the all members of Ogawa groups for all their help and support during undertaking this course.

The last but not least, heartfelt gratitude to my parents Drs. H. Muh. Arsyad and Hj. Sitti Faisah, my wife Hj. Sri Irmayana Ahmad, and my beloved children; Raihana Clemira, Aisyah Kimiko, Khalid Hideyo for their full support with love to achieve my dream.

January 5th, 2021

Muammar Fawwaz